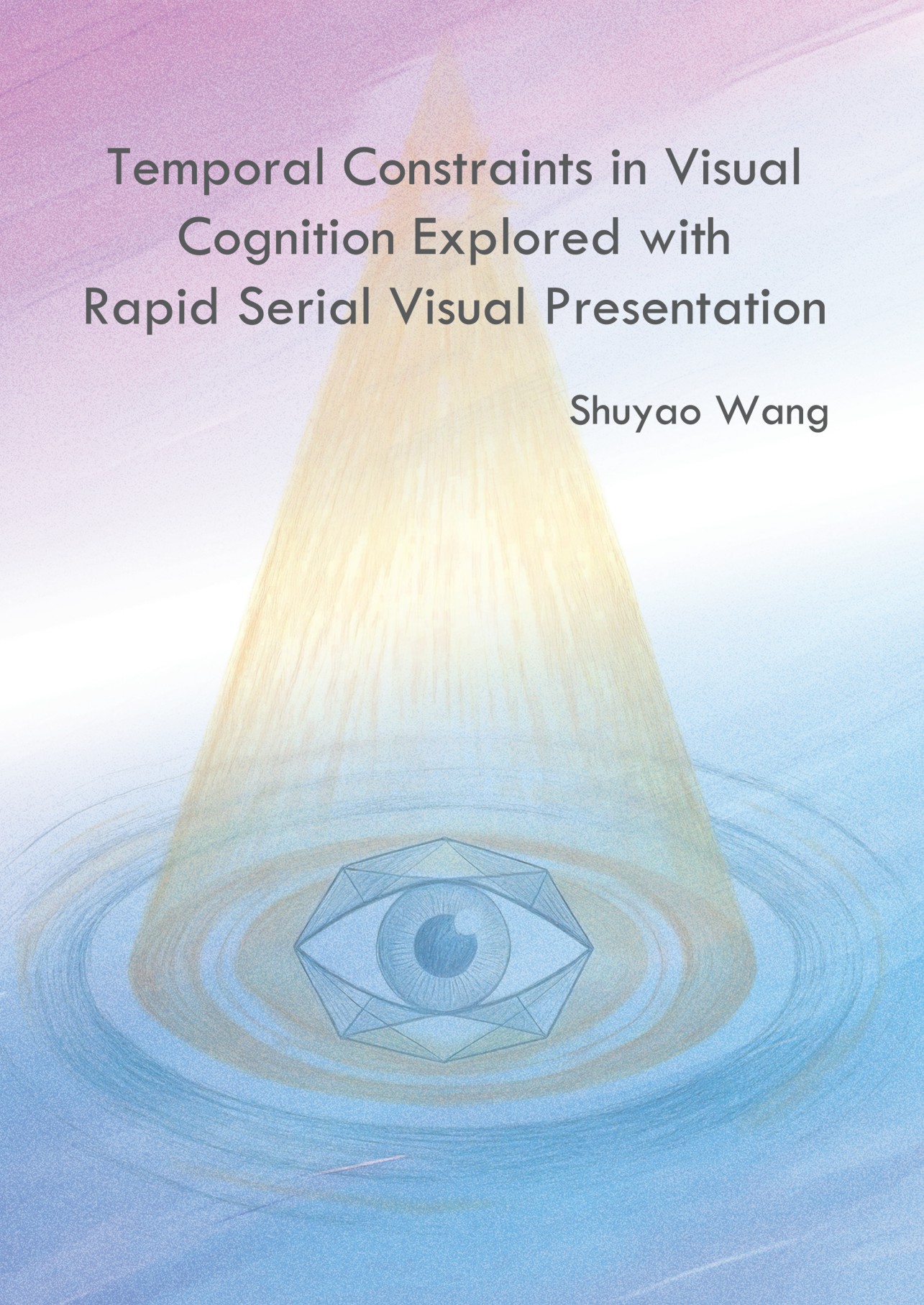
Temporal Constraints in Visual Cognition Explored with Rapid Serial Visual Presentation

Shuyao Wang



Propositions

1. The human brain is not a passive recorder of visual information; it is a dynamic system that regulates access to consciousness.

2. Modeling the shape of errors, rather than just counting their frequency, is essential to distinguish whether information under temporal pressure is completely lost or merely less precise (**Chapter 2**).

3. We can adaptively adjust the 'zoom ' of our attention, but this flexibility depends on stable habits and learned patterns rather than instant, trial-by-trial reactions (**Chapter 3**).

4. Conscious perception under pressure is not strictly all-or-none or gradual; it is a flexible state that shifts from a complete 'blink' to a partial 'blur ' depending on the 'zoom ' of our attention (**Chapter 3**).

5. The fundamental limit of working memory in dynamic environments is not only the size of its storage, but also the speed of its encoding.

6. The brain automatically prioritizes information with personal significance, even when we are consciously committed to ignoring it (**Chapter 4)**.

7. Rapid visual streams are effective for detecting hidden information because they move too quickly for the conscious mind to hide its own recognition (**Chapter 4**).

8. The true challenge of cognitive science is not finding a mechanism in an isolated lab setting, but proving it still holds true in the natural complexity of daily life.

9. Great things are not done by impulse, but by a series of small things brought together. — **Vincent van Gogh**

Temporal Constraints in Visual Cognition Explored with Rapid Serial Visual Presentation

Shuyao Wang

Cover Design & Layout: Shuyao Wang

Printing: ProefschriftMaken

© 2026 Shuyao Wang

All rights reserved. No parts of this publication may be reproduced or transmitted in any form or by any means, electronic or mechanical, including photocopying, recording, or any information storage and retrieval system, without the written permission of the author.



university of groningen



university of groningen

Temporal Constraints in Visual Cognition Explored with Rapid Serial Visual Presentation

PhD thesis

to obtain the degree of PhD at the
University of Groningen
on the authority of the
Rector Magnificus Prof. J.M.A. Scherpen
and in accordance with
the decision by the College of Deans.

This thesis will be defended in public on

Thursday 25 June 2026 at 11.00 hours

by

Shuyao Wang

born on 26 March 1993
in Shaanxi, China

Supervisor

Prof. E.G. Akyürek

Co-supervisor

Dr. A. Karabay

Assessment Committee

Prof. D.H. van Rijn
Prof. M.E. Timmerman
Prof. H. Bowman

Contents

Chapter 1 1
General Introduction 1
Chapter 2 15
Working Memory Representations under Temporal Constraints ... 15
Chapter 3 75
Visual Awareness under Temporal Constraints 75
Chapter 4 109
Covert Recognition under Temporal Constraints 109
Chapter 5 135
General Discussion 135
References 145
English Summary 165
Nederlandse Samenvatting 169
Acknowledgements 173

Chapter 1

General Introduction

When I arrived in Schiphol Airport in 2019 to begin my PhD journey, I found myself, jet-lagged and slightly disoriented, standing at the baggage claim, eyes locked on the rotating belt. My goal was simple: spot and grab my suitcases before anyone else mistook them for theirs. I watched each black rectangle roll by. In hindsight, choosing a black suitcase might not have been the wisest decision. Had I known anything about the rapid serial visual presentation (RSVP) paradigms back then, or conducted even a few pilot experiments, I might have opted for something slightly more distinctive. I scanned for labels, straps, dents. Despite being so focused, I still missed one of my bags on the first round. I also failed to notice that my friend had already collected theirs and was standing right beside me. Despite the sense that I was fully attentive, with eyes wide open and determined not to blink, my targets slipped by unnoticed, along with many other potentially relevant cues: a gate change announcement, a message on my phone, a human presence just to my side. Fortunately, I eventually retrieved all my luggage. Still, the incident pointed to a common limitation in visual processing. Even when attention is focused, some information can go unnoticed, not because of distraction, but due to inherent constraints in how visual input is selected and encoded.

Human visual information processing operates under structural constraints that limit both how much information can be processed and how fast such processing can occur. Attention serves as a fundamental mechanism for managing these constraints. Its primary function is to focus processing resources on a subset of sensory input, thereby enabling goal-directed perception and action (Carrasco, 2011; Desimone & Duncan, 1995). For example, in the spatial domain, attention prioritizes specific locations, improving target processing in that region, at the expense of others (Posner, 1980). In the temporal domain, attention similarly selects stimuli appearing at certain moments, but especially when other stimuli then occur in close succession, they may not be fully processed (Broadbent & Broadbent, 1987).

To investigate how the visual system copes with such temporal limitations, researchers have developed experimental paradigms that isolate time as a critical factor while minimizing spatial confounds. A widely used method is the RSVP paradigm (Potter & Levy, 1969), in which stimuli are presented sequentially at the same spatial location, typically at a rate of 10 items per second. Since the 1970s, RSVP has mapped how meaning is extracted at speed, how attention is distributed over time, and how stimuli are consolidated into working memory (WM) (Lawrence, 1971; Potter, 1976). RSVP has enabled researchers to examine the extraction of semantic meaning from rapidly presented visual input, the distribution of attention across time, the consolidation of sequential stimuli into WM, and the perceptual integration of temporally adjacent items (Akyürek et al.,

2012; Chun & Potter, 1995; Karabay et al., 2022; Klein & Dick, 2002; Pastukhov et al., 2013; Raymond et al., 1992; Shapiro et al., 1994).

The Attentional Blink and Its Theoretical Accounts

One notable attentional limitation revealed by RSVP is the attentional blink (AB) phenomenon. In dual- target RSVP, when a second target (T2) follows the first one (T1) after ~200–500 ms in a stream of distractors, report of T2 is impaired, which is called the attentional blink (AB) (Broadbent & Broadbent, 1987; Raymond et al., 1992). This deficit reflects a time- limited selection/encoding window rather than simple distraction.

The AB has since been extensively studied as a tool to investigate the temporal dynamics of attention and further cognitive processing (see reviews by Dux & Marois, 2009; Martens & Wyble, 2010). For example, it has been used to investigate how long attention dwells on an item for identification (Duncan et al., 1994) and to examine the dynamics of attentional allocation and memory consolidation (Martens et al., 2006; Nieuwenstein et al., 2005). Moreover, the AB has also served as a useful tool for exploring the mechanisms by which information gains access to consciousness. (Sergent & Dehaene, 2004; Sergent et al, 2005). Despite decades of research, the underlying mechanisms of the AB remain debated, and several theoretical accounts have been proposed. Two broad perspectives have been particularly influential: inhibition-based theories and capacity-limitation (bottleneck) theories.

Inhibition-based Theories

Inhibition-based theories can be traced back to Raymond et al.'s (1992) Attentional Gating Theory, which proposes that selective attention operates like a "gate". This attention gate opens to allow T1 for identification and then inhibits subsequent items to prevent featural confusion. The gate remains closed until T1's identification is complete. Because of this, a closely following T2 cannot pass through this 'gate', resulting in the AB. It is important to point out an exceptional case during the AB, known as the "lag-1 sparing effect". Here, *lag* refers to the number of intervening distractor items between T1 and T2 in the RSVP stream. A lag of 1 thus means that T2 immediately follows T1. The lag-1 sparing effect refers to the phenomenon where T2 can be correctly identified at lag 1, thereby avoiding the typically observed "blink". According to this Attentional Gating Theory, both T1 and T2 can be processed simultaneously at lag 1, since the gate cannot shut quickly enough, resulting in no deficit in reporting T2.

Building on this idea, Olivers and Meeter (2008) proposed the "Boost and Bounce" theory. They argued that the AB is caused by the suppression of the immediate distractor following T1 (T1+1), rather than to the prevention of feature-

binding errors between T1 and T1+1. This theory suggests that T1 receives an attentional boost, facilitating its entry into WM. Initially, the T1+1 distractor also receives an attentional boost due to its close temporal gap with T1. However, because it does not match the target template, it is swiftly suppressed (a bounce), which suppresses subsequent items' entry into WM, producing the AB. The lag-1 sparing effect is explained in this account by the overlap in the attentional boost duration for T1 and T2, which allows both targets access to WM.

Capacity-limitation (Bottleneck) Theories

The second category of theories originated from Chun and Potter's (1995) Two-Stage Model. They found that the AB still occurred in conditions where featural confusions were unlikely to happen, such as when searching for two black letter targets amidst black digit distractors. This observation challenged the gating theory proposed by Raymond et al. (1992). To account for it, Chun and Potter introduced a two-stage model. In the first stage, all items are briefly processed with a focus on feature detection, but the resulting conceptual representations are unstable. For information to be reportable, it must advance to the second stage, where it is consolidated into WM through slower, serial processing with limited capacity. According to this model, T2 cannot be encoded into WM until T1 has been fully processed in both stages. Although T2 can still undergo the first stage, its representation is vulnerable to decay or disruption by the subsequent item (e.g., T2+1). At lag 1, both targets can reach the second stage together due to the sluggish dynamics of the attentional system. Subsequent studies elaborated on this framework (e.g., Dux & Harris, 2007; Jolicoeur, 1998,1999; Jolicoeur & Dell'Acqua, 1998; Potter et al., 2002), further reinforcing the interpretation of the AB as a consequence of central capacity limitations.

However, bottleneck theories are challenged by 'spreading the sparing'—accurate identification of multiple successive targets without a blink (Di Lollo et al., 2005; Nieuwenstein & Potter, 2006; Olivers et al., 2007; Potter et al., 2008). To account for this, Wyble et al. (2009; Bowman & Wyble, 2007) introduced the (episodic) simultaneous type/serial token (eSTST) model, building further upon the Two-Stage model. The eSTST model consists of three fundamental components: *types* (conceptual representations), *tokens* (episodic representations in WM), and a temporal attention mechanism referred to as the '*blaster*'. According to the eSTST model, every item in the RSVP is first identified at the type level. However, to be accessible for reporting, these types must be bound to tokens, with the blaster facilitating this binding. In an AB task, detection of T1 activates the blaster, enabling its type to be bound to a token and consolidated in WM. The blaster is then briefly suppressed to protect this process, which prevents subsequent items – including T2 – from being tokenized. Importantly, this attentional suppression

reflects the inherent limitation of WM consolidation, which cannot encode two items into distinct temporal positions simultaneously. Accordingly, the blink arises from the interplay between the suppression mechanism and the consolidation bottleneck. At lag 1, however, T1 and T2 may be bound in parallel, sparing T2 but often impairing T1 accuracy, or leading to order reversals (i.e., T2 bound to Token 1, T1 to Token 2). Regarding the "spreading the sparing" effect, the eSTST suggests that multiple successive targets facilitate a sustained deployment of attention. While this sustained attention enables accurate identification of multiple consecutive targets, the eSTST model suggests that it comes at the expense of episodic information, such as the precise temporal order of items (but see also Hommel & Akyürek, 2005; Akyurek et al., 2012; Akyurek & Wolff, 2016).

Working Memory Encoding under Temporal Constraints

Building on these theoretical and behavioral findings, prior research has consistently shown that AB arises when the consolidation of T1 temporarily occupies limited WM resources, thereby disrupting the consolidation of T2 and leaving it vulnerable to decay or interference. This section reviews physiological evidence demonstrating that T2 consolidation in WM is disrupted during the AB at the neural level.

Electrophysiological studies commonly indicate that, during the AB, early perceptual processing is largely preserved whereas indices of WM consolidation (e.g., P3/P3b) are attenuated or delayed. Vogel et al. (1998) provided one of the earliest ERP demonstrations of a post-perceptual locus of the AB. By contrasting single- and dual-target RSVP tasks, they showed that early perceptual (P1, N1) and semantic responses (N400) to T2 were unaffected, whereas the T2-evoked P3 was eliminated during the blink interval, clearly linking the deficit to a failure of WM consolidation rather than perceptual suppression. Subsequent studies replicated this dissociation, consistently finding intact early and semantic processing but attenuated or absent P3s for blinked T2s (Kranczioch et al., 2003; Rolke et al., 2001).

Importantly, subsequent work showed that T2 consolidation is not always eliminated but can be postponed. Vogel and Luck (2002) directly compared masked and unmasked T2s within the blink window. When T2 was masked, the P3 component was fully suppressed despite intact early perceptual responses (e.g., P1/N1; but see Zhao et al., 2025 for evidence of early modulation), suggesting failed consolidation. In contrast, when T2 was unmasked, the P3 was not eliminated but delayed by about 100ms relative to long-lag trials, indicating that consolidation can be temporally postponed. Sessa et al. (2007) further corroborated this account by showing that T2-related P3s during the blink period were both reduced in amplitude and shifted in latency. Chennu et al. (2009) suggested that the AB also

reflects a reduction in the temporal acuity of selective attention. Specifically, they found increased temporal variance in the P3s evoked by targets within the AB window. Chennu et al. (2009) suggested that the AB also reflects a reduction in the temporal acuity of selective attention. Specifically, they found increased temporal variance in the P3s evoked by targets within the AB window.

Further evidence links the AB to serial WM encoding mechanisms, in line with the eSTST model (Wyble et al., 2009; 2011). Craton et al. (2009) combined ERP data with computational modeling and showed that T2-related P3s were suppressed during the blink while T1-related P3s remained unaffected, indicating that items are consolidated strictly one after the other rather than in parallel. Dell'Acqua et al. (2015) extended this line by dissociating detection and encoding processes using different ERP components: the P3a, associated with attentional allocation, was reduced in amplitude without latency shifts, whereas the P3b, indexing WM encoding, was both attenuated and delayed, particularly under higher target loads.

Additionally, the extent of the AB has been shown to vary with the processing of demands of T1 itself. Akyürek et al. (2010) demonstrated that higher T1 loads increased the suppression of T2-related P3s, while Robitaille et al. (2007) reported that rare or demanding T1 tasks elicited larger P3s and disrupted both T2-locked P3s and sustained contralateral negativities which is associated with WM maintenance. Together, these results indicate that increasing the demands of T1 processing further impair T2 consolidation.

Finally, ERP studies have shown that the consolidation bottleneck underlying the AB is not modality-specific. Attenuated and delayed T2-locked P3s have been observed regardless of whether the RSVP stream consisted of visual, auditory, or cross-modal targets, demonstrating that the bottleneck reflects a central rather than sensory-specific limitation (Arnell, 2006; Dell'Acqua et al., 2003; Ptito et al, 2008, but see also Duncan et al., 1997).

Conscious Awareness during the Attentional Blink

The WM consolidation bottleneck observed in the AB is closely related to conscious access. In the eSTST model (Bowman & Wyble, 2007; Wyble et al., 2009), perceptual processing first activates a type representation; consolidation then binds this representation to a token, which makes it stable in WM and accessible to awareness. From this perspective, the consolidation bottleneck governs access to awareness, leading to the question of how awareness emerges during the AB.

Conscious processing is commonly distinguished from initial perceptual processing. Block (1995, 2005) emphasized that access consciousness is defined by information becoming stabilized and available for report, reasoning and action. From a neural perspective, Lamme (2004) argued that while feedforward activity

may support perceptual discrimination without awareness, conscious experience requires recurrent processing that stabilizes perceptual representations. These accounts suggest that becoming aware of a stimulus requires more than initial perceptual processing; it relies on additional processes that make the representation stable and cognitively accessible.

Whether such awareness emerges in an all-or-none fashion or a graded manner is debated in the field of consciousness research. On a discrete, all-or-none view, stimulus information either enters awareness fully or remains entirely unconscious. By contrast, graded accounts hold that conscious perception may vary gradually along a continuum, rather than reflecting a binary distinction between 'seen' and 'unseen'. To test these competing accounts, researchers have often turned to the AB paradigm. Critically, when T2 occurs within the blink window, physically identical targets are sometimes accurately reported on some trials but missed on others. This dissociation between identical sensory input and divergent conscious outcomes makes the AB a powerful paradigm for exploring the nature of awareness.

All-or-none Accounts

The all-or-none perspective is supported most prominently by the Global Neuronal Workspace (GNW) model (Baars, 1989; Dehaene et al., 1998; Dehaene et al., 2003). According to this framework, consciousness occurs only when stimulus-evoked activity exceeds a critical threshold, triggering a self-sustained and distributed pattern of activation – often referred to as "ignition". By contrast, if activation remains below threshold, processing is restricted to local, short-lived representations that do not propagate into the workspace and thus fail to reach awareness. Within this account, the AB can be understood as a failure of ignition for the second target: although T2 receives normal early perceptual analysis, the global workspace is already engaged by the ignition elicited by T1. Consequently, the top-down amplification required for T2 to cross threshold and gain conscious access is temporarily unavailable, preventing it from entering awareness.

The prediction of the GNW model for the AB – that T2 should either reach awareness fully or fail entirely – has been tested both in behavioral and physiological studies. Sergent and Dehaene (2004) asked participants to rate T2 visibility on a continuous scale and modeled the response distributions with regression analyses. They found that subjects' ratings clustered into a bimodal distribution: T2s were either fully seen or completely missed, with little evidence for intermediate states. Conscious access thus appeared to follow a discrete transition at threshold, as predicted by the GNW framework.

Sergent et al. (2005) subsequently compared the neural cascade elicited by seen and unseen T2s, categorized using subjective visibility ratings. In their

findings, early components (P1, N1, N400) were preserved regardless of conscious state, indicating intact perceptual and semantic processing. By contrast, unseen T2s failed to evoke a P3b and showed reduced long-range beta-band synchronization, both markers of global workspace ignition. Additionally, they found that faster decay of the T1-evoked P3b was associated with greater T2 visibility, consistent with competition for limited workspace resources, and in line with an all-or-none account.

In a different approach, Asplund et al. (2014) used mixture-modeling analyses to dissociate the probability of perceiving T2 from the precision of reports when perceived. Manipulating the interval between T1 and T2 revealed that only the likelihood of reporting T2 was affected, while representational precision remained stable. Critically, this likelihood dropped significantly at lag 2, corresponding to the blink window. These findings indicate that the blink reflects a reduced probability of T2 reaching awareness rather than a degradation of its representation quality, again consistent with the all-or-none account of consciousness.

Graded Accounts

A number of studies have nevertheless challenged the all-or-none claim and argue that awareness is more continuous in nature. Overgaard et al. (2006) introduced the Perceptual Awareness Scale (PAS) and showed that intermediate awareness ratings occurred systematically. PAS scores increased with stimulus duration and were positively correlated with objective accuracy, indicating that these subjective reports reflected meaningful gradations of awareness rather than arbitrary choices. Nieuwenhuis and de Kleijn (2011) likewise reported gradual conscious perception in a series of AB experiments. Specifically, by replacing word stimuli that are susceptible to post-hoc reconstruction with single characters, they minimized opportunities for guessing and observed reliable intermediate ratings, thereby providing evidence against a strictly dichotomous view of awareness. In direct contrast to the results of Sergent and Dehaene (2004), they argued that the divergences may partly stem from methodological factors. More recently, Cohen et al. (2023) provided further support for gradual awareness. Using continuous reproduction tasks across four different paradigms – AB, backward masking, iconic memory, and retro-cueing – they showed that behavioral performance was best explained by the target confusability competition model, which characterizes awareness as a gradual change in representational strength.

Hybrid Accounts

An emerging line of research has sought to reconcile these apparently conflicting findings by suggesting that awareness can be both graded and discrete,

depending on contextual factors. Sy et al. (2021) first demonstrated that the loss of awareness during the AB can take graded or discrete forms depending on task conditions. When T1 and T2 were perceptually similar and both required orientation reports, the blink was marked by a graded reduction in T2 precision without a change in guess rate. In an attentional switch condition, where participants report T1 color and T2 orientation, both precision loss and increased guessing were observed. However, when T1 and T2 were perceptually distinct and required a task switch, the blink was associated only with an increase in guess rate of T2, indicating discrete loss of awareness.

Karabay et al. (2022) reported complementary findings across a series of experiments manipulating the width of attentional allocation during the AB. When attention was narrowly focused on a predictable T1 location, T2 performance showed higher guess rate, consistent with discrete failures. In contrast, broader attentional allocation (e.g., an unpredictable T1 location) yielded reduced precision without changes in guessing, indicative of graded awareness. They suggested that attentional allocation to T1 influences whether T2 awareness loss appears discrete or gradual.

Practical Application of RSVP in the Concealed Information Test

As outlined in the previous sections, RSVP has proven to be a valuable tool in the study of the temporal dynamics of attention, perception, WM and consciousness. Its main characteristics are the rapid presentation of stimuli and the need for continuous monitoring under high temporal pressure. Importantly, RSVP studies have identified the P3 component as a reliable marker of item identification: when an item is consciously perceived, its presentation elicits a clear P3 response, whereas distractors or missed targets typically do not, as reviewed in the previous section. These same properties make RSVP attractive for concealed information detection. The speed and attentional demands of RSVP furthermore reduce the possibility for deliberate strategic control, making it difficult to manipulate behavioral and/or physiological responses to critical items.

In forensic science, concealed information tests (CITs) already exist in various forms. At its heart, a CIT aims to assess whether an individual recognizes concealed information, such as crime-relevant or personally significant details. To this end, behavioral and/or physiological responses to *probe* items - stimuli known only to the knowledgeable person - are compared with responses to matched but irrelevant *control* items. CIT studies have shown reliable probe-control differences in a variety of measures (Ben-Shakhar & Elaad, 2003; Verschuere et al., 2011). These include autonomic responses such as skin conductance, heart rate, respiration, and pupil size (see Gamer, 2011 for a review), as well as central nervous

system markers, most prominently the P300 component of ERP (see a review in Rosenfeld, 2020), and fMRI-based indices (Ganis et al., 2003).

A persistent challenge for existing CITs is vulnerability to countermeasures. Because stimuli are usually presented at a relatively slow pace, participants can intentionally alter their responses to reduce probe-control differences. Countermeasures can be physical, such as covert muscle movements or controlled breathing (Honts et al., 1996; Mertens & Allen, 2008; Rosenfeld et al., 2004), and mental strategies, such as deliberately focusing on control items or recalling irrelevant details (Rosenfeld et al., 2004). Empirical studies have demonstrated that such strategies can markedly reduce the sensitivity across a range of physiological measures, thereby affecting the reliability of the CIT (Ben-Shakhar, 2011; Peth et al., 2016).

However, RSVP has the potential to counteract the effect of countermeasures. By presenting items at a rapid rate, RSVP imposes high temporal pressure that narrows the time window for voluntary modulation, making it more difficult to selectively alter responses to probes or controls. Importantly, recognition-related signals remain detectable under these rapid conditions. Bowman et al. (2013) were the first to examine this combined RSVP-CIT approach and found that participants' own names elicited a reliable P3 response compared to control names. In a follow-up study, they further demonstrated that probe-control P3 differences persisted even when participants were instructed to apply countermeasures strategies (Bowman et al., 2014). Alsufyani et al. (2019) extended this work to face stimuli and found that famous faces triggered enhanced ERP responses (N400f and P600) and increased low-frequency theta power, distinguishing them from unfamiliar faces. More recently, Chen et al. (2023) investigated whether pupillometry could be used as an indicator in RSVP- CIT. Their study showed that participants' real names elicited greater pupil dilation than control names. Together, these studies show that RSVP-CIT has potential.

Thesis Overview

As sketched above, RSVP can be used as a means to investigate a range of cognitive processes and phenomena. As such, RSVP is at the core of this dissertation, which comprises three empirical studies that investigate visual cognition under temporal constraints, with a focus on WM encoding, the modulation of conscious perception, and physiological markers of covert recognition. While each chapter addresses a distinct aspect of RSVP-based cognition, together they trace a progression from theoretical models of WM to the dynamics of conscious access, and finally to the application of RSVP in concealed information detection. This structure illustrates how RSVP paradigms can be used

both to refine theoretical accounts of temporal cognition and to explore their practical implications.

Chapter 2 examined the limitations of WM consolidation by systematically comparing seven WM computational models in the context of the AB. Using four empirical datasets from three independent laboratories, we evaluated the capacity of these models to account for target consolidation failures under temporal pressure. Specifically, each model was fitted to the data and assessed using the Akaike Information Criterion values at an individual level, across different conditions and experiments, which served as the basis for model comparison.

Chapter 3 investigated the adaptive control of attentional scaling and its influence on the nature of conscious experience during the AB. The location of T1 was manipulated either session-wise, trial-wise, or through a biased distribution that could be learned across a block of trials. Participants were explicitly required to attend to T1's location. We assumed that differences in T2 awareness reflect differences between narrow and broad attentional scales. The central question was whether participants could learn to adapt their attentional scale under these different conditions. We expected that the session-wise cue could allow sustained adjustment by providing stable information across an extended period, while the biased distribution would support adaptation through implicitly learning. In contrast, the trial-wise cue provided prediction on each trial, but required immediate adaptation, which likely prevented successful adjustment of the attentional scale. In our study, we examined T2 awareness under each condition, using mixture modeling to dissociate the probability that T2 was consciously perceived from the precision of its representation.

Chapter 4 extended the RSVP paradigm to the practical domain of CIT, combining EEG and pupillometry to assess covert recognition of personally significant information. Participants viewed RSVP streams of face stimuli while performing a gender-based target detection task. Within each stream, a critical stimulus was embedded that could be a task-relevant target (opposite gender face), a probe face, a control face, or a distractor face. Probe faces were either personally familiar (a parent's face) or unfamiliar, depending on block condition. Thus, participants focused on detecting gender-defined targets while personally familiar but task-irrelevant faces appeared among distractors. EEG and pupillometry were concurrently recorded throughout the task, and our analyses focused on four measures: ERP amplitude at the Pz electrode, theta-band (4-8 Hz) power, pupil size and pupil size change, in response to personally familiar information.

Chapter 5 presents the general discussion of the dissertation. It integrates the main findings of the three empirical chapters, considers their broader theoretical implications, and outlines potential directions for future research.

Author Contributions

Chapter 2

Shuyao Wang contributed to the conceptualization of the experiments, and served as lead for data curation, formal analysis, methodology, visualization, and writing – original draft. Aytaç Karabay supervised the project, contributed to methodology and writing – review & editing. Elkan Akyürek served as lead for project administration and supervision, and contributed to the conceptualization of the experiments and writing – review & editing.

Chapter 3

Shuyao Wang contributed to the conceptualization of the experiments, and served as lead for data curation, formal analysis, methodology, visualization, and writing – original draft. Aytaç Karabay supervised the project, contributed to methodology and writing – review & editing. Elkan Akyürek served as lead for project administration and supervision, and contributed to the conceptualization of the experiments and writing – review & editing.

Chapter 4

Shuyao Wang contributed to the conceptualization of the experiments, and served as lead for data curation, formal analysis, methodology, visualization, and writing – original draft. Robbert van der Mijn contributed to data collection, formal analysis, and reviewed the final manuscript. Aytaç Karabay supervised the project, and contributed to methodology and writing – review & editing. Elkan Akyürek served as lead for project administration and supervision, and contributed to the conceptualization of the experiments and writing – review & editing.

Chapter 2

Working Memory Representations under Temporal Constraints

Preprinted as:
Wang, S., Karabay, A., & Akyürek, E. G. (preprint). Evaluating working memory representations during the attentional blink: A comparative modeling approach. bioRxiv. https://doi.org/10.1101/2022.09.15.508098

Abstract

The nature of working memory (WM) limitations has been a topic of long-standing debate, with several models proposed to elucidate this issue. In this study, we conducted a systematic comparison of seven visual WM models to assess their ability to account for target consolidation during the attentional blink (AB). The AB phenomenon refers to where participants often fail to encode the second of two targets when there is a short time interval of ~500 msec or less between them, providing an opportunity to evaluate commensurate WM limitations. Despite the growing consensus on the applicability of some WM models, such as the standard mixture model and the variable precision model, to the AB domain, no study has systematically evaluated these models in this context. We compared the performance of seven widely adopted visual WM models in four different AB datasets, drawn from three separate laboratories. We fitted each model and computed the Akaike Information Criterion (AIC) values at an individual level, across different conditions and experiments, based on which we compared the models. Slot- family models most often minimized AIC for second-target reports at short lags, while variable-precision models improved at longer lags and with color targets, indicating predominantly discrete consolidation during the AB, with feature- and lag- dependent graded components. These patterns imply that failure- to- encode (guessing) dominates over low- precision encoding, except when feature content or lag affords partial consolidation, refining theories of episodic tokenization and WM consolidation during the AB.

Keywords: working memory; attentional blink; computational models; model comparison

1. Introduction

Visual working memory (WM) is essential for information processing, yet it is challenging to encode all information completely. A substantial amount of research has focused on investigating the limitations of WM, which include storage limitations – the capacity of how many items can be encoded (Cowan, 2001; Miller, 1956; Pashler, 1988); but also processing limitations – the difficulties faced when processing and consolidating multiple items that appear either concurrently or in a rapid succession (Jolicœur & Dell'Acqua, 1998; Ricker & Cowan, 2014).

To investigate the limits of WM, an analysis of the kind of representation errors that occur in WM tasks has proven fruitful. Several WM models on the nature of these errors have been proposed. One perspective suggests that WM is comprised of a fixed, limited number of discrete "slots" dedicated to item storage, with large memory errors (i.e., those far away from the target value) occurring when items are not stored in WM, reflecting pure guessing (Alvarez & Cavanagh, 2004; Bays et al., 2009; Zhang & Luck, 2008). Another set of models proposes that WM is a continuous resource that can be distributed freely over items (Fougnie et al., 2012; van den Berg et al., 2012). According to this view, large memory errors arise when items are encoded with extremely low precision as opposed to high precision. Still other models focus on perceptual confusability and on the degree to which items are processed as an integrated ensemble. (Brady & Alvarez, 2011; Schurgin et al., 2020).

Although such model-based analyses of representation errors originate from, and have mainly been applied in, experimental tasks that target WM specifically, maintaining stimulus representations is critical to a myriad of cognitive functions, including selective attention, where target items have to be identified, selected, and reported on, sometimes also after a small delay. Through the application of model-based analyses, here we asked how targets are (mis-)reported in a temporal attention task, to assess the nature of representation during the attentional blink (AB) phenomenon.

The AB refers to the failure to identify the second (T2) of two briefly presented target stimuli, when the time interval (or lag) between them is within 200 – 500 msec (Broadbent & Broadbent, 1987; Raymond et al., 1992). Recent models of the AB suggest that the blink occurs due to the ongoing consolidation of the initial stimulus (Wyble et al., 2009, 2011; but see Zhao et al., 2024). During the consolidation of the first target (T1) into WM, attention is suppressed, which impairs the ability to identify new stimuli (e.g., T2). Event-related potential (ERP) studies provided evidence that the consolidation of T2 information is impaired, as shown by a decrease in the P3 component's amplitude (Bourassa et al., 2015; Dell'Acqua et al., 2003; Vogel et al., 1998; Sergent et al., 2005; for a review see

Zivony & Lamy, 2022). Further evidence for the involvement of WM in the emergence of the AB phenomenon has come from experiments showing that AB magnitude is increased when WM load is higher (Akyürek et al., 2007), which is also accompanied by reduced P3 amplitude (Akyürek et al., 2010).

Traditionally, AB research has utilized categorical items such as letters, numbers, or images in the rapid serial visual presentation (RSVP) paradigm (for a review, see Dux & Marois, 2009; Martens & Wyble, 2010). While this typical paradigm has proven to be an effective method for studying the AB itself, it presents inherent challenges in evaluating the quality of target representations maintained in WM during the AB window. In response to this challenge, recent studies have incorporated the continuous report task into the RSVP paradigm, as is also frequently utilized in the visual WM field (Bays et al., 2009; Fougnie & Alvarez, 2011; Kool et al., 2014; Oberauer et al., 2017; Zhang & Luck, 2008). During the task, participants are required to memorize targeted visual items, which are identified by a basic visual property that varies on a continuous, usually circular, dimension, such as color or orientation. In the reproduction stage, participants are then asked to recall the target on a continuous response scale, such as recreating its orientation by rotating a Gabor (Wilken & Ma, 2004). Consequently, the performance of a continuous report task is not measured in a binary format, but rather as the divergence between the target value and the corresponding response, making it possible to quantify the target representations stored in WM. Thus, by combining the AB paradigm with continuous report tasks, we can measure the structure of T2 errors, and assess whether target report failures arise from the rate of all-or-none losses or from (overall) degradation in precision.

Several previous studies have explored this approach. For instance, Asplund et al. (2014) applied a mixture-model analysis (Zhang & Luck, 2008) to data obtained by explicitly asking participants to recall their perception of T2 along a continuous circular dimension. Through this approach, the authors were able to quantify the precision of T2 representations and the proportion of guess responses for T2. Their findings indicated that AB affects T2 perception in an all-or-none manner, with an increased percentage of random guess trials at shorter lags, while lag had no effect on T2 precision.

In a similar vein, Karabay et al. (2022) employed hierarchical Bayesian estimation to explore the variability in the precision and guess rate parameters of the standard mixture model at different time intervals between two targets. Their study showed that T2 awareness during the AB can be both gradual and discrete. Specifically, when the identification of the first target (T1) required the focus of attention on a single spatial location, T2 awareness was discrete, with the guess rate varying significantly; on the contrary, when T1 identification induced a spatial spread of attention, T2 awareness was gradual, with variations in precision. Sy et al.

(2021) utilized both the standard mixture and variable precision models, and also found that the temporal loss of T2 information during the AB might be either gradual or discrete. Specifically, when two targets (T1 and T2) shared a visual feature, their results indicated a gradual loss of T2 precision, with the variable precision model providing a better fit to the data. In contrast, they observed a discrete loss of T2 information when participants had to switch their attention to different target features (i.e., color for T1 and orientation for T2), and in this case the mixture model performed better than the variable precision model in terms of fitting the data. While the primary objective of Sy et al. was to discern whether perception during the attentional blink is discrete or graded, it is worth noting that their results present mixed results in terms of model performance.

Despite these previous efforts to apply WM models to AB tasks, a comprehensive account of target representation during the AB has not yet emerged. In large part, this may be due to the variable outcomes, which could be due to differences in task paradigms and sample variability that have not been assessed systematically. Moreover, most comparisons among WM models have primarily focused on the standard mixture and variable precision models, potentially overlooking other relevant components which could affect WM representations. For example, the influence of non-target items proposed by the ensemble integration model (Brady & Alvarez, 2011) may be relevant in the context of the AB. This hypothesis is supported by Akyürek and Hommel (2005; Akyürek et al., 2012), who discovered that temporal integration occurs with successive targets in RSVP. This suggests that representational errors during the blink may also reflect interactions with temporally adjacent items in the stream.

Against these open questions, the current study examines how WM representations are shaped under temporal constraints, by applying a broader set of WM models to continuous report data gathered from multiple AB tasks. We start by selecting seven commonly used visual WM models: the standard mixture model, the slot model, the slots plus resource model, the swap model, the ensemble integration model, and two versions of the variable precision model. These models fundamentally diverge in how they interpret memory errors in the continuous reproduction task. We also considered the target confusability competition model (Schurgin et al., 2020), due to its new perspective on modeling working memory representations, but it was ultimately excluded from our analysis. The target confusability competition model quantifies psychophysical similarity within a given feature space (e.g., color), elucidating how familiarity propagates within that specific stimulus field. However, we found that it produced unstable fits across features under RSVP timing depending on the specific feature, likely due to psychophysical similarity functions inadequately estimated under RSVP. To ensure the generalizability and robustness of our results, we analyzed continuous report

data from three previously conducted AB studies by distinct research groups (Asplund et al., 2014; Karabay et al., 2022; Tang et al., 2020), together with data from a new experiment we have undertaken ourselves.

2. Method

2.1. Model Details

Slot model family: Models with limited number of WM slots.

The family of slot models, including the standard mixture, slot and slots plus resource models is built upon the core assumption that WM consists of a limited number of discrete slots for storing visual representations (Cowan, 2001; Luck & Vogel, 1997). If the target object has been stored in one of these slots, its information is maintained in WM. In contrast, if the item has not been stored in any of these slots, then no information about it remains in WM.

Standard mixture model (StM). The StM model (Zhang & Luck, 2008) proposes a mixture distribution for responses. When items are successfully stored into WM, the corresponding response values tend to cluster around the actual value, thereby forming a Von Mises distribution. Conversely, when item information is not available in WM, the reported values are expected to be random, conforming to a uniform distribution. The probability of this guessing is denoted by the height of this uniform distribution. Taken together, the response error distribution in the StM model is given by:

$$p(x|s, g, sd) = (1 - g)VM\big(x - s; 0, k(sd)\big) + g\frac{1}{2\pi},$$

where x is the reported value, s is the target value. The model parameter g, or the guess rate, indicates the proportion of trials where subjects are presumed to make random guesses. The von Mises distribution is expressed as:

$$VM(x - s; 0, \kappa) = \frac{1}{2\pi I_0(\kappa)} e^{(\kappa \cos(x-s))}.$$

In this formula, κ, the concentration parameter of the Von Mises distribution, signifies the precision of memory representations. It is analogous to the standard deviation sd in the normal distribution. $I_0(\kappa)$ is the modified Bessel function of the first kind of order 0, which ensures that the total probability density integrates to 1.

Slot model. The Slot model (Cowan, 2001; Luck & Vogel, 1997), which serves as the classic representation of this family, posits that there is a fixed number of storage slots in WM. When the number of items to be remembered, known as the set size, exceeds the maximum number of available slots, any excess items are disregarded. Consequently, in the Slot model, the guess rate (g) is correlated with the maximum number of slots. The response error distribution is formally given by:

$$p(x|s, g, sd) = (1 - g)VM\big(x - s; 0, \kappa(sd)\big) + g\frac{1}{2\pi},$$

The guess rate g depends on the model parameter, capacity (K), according to the following relationship. When $K \geq N$ (set size), all items can be remembered, and the guess rate would equal zero. When $K < N$:

$$g = 1 - \frac{K}{N}.$$

Slots plus resource model (SR). The SR model (Awh et al., 2007; Zhang & Luck, 2008), like previous models, hypothesized a fixed, finite capacity of WM wherein a certain number of items can be stored. What distinguishes the SR model is its unique approach to WM resource allocation. Specifically, most WM resources are preferentially assigned to a probed item, with only a minimal amount for other items that are considered less relevant. The SR model proposes that when the number of items is fewer than the slots available, the surplus resources improve the precision of the stored items. In such instances, we anticipate significant variance in the precision (standard deviation, sd) of WM, depending on the set size. Formally, the response error distribution is given by:

$$p(x|s, g, sd) = (1 - g)VM\big(x - s; 0, \kappa(sd)\big) + g\frac{1}{2\pi}.$$

Here, the sd is extrapolated using the SR model's parameters, bestSD and the number of probed items n, as follows:

$$sd = \text{bestSD} \times \text{sqrt}(n),$$

where bestSD denotes the precision when all WM resources are used for storing a single item, and n is the number of items that can be stored in WM, depending on the capacity K and set size N:

$$n = \min(\text{capacity } K, \text{set size } N).$$

The guess rate is linked to the capacity K in the same way as in the Slot model.

It should be noted that the key difference between the StM model and the other two slot models (the Slot and SR models) is that the latter explicitly proposes hypotheses about the effect of set size on error distribution. In the AB paradigm, the set size is typically considered to be 2, which may result in similar performance across these models due to the consistent set size. However, we also consider the condition where T1 is incorrectly reported (see **Section 2.4**, Data Preparation, for a detailed explanation). We expect that this condition will reveal differences in the models' performance as the set size changes.

The variable precision models: Models that assume WM consists of a resource pool.

The variable precision models (Fougnie et al., 2012; van den Berg et al., 2012) propose that WM resources are allocated to items in a continuous and variable manner, which causes the precision of WM representation to vary across items and trials. Although the variable precision models and the SR model both

suggest that WM is not (entirely) quantized, there are two primary distinctions between them. First, the variable precision models define WM limitations by the quality of the representation, as opposed to the number of items memorized. This is in contrast to the SR model, which puts emphasis on the item count. Second, the variable precision models imply a variability of WM resources across trials and items. The SR model, in contrast, implies an equal level of precision across all items and trials, when the set size is fixed.

Variable precision model (VP). In the VP model proposed by van den Berg et al. (2012), item information does not undergo a total loss. Instead, the quality of the item representation may severely degrade, resulting in extremely low precision. Therefore, the response error distribution is given by:

$$p(x|s, J) = VM(x - s; 0, \kappa(J)).$$

Here, each item is encoded with precision J , which is defined as the Fisher information. The concentration parameter κ is related to J through the following relationship:

$$\mathrm{J} = \kappa \frac{\mathrm{I}_1(\kappa)}{\mathrm{I}_0(\kappa)},$$

where I_0 represents the modified Bessel function of order zero and I_1 represents the modified Bessel function of order one.

The core hypothesis in the VP model is that the precision J varies independently across items and trials. Furthermore, the precision J itself follows a specific distribution as a random variable. Van den Berg et al. (2012) further assume this specific distribution of precision J to be Gamma with mean precision $\bar{J}$ and scale parameter τ:

$$p(J|\bar{J};\tau) = Gamma(J|\bar{J};\tau).$$

Therefore, the response error distribution of the VP model is a mixture of an infinite set of Von Mises distributions:

$$p(x|s;\bar{J},\tau) = \int VM((x - s; 0, \kappa(J))Gamma(J|\bar{J};\tau)\, dJ.$$

Variable precision model with guess rate (VPG). In the current study, we also employed another version of the VP model with an extra *guess rate* parameter (Fougnie et al., 2012). Mathematically, the response distribution is then given by:

$$p(x|s, g, mo, sd) = (1 - g) \int VM((x - s; 0, \kappa(J))Gamma(J|mo; sd)\, dJ + g\frac{1}{2\pi}.$$

Thus, the VPG model has three free parameters: guess rate (g), the mode (mo) and the standard deviation (sd) of the Gamma distribution of precision J.

Interference models: Models that assume there are interaction between items.

Ensemble integration model (EnsInt). The aforementioned models suggest that each item is stored in WM independently, which implies there is no

interaction between these items. However, Brady and Alvarez (2011) demonstrated that the representation in WM is not only affected by the item itself, but also by the integration of information of all the stimuli that are displayed. Their results showed that the reported size of a target item was shifted toward the mean size of the items with the same color, as well as the mean size of all items displayed. The EnsInt model implemented in the current study is a simplified version of the Brady & Alvarez (2011) model, which introduces a parameter that represents the bias towards the mean value of all distractors. Since the first target is the only other relevant item in typical continuous-report AB tasks, we used T1's value for this parameter, slightly simplifying the model. Formally, the error distribution of the EnsInt model is given by:

$$p(x|\mu_s, g, sd) = (1-g)VM\big(x-\mu_s; 0, \kappa(sd)\big) + g\frac{1}{2\pi},$$

where μ_s refers to the biased mean value, which is estimated based on the differences between the target (T2) and the other item (T1).

Swap model. This model can be considered as an extension of the StM model. In addition to the two components of the response error distribution, namely a uniform distribution that indicates the proportion of random-guessing trials and a Von Mises distribution that represents the memory precision, Bays et al. (2009) introduced a third source of error: The probability of incorrectly reporting non-target items. Consequently, the Swap model has a three-component structure, including precision, guess rate, and swap rate (estimated by the measurement of the distance between reported values and non-target items):

$$p(x|s, g, sd, \beta) = (1-g-\beta)VM\big(x-s; 0, \kappa(sd)\big)$$
$$+\beta\frac{1}{m}\sum_i^m VM(x-\theta_i; 0, \kappa(sd)) + g\frac{1}{2\pi},$$

where β, the swap rate, denotes the probability of incorrectly reporting the non-target items (distractors, i.e., T1) and where $\{\theta_1, \theta_2, \ldots\theta_m\}$ are the values of a set of m distractors.

2.2. Datasets

As summarized in Table 1, we obtained three existing datasets from three separate laboratories (Asplund et al., 2014; Karabay et al., 2022; Tang et al., 2020), and added a fourth, new dataset in the present paper (Wang et al.).

Asplund et al. (2014). The first dataset was obtained from Experiment 1 in Asplund et al. (2014), where square-shaped targets were embedded in circle-shaped colored distractors. T1 was filled with either black or white, while the T2 color was randomly chosen from 180 equiluminant colors. T2 appeared at the first, second, fourth, or eighth position (labeled as Lag 1, Lag 2, Lag 4, and Lag 8) following T1. The stimulus duration for each participant was set by a staircase method and resulted in an average value of 150 ms (*SD* = 10 ms). At the end of the

stimulus stream, participants were asked to reproduce T2 using a color wheel, and to report whether the first target was black or white.

Tang et al. (2020). The second dataset was retrieved from two behavioral experiments in the AB study by Tang et al. (2020), where a RSVP task was again employed. Specifically, there were 20 Gabor patches, and the orientation of the Gabors were integer angles ranging from 0 to 179 degrees, without replacement. Participants were instructed to memorize two targets (high-frequency Gabors) among distractors (low-frequency Gabors) and reproduce them at the end of each trial. Each target or distractor appeared for 40 ms, and the next item followed after a blank interval of 80 ms. The time interval between two targets was manipulated by presenting different numbers of distractors in-between (lag). In Experiment 1, there were five lag conditions (1, 2, 3, 5, 7), while in Experiment 2, there were two lag conditions (3, 7).

Karabay et al. (2022). Karabay et al. (2022) used two different paradigms, dwell time (DT) and RSVP, both with continuous report tasks, to examine the nature of awareness in the AB. We acquired seven datasets from their experiments. Experiment 1A, 1B, 2A, and 2B were run with the DT paradigm. Both targets were orientation gratings (in Experiment 1A and 1B) or colors (in Experiment 2A and 2B). T1 and a distractor were presented, at the same time, above or below the fixation dot, at an equal distance. The display of T2 was the same as T1, except the location changed to the left or right side of the fixation dot. On each trial, T1 and T2 target arrays were followed by a mask. The stimulus-onset asynchrony (SOA) between T1 and T2 was set to 250 ms and 800 ms. The RSVP paradigm was used in Experiment 3, 4, and 5, in which the targets were always orientation gratings. The number of distractor items between two targets was 2 (Lag 3, 300 ms SOA) or 7 (Lag 8, 800 ms SOA). In Experiment 3, the two targets appeared among a stream of distractors, similar to the design in Tang et al. (2020). In Experiment 4, there were simultaneously two streams of stimuli at the left and right sides of the fixation dot. In Experiment 5, T1 was presented within a single stream of distractors, but split into a dual stream with the presentation of T2, as in Experiment 4.

Table 1

Details of the data sets.

Datasets	Exp	SOA (ms)	Lag	T1 feature	T2 feature	subject number
Asplund et al., 2014	Exp 1	NA	1, 2, 4, 8	Categorical	Color (1°-360°)	25[1]
Tang et al., 2020	Exp 1	50, 240, 360, 600, 720	1, 2, 3, 5, 7	Orient. (1°-180°)	Orient. (1°-180°)	22
	Exp 2	360, 720	3, 7	Orient. (1°-180°)	Orient. (1°-180°)	23
Karabay et al., 2022	Exp 1A	250, 800	NA	Orient. (1°-180°)	Orient. (1°-180°)	23
	Exp 1B	250, 800	NA	Orient. (1°-180°)	Orient. (1°-180°)	21
	Exp 2A	250, 800	NA	Color (1°-360°)	Color (1°-360°)	26
	Exp 2B	250, 800	NA	Color (1°-360°)	Color (1°-360°)	27
	Exp 3	300, 800	3, 8	Orient. (1°-180°)	Orient. (1°-180°)	24
	Exp 4	300, 800	3, 8	Orient. (1°-180°)	Orient. (1°-180°)	24
	Exp 5	300, 800	3, 8	Orient. (1°-180°)	Orient. (1°-180°)	23
Wang et al. data	Exp 1	90, 300, 800	1, 3, 8	Orient. (1°-180°) or Color (1°-180°)	Orient. (1°-180°) or Color (1°-180°)	28

Note. Exp = Experiment; Orient. = Orientation; Wang et al. data refers to the new dataset collected in the present study.

2.3. Wang et al. data

In the new experiment, we manipulated feature-dimension changes between targets in the AB task (same or different), hypothesizing that matching target feature-dimensions might cause mutual bias in target reports, which might affect the model selection. Like the other studies, this experiment also featured continuous report of targets.

2.3.1. Participants

The minimum sample size of 24 subjects was determined by means of a G-power analysis (Faul et al., 2007), with the following parameters: significance level (α = .05), beta-level (β = .2), and a medium to large effect size (Cohen's dz = .6). Twenty-eight undergraduate students (seventeen females and eleven males) from the University of Groningen were recruited in exchange for course credits (mean age = 19.6, range = 18-27). All participants reported normal or corrected-to-normal

[1] Three subjects were removed from the original data set due to a lack of trials in the T1 incorrect condition. For consistency, we also excluded these subjects from all analyses of Asplund et al.'s data.

visual acuity and no color blindness. Informed consent forms and instructions were given to the participants prior to participation. Prior to its execution, ethical approval was obtained from the ethical committee of the Psychology Department of the University of Groningen (Approval code PSY-1819-S-0209). The study was conducted in accordance with the Declaration of Helsinki (2008).

2.3.2. Apparatus and stimuli

Participants were individually seated on a desk chair in sound-attenuated lab chambers, at a viewing distance of approximately 60cm from a 22" CRT monitor (Iiyama MA203DT). The screen was set at a 1280 x 1024-pixel resolution, 16-bit color depth, and a 100Hz refresh rate. The trials were prepared and run in OpenSesame 3.2 (Mathôt et al., 2012) with the PsychoPy back-end (Peirce, 2007; 2009), under the Microsoft Windows 7 operating system. All the stimuli were displayed in the center of the screen on a grey background (RGB: 128,128,128), as shown in Figure 1A. There were two kinds of target stimuli in the RSVP stream (Figure 1B). The first kind of target consisted of orientation gratings with a spatial frequency of 1.8 cycles/degree of visual angle, presented within a circle of 2.2° of visual angle. The orientation of the gratings was chosen randomly from the range of 0°-179°. The other kind of target consisted of circles (2.2° of visual angle) filled with one of 360 colors, which were chosen randomly from the HSL color spectrum. The distractors were grey-scale mosaic images (2.2° × 2.2° of visual angle), retrieved from Karabay et al. (2022).

2.3.3. Procedure

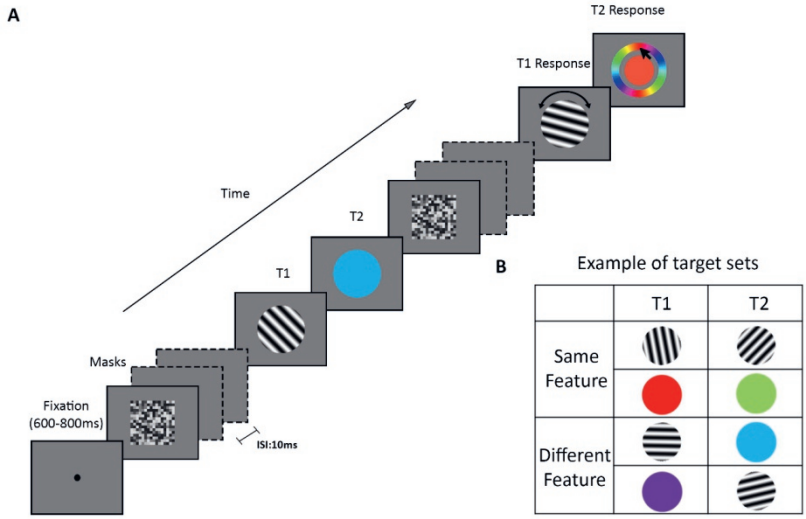
A 2 (Target feature-dimension: same or different) x 3 (Lag: 1, 3, 8) factorial design was implemented in this experiment. Two practice blocks, each including 16 trials, were administered at the beginning, which were excluded from the analysis. After that, there were 540 experimental trials evenly distributed into 15 blocks. Each trial started with a fixation dot that randomly lasted for 600-800ms. There were 18 items within the RSVP stream. Each item was shown for 80 ms, separated by a 10 ms inter-stimulus interval (ISI). T1 was randomly presented at the fifth, sixth, or seventh position of the stream. T2 was presented consecutively (Lag 1), after two items (Lag 3), or after seven items (Lag 8), following T1. T1 and T2 could have either the same feature-dimension (color or orientation), or different feature-dimensions. At the end of the stream, after a blank interval of 500ms, two response prompts were displayed successively.

Participants were asked to reproduce the two targets in the correct order. They were asked to reproduce the target orientation by rotating a probe grating, or to reproduce the target color by choosing the exact color from a color wheel. Responses were collected with a standard mouse. Trial-based feedback was

provided only in practice trials: A happy smiley was shown for correct trials, and an unhappy smiley for incorrect trials. Responses close to target values (below 22.5° reproduction error) were considered correct responses for feedback. In the experimental blocks, the average performance on T1 and T2 were displayed at the end of each block. During the experiment, participants could have a self-paced break between blocks. The whole session took about 90 minutes to complete.

Figure 1

Illustration of the design of the newly conducted experiment.



Note. **(A)** An example trial of the dual-target RSVP task at Lag 3. In this instance, the two targets have different feature-dimensions. **(B)** Examples of possible targets in all combinations and orders of the two targets.

2.4. Data Preparation

As indicated, all the data sets we gathered for analysis were obtained from continuous-report AB tasks. We reorganized the datasets to form a uniform structure, as per the following procedure:

1. For each trial, response error for each target (T1 and T2) was calculated by subtracting the response value from the actual one.

2. To avoid cases of trivial near- identity and ambiguous swap/integration, trials in which the absolute deviations between T1 and T2 values were less than 22.5 degrees were discarded.

3. Response errors were limited to a range from -90° to 90° for orientations and from -180 to 180 for colors.

4. Performance of T2 was evaluated in two distinct conditions:

a. T1 correct Condition (T2|T1) – This condition is often employed in AB studies. In this condition, we included only the trials in which the absolute error of T1 was less than or equal to 22.5 degrees for orientations (45 degrees for colors).

b. T1 incorrect condition – This condition included the trials in which the absolute error of T1 exceeded 22.5 degrees for orientations (45 degrees for colors). This condition served as a proxy for reduced effective load, but since it is not fully equivalent to a true single- item set size, our conclusions using this proxy are bracketed accordingly.

Given that the set size remained constant across all our data sets, we took into account that some models (e.g., the SR model) incorporate set size for parameter estimation. Hence, we also analyzed T2 performance when T1 was reported incorrectly, as this represents a scenario where the set size equals one. Although this condition does not strictly correspond to a true single set size condition, it does provide a valuable approximation of model performance when the memory load is set to one, while the typical T2|T1 performance analysis evaluates the models' performance when the memory load is two.

2.5. Model fitting

We employed maximum likelihood estimation (MLE) as our chosen approach to fit all of the aforementioned models to our data sets. The general logic of MLE is to maximize the likelihood function to find the specific parameter value, with which the chosen probabilistic model is most "likely" to generate the observed data. Specifically, for each subject and condition within a single experiment, we carried out model fitting using the built-in MLE function in MemToolbox (Suchow et al., 2013). This allows us to obtain the best estimates of the model parameters at the individual level (See Supplementary Materials A for details of parameter estimates).

2.6. Model comparison

In terms of model comparison and selection, it is important to strike a balance between model flexibility and overfitting. Although flexible models can accommodate a wide range of datasets by introducing additional parameters, they may lack supporting evidence and can lead to overfitting (Ziegel, 2003). To assess the fitness of the models and determine the best model for describing our data, we used the Akaike Information Criterion (AIC; Akaike, 1974) as a common penalized model comparison measure.

The AIC values were calculated based on the natural logarithm of the likelihood function, also known as the log-likelihood. Specifically, the AIC was calculated using the formula:

$$AIC = 2k - 2\ln L,$$

where k represents the number of parameters, and L denotes the maximized value of the likelihood function. At the individual level, we obtained the AIC values using the model comparison function implemented in MemToolbox (Suchow et al., 2013; memtoolbox.org). Lower AIC values indicate a better fit of the model to the data. By subtracting the lowest AIC value (corresponding to the most likely model for each subject) from the AIC values of other models, we obtained the relative AIC values at the subject level.

Additionally, to extend our analysis to the group level, we investigated the model performance against group data. In detail, we first averaged the relative AIC values across all subjects for each experimental condition (e.g., lag). Second, we ranked the models according to their AIC values for each subject and presented the average rankings across all subjects, separately for each condition. This allowed us to gain insights into the overall model performance and make meaningful comparisons among the models within each condition.

2.7. Simulation analysis

Although the AIC indicates how well a model fits the experimental data compared to other models, it does not provide a comprehensive assessment of each model's absolute performance. To gain a more detailed understanding of how well each model captures different aspects of the data, we conducted a simulation analysis. This involved generating simulated data sets from these assessed models and comparing the model predictions to the actual T2 errors in the observed data.

To perform the simulations, we utilized the most probable parameter values from the model fitting procedure described earlier (See 2.5. Model fitting). These parameters were applied to their respective models for each subject and each condition. We then generated simulated datasets with the same number of data points as those collected from each subject in the corresponding condition. Subsequently, we calculated the summary statistics of T2 errors separately for the simulated data, and the actual data gathered from different studies. This simulation procedure was implemented with a custom-made function in MATLAB, based on the SampleFromModel function in Memtoolbox.

3. Results

3.1. Asplund et al. (2014)

3.1.1. Model comparison

Figures 2 and 3 present the model comparison analysis for the Asplund et al. (2014) data. Since Asplund et al.'s data consisted of entirely different T1 and T2

stimulus, the EnsInt model and the Swap model were excluded as they both need a third parameter for the similarity of two targets that was absent here.

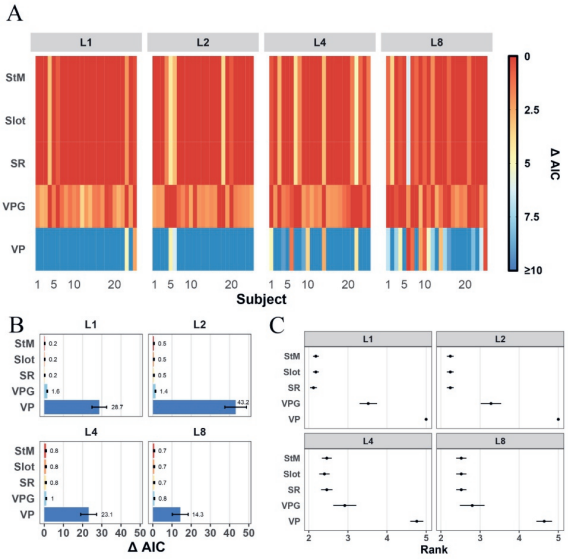
Figure 2 shows the results of the T1 correct condition, that is, T2|T1 performance. At the individual level (Figure 2A), the StM, Slot, and SR models consistently exhibited the best fit across most subjects' data. In terms of the VP model, it consistently showed the poorest performance across almost all subjects, particularly at Lag 1 and 22. Interestingly, the VPG model fitted better than the VP model. As the lag increased, the performance of the StM, Slot, and SR models declined for some subjects, while the performance of the VPG model improved.

To further assess model performance at the group level, we summarized the individual model fitness values in several ways. First, we calculated the AIC values relative to the best-performing model and then derived their average values across all subjects for each lag (as illustrated in Figure 2B). All models performed commendably across all lags, except for the VP model, which exhibited smaller relative AIC values as the lag increased. Next, we ranked the models for each subject based on their AIC values and averaged these ranks over all subjects for each lag (Figure 2C). This pattern closely mirrored the model performance depicted in Figure 2B. The StM, Slot, and SR models consistently achieved the lowest ranks (and thus, superior) across all lags. The VPG model, while ranking higher (thus poorer) at Lag 1 and 2, improved its performance at longer lags (Lag 4 and 8). This is consistent with the model comparison results of the VPG model at the individual level, with more subjects getting lower AICs when lag increased. Moreover, the consistency of the general model performance across different lags indicated that the AB itself (in particular at Lag 2) did not change the shape of the response error distributions, compared to other lags.

[2] To verify the robustness of the fitting procedure, we conducted grid searches for the two VP parameters over wide ranges. Grid searches were performed on both the orientation and color datasets. Across all datasets, the best parameters from grid searches consistently fell at the lower boundary for the mode precision and showed very small values for the sd precision. This pattern closely aligned with the estimates obtained from MLE, indicating that the VP model's poor performance is not due to optimization failure (e.g., the fitting procedure got stuck in a local minimum). Moreover, the model comparison results showed that the VPG model achieved better fits, which also suggest that the VP model's poor performance reflects a mismatch between its predictions and the empirical data, rather than a parameter estimation issue.

Figure 2

Model comparison for T2 performance when T1 was correct (T2|T1).

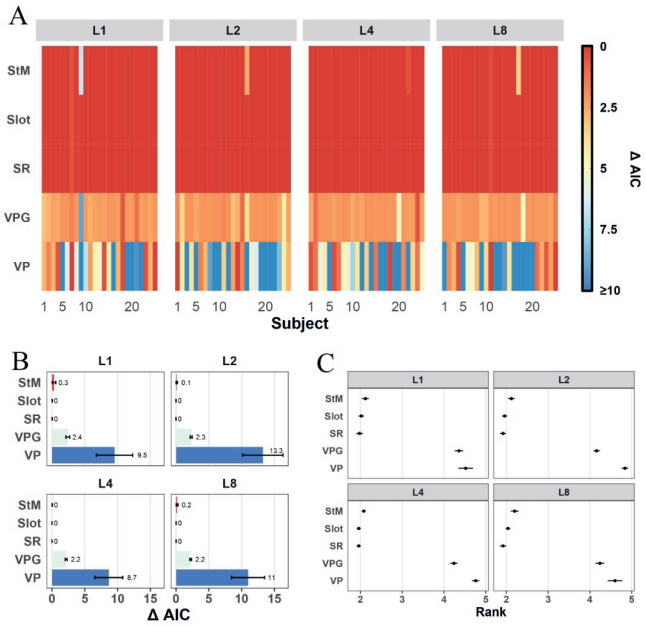


Note. (**A**) Model comparison results at the subject level, using the data from Asplund et al. (2014). Each column represents a subject, and each row represents a specific model. Each panel represents a lag condition. L1 = Lag 1; L2 = Lag 2; L4 = Lag 4; L8 = Lag 8. Cell color indicates each model's relative AIC value. Larger relative AIC values mean worse performance. (**B**) Relative AIC values compared to that of the best-performing model, averaged across all subjects. Error bars indicate standard error. (**C**) Model ranking. The ranks were obtained by averaging the per-subject ranks for each specific lag. Larger ranks mean worse performance. The model abbreviations are mentioned in the Method (see *2.1. Model details*).

Figure 3 presents the results of model comparison for T2 performance in the T1 incorrect condition. The model comparison pattern bears a resemblance to that in the T1 correct condition, observable at both individual and group levels. Having superior performance across all lags were the StM, Slot, and SR models. In contrast, the VP model consistently demonstrated poor performance.

Figure 3

Model comparison for T2 performance when T1 was incorrect.



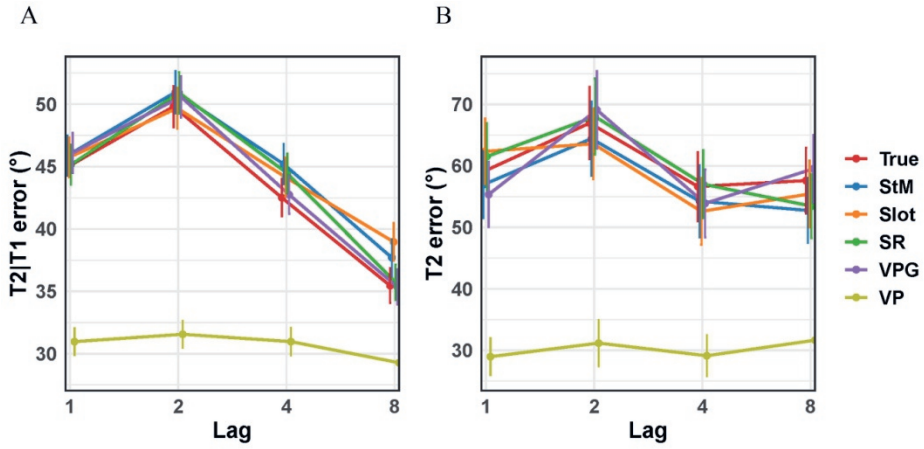
Note. (**A**) Model comparison results at the subject level, using the data from Asplund et al. (2014). (**B**) Relative AIC values, averaged across all subjects for each lag. (**C**) Model ranking at the group level. Figure conventions follow Figure 2.

3.1.2. Simulation analysis

We compared experimentally observed and simulated T2 accuracy for each respective lag. Figure 4 displays the average T2 accuracy across all subjects in both T1 correct and incorrect conditions. Of particular interest was the response error of the second target when the time interval between the first and second target fell between 200 – 500 ms (primarily at Lag 2), to get an idea if these models can actually describe the data well within the AB window. In general, the pattern of the simulated data was more or less similar to that of the actual data, except for the simulated data obtained from the VP model. The VP model had difficulty in mimicking a 'blink' shape in the error, presenting relatively similar T2|T1 errors across lags and generally lower values compared to the actual data and other model simulations In terms of T2 performance when T1 was incorrect, there was still a large divergence between the simulated data of the VP model and the actual data.

Figure 4

Comparison of model simulations and experimental data based on T2 accuracy.



Note. Model simulation results using the data from Asplund et al. (2014). (**A**) Average T2 errors in the T1 correct condition. (**B**) Average T2 errors in the T1 incorrect condition. True = experimentally observed data.

3.2. Tang et al. (2020)

3.2.1. Model comparison3

Figure 5 depicts the model comparison results for T2|T1 performance. At the individual level, the StM, Slot and SR models performed almost identical (Figure 5A). At Lag 1, 2 and 3, these three models showed a good fitness for some individuals, while they behaved poorly for the others (ΔAICs ≥ 16). As lag increased, model performance was improved, and the number of bad individual fits decreased. However, it can clearly be seen that the Swap model consistently showed excellent, if not best, fitness across all subjects and persistently at all lags. It is also worth noting that the number of participants for which the Swap model was the winning one dropped as a function of lag. At Lag 1, 2, and 3, the EnsInt model was the best model for a subset of subjects. The extent of preference for the EnsInt model decreased at Lag 5 and 7, where the EnsInt model showed a relatively consistent and moderate performance across all subjects. The VPG model's performance was only better than its variant, the VP model, for some subjects at short lags (Lag 1, 2, and 3). However, at long lags (Lag 5 and 7), its performance was improved for most subjects. In contrast, the VP model was always the worst fitting one for all subjects

[3] For the data from Tang et al. (2022), we also conducted further analysis of the Ensemble Integration and Swap models, to investigate the potential interactions between T2 and its subsequent item of T2. Those analyses are presented in the Supplementary Materials (see Supplementary Materials B)

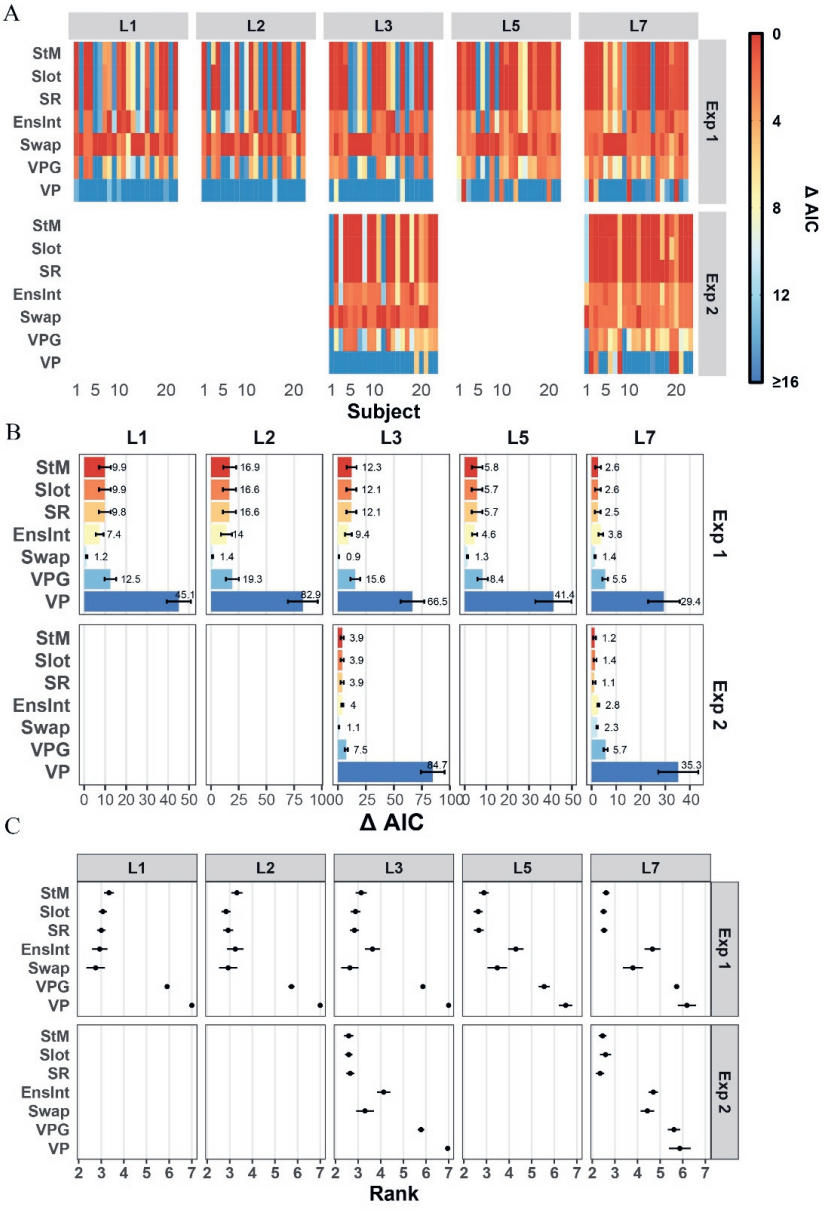
at all lags, except for some individuals at Lag 5 and 7. In Experiment 2, there were two lag conditions (Lag 3 and Lag 7). The results presented a similar pattern to Experiment 1 with regard to lag. It was noteworthy that the Swap model was again the winning model for a subset of subjects at Lag 3, but only for two subjects at Lag 7. The swap model's superiority at Lag 1–3 and decline at Lag 5–7 is consistent with the occurrence of temporal integration / order reversals at short lags, and reduced nontarget-influence at longer lags.

The averaged relative AIC values (as displayed in Figure 5B) indicated a lag-dependent change in the models' fitness. During Experiment 1, the StM, Slot, SR and EnsInt models reached their peak relative AIC values at Lag 2, followed by a decrease at Lag 5 and 7. The VP and VPG models exhibited a similar pattern. Remarkably, the Swap model consistently registered the smallest ΔAIC values at all lags, maintaining a value of less than 2 points. This finding is coherent with existing AB theories such as the eSTST (Bowman & Wyble, 2007; Wyble et al., 2009), and with the notion of temporal integration (Akyürek & Hommel, 2005). These suggest that targets are bound to same episodic event if they are successively shown, possibly when the second target is processed (tokenized) more quickly than the first one. Then, timestamps of the targets might be confused, which causes T2 to be reported as T1 and vice versa. For Experiment 2, the Swap model recorded the lowest mean ΔAIC at Lag 3 (1.1), but a slightly higher value (2.3) at Lag 7, at which the StM, Slot and SR models took over the leading positions. Generally, the comparison results from Experiment 2 displayed a similar pattern to that observed in Experiment 1.

The average model ranking at the group level is shown in Figure 5C. For Experiment 1, at Lag 1, 2 and 3, the StM, Slot, SR, EnsInt and Swap models dominated the top ranks with minimal divergence between them. At Lag 5 and 7, however, the EnsInt and Swap models experienced an increase in ranks (indicating poorer performance) compared to the leading models (the StM, Slot and SR). The VP and VPG models, on the other hand, consistently ranked last. What stood out in this comparison was the differences in rank across different lags for the EnsInt and Swap models in Experiment 1, a feature not observed in the other models. In Experiment 2, the StM, Slot and SR models achieved the smallest ranks (thus, superior performance) at both Lag 3 and 7.

Figure 5

Model comparison for T2 performance when T1 was correct (T2|T1).

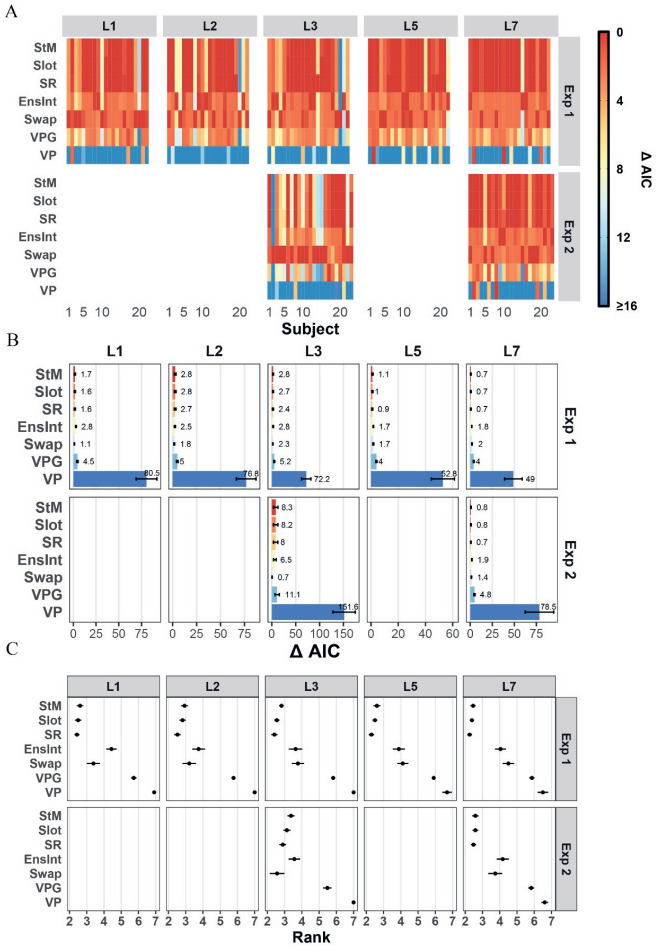


Note. (**A**) Model comparison at the subject level, using the data from Tang et al. (2020). L1 = Lag 1; L2 = Lag 2; L3 = Lag 3; L5 = Lag 5; L7 = Lag7. Exp = Experiment. (**B**) Relative AIC values compared to that of the best-performing model, averaged across all subjects. (**C**) Average model ranking. Figure conventions follow Figure 2.

We observed that when T1 was incorrect, the performance of the models exhibited a more uniform pattern across subjects and lags in both Experiment 1 and Experiment 2. Evidently, the VP model underperformed at both the individual and group level, whereas other models presented either good or moderate fitness. Moreover, the divergences among the top-performing models were fairly minimal.

Figure 6

Model comparison for T2 performance in the T1 incorrect condition.



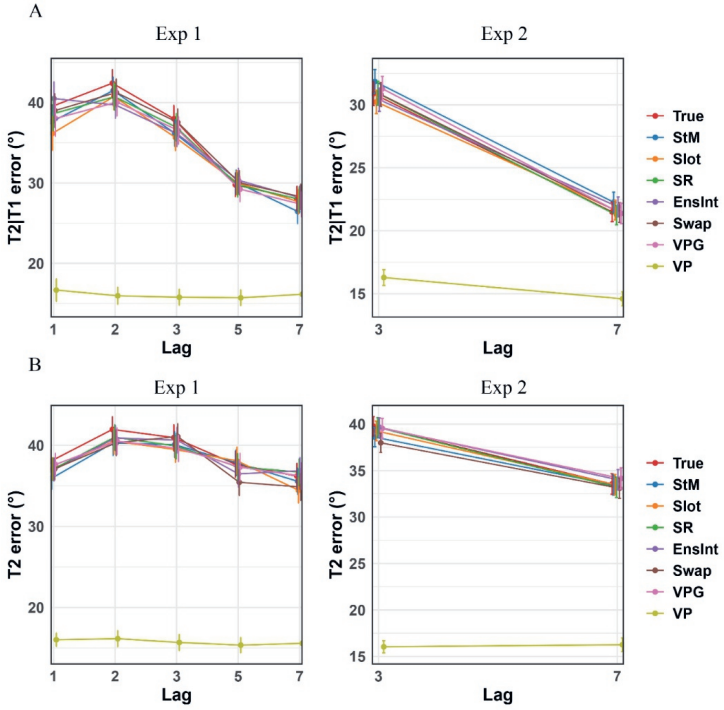
Note. (**A**) Model comparison results at the individual level, using the data from Tang et al. (2020). (**B**) Relative AIC values, averaged across all subjects for each lag and each experiment, respectively. (**C**) Average model ranking. Figure conventions follow Figures 2 and 5.

3.2.2. Simulation analysis

Figure 7 displays the summary statistics for simulated T2 errors from seven models alongside the experimentally observed T2 errors from Tang et al.'s study (2021). It is evident that there was a considerable deviation between the simulated data from the VP model and the other models, compared to the clustering of the simulated data from these latter models around the experimental T2 errors. The differences between these models (except the VP model) and the experimental data were relatively narrow. However, it's worth noting that in Experiment 1 and the T1 correct condition, the EnsInt model generated a distinct T2 response shape, with T2|T1 errors continually decreasing as lag increased (Figure 7A), while the True data set exhibited its highest T2|T1 errors at Lag2 (the AB effect). The discrepancy indicates a potential mismatch between the EnsInt model's simulation and the actual experimental T2 responses.

Figure 7

Comparison of model simulations and experimental data based on T2 accuracy.



Note. Model simulation results using the data from Tang et al. (2020). Exp = Experiment. (**A**) Average T2 errors in the T1 correct condition. (**B**) Average T2 errors in the T1 incorrect condition. True = experimentally observed data. See Method for model abbreviations.

3.3. Karabay et al. (2022)

3.3.1. Model comparison

Figure 8 presents the model comparison results for T2|T1 performance. When comparing these results across the various experiments within Karabay et al.'s (2022) study, the most apparent observation was that the models' goodness-of-fit in Experiment 2 was clearly different from those in other experiments, which was evident at both the subject and group level.

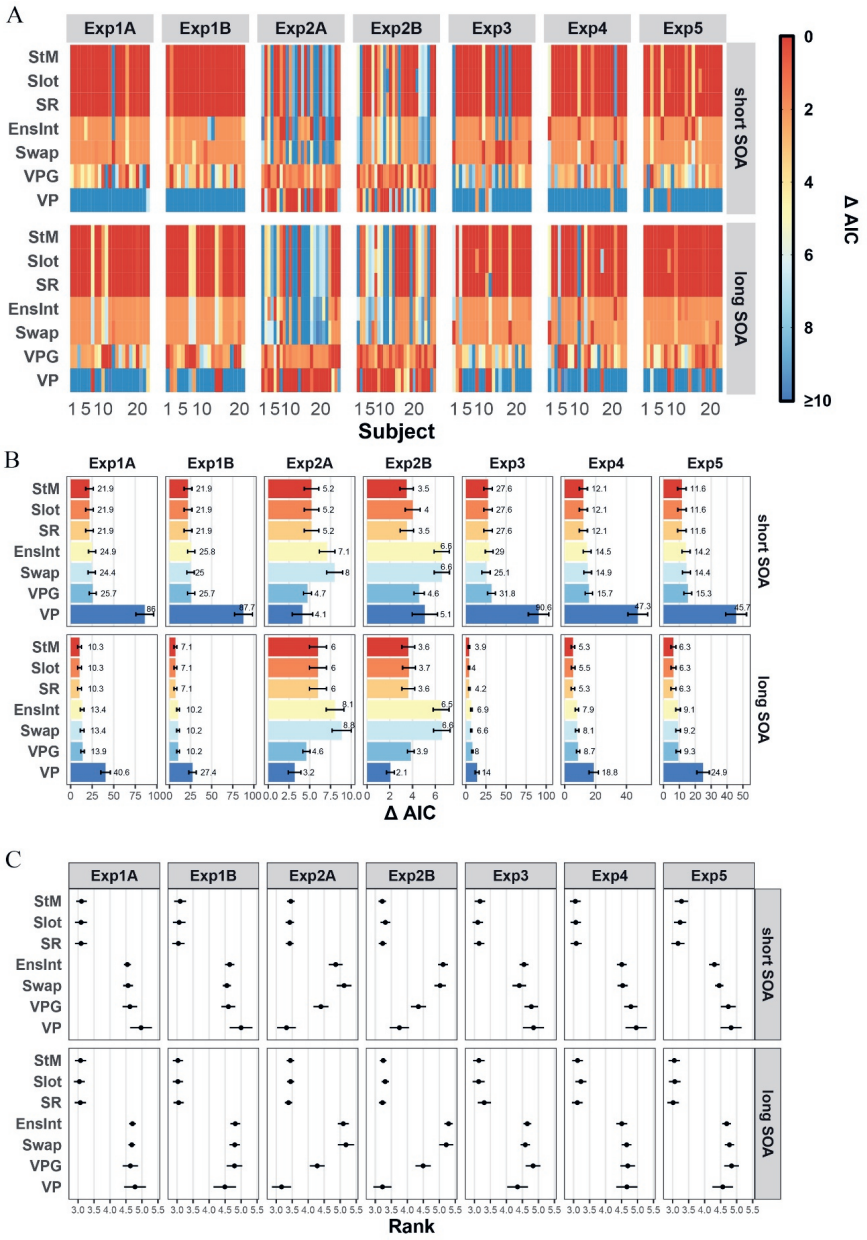
Delving into the results at the subject level, in Experiment 2A and 2B, where the targets had only a color feature, the VP and VPG models exhibited a good fit for most subjects at two distinct SOAs. Particularly at long SOA, the VP model outperformed all of its competitors for over half of the subjects. Conversely, the EnsInt and Swap models produced the least accurate data fit, maintaining either relatively higher or the highest ΔAIC values across all subjects. Intriguingly, here the StM, Slot, and SR models showed two extremes of fitness, either being the best or the worst.

In the results of the other experiments, a similar pattern of model fitness is observable. In detail, the StM, Slot, and SR models maintained the lowest ΔAIC values for the majority of subjects; the EnsInt and Swap models had relatively higher ΔAIC values. Additionally, although the VPG model's fitness was the poorest for a subset of subjects, it demonstrated a moderate performance for the others, while the VP model scored the highest ΔAIC values for a majority of individuals.

In line with the results at the subject level, the VP and VPG models showed superior fitness at the group level in Experiment 2A and 2B, compared to other experiments, as depicted in Figure 8B. Furthermore, the range of mean ΔAIC values in Experiment 2A and 2B was markedly narrower than those observed in the other experiments. In terms of the model ranking (Figure 8C), the StM, Slot and SR models consistently claimed the leading positions in all experiments, with the exception of Experiment 2A and 2B. It is also worth noting that the EnsInt and Swap models ranked last in these two experiments.

Figure 8

Model comparison for T2 performance when T1 was correct (T2|T1).

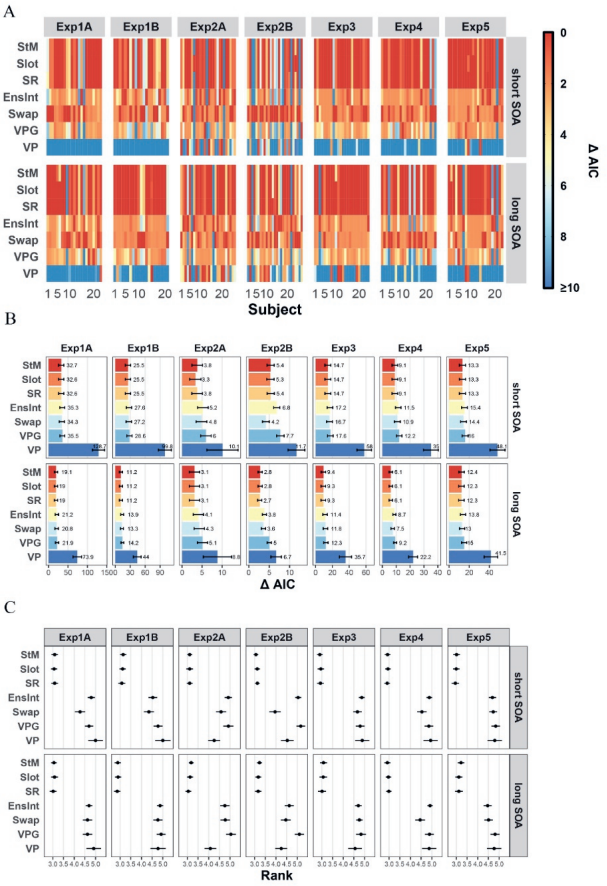


Note. (**A**) Model comparison at the subject level, using the data from Karabay et al. (2022). Exp = Experiment; SOA = stimulus onset asynchrony. (**B**) Relative AIC values compared to that of the best-performing model, averaged across all subjects. (**C**) Average model ranking. Figure conventions follow Figure 2.

Figure 9 presents the model comparison results for T2 performance when T1 was incorrect. Generally, the models demonstrated a relatively consistent performance across all subjects at the individual level. In addition to this, the pattern of model ranking, as inferred from their averaged ΔAIC values and their average ranks, mostly reflected those observed in the T1 correct condition. Yet, there were certain differences in comparison to the T1 correct condition. For example, although the VP and VPG models presented their best fit in Experiment 2A and 2B compared to other experiments, they still occupied the bottom ranks in Experiment 2A and 2B.

Figure 9

Model comparison for T2 performance when T1 was incorrect.



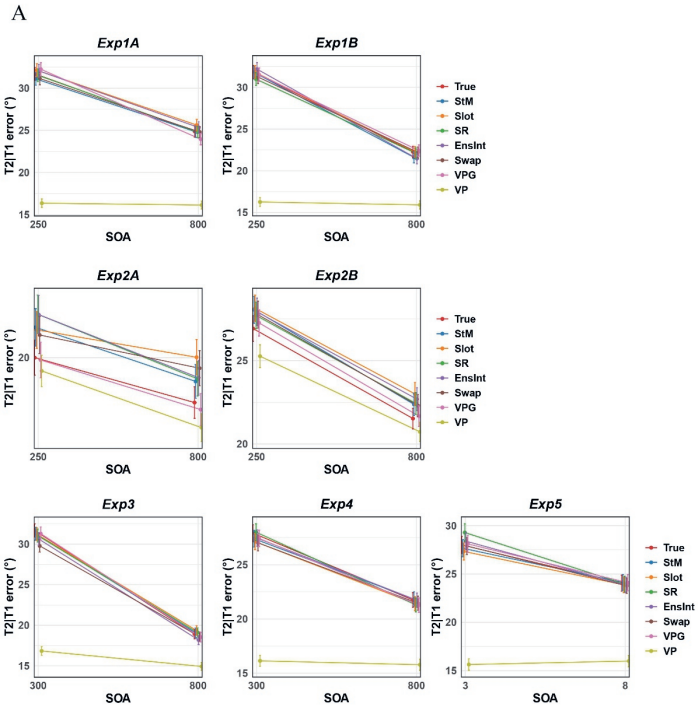
Note. (**A**) Model comparison at the subject level, using the data from Karabay et al. (2022). Exp = Experiment; SOA = stimulus onset asynchrony. (**B**) Relative AIC values compared to that of the best-performing model, averaged across all subjects. (**C**) Average model ranking. Figure conventions follow Figure 2.

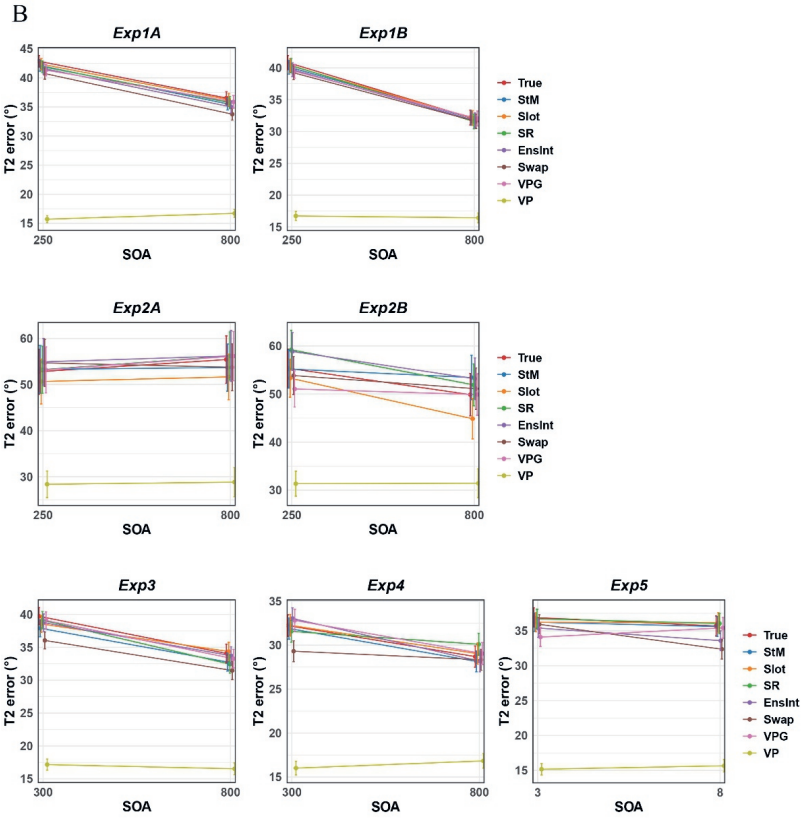
3.3.2. Model Simulation

Figure 10 shows a comparison between the experimental data and the simulated data derived from all seven models. A notable discrepancy was again observed between the VP model and the other seven models. Specifically, most of the models (except for the VP model) provided simulations that were closely aligned with the experimental T2 response errors, regardless of whether T1 was correct or incorrect. Interestingly, in the T1 correct condition (Figure 10A), when the targets were colors (in Exp2A and 2B), the VP model's pattern closely mirrored that of the other models, presenting a similar trend of T2 error across two distinct SOAs (or Lags). However, this good performance of the VP model was not observed in the T1 incorrect condition (Figure 10B).

Figure 10

Comparison of model simulations and experimental data based on T2 accuracy.





Note. Model simulation results using the data from Karabay et al. (2022). (**A**) Average T2 errors in the T1 correct condition, shown separately for each experiment. (**B**) Average T2 errors in the T1 incorrect condition. Exp = Experiment. True = experimentally observed data. See Method for model abbreviations.

3.4. Wang et al. data

3.4.1. Model comparison

In the model comparison in the T1 correct condition, a standout characteristic of Wang et al.'s data, compared to prior studies, lies in the minimal discrepancies among the candidate models (see Figure 11).

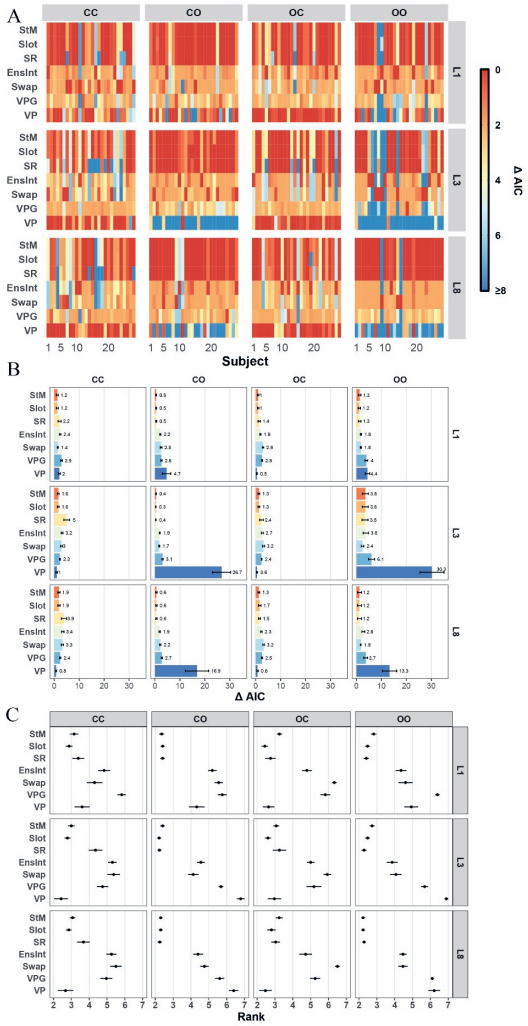
Analyzing at the subject level, we can group these models into three categories based on their performance (Figure 11A). First, the StM, Slot and SR models consistently demonstrated strong fitness across most subjects under different experimental conditions (lags and target pairs), as indicated by their comparatively lower or the lowest ΔAIC values. Notably, though, the SR model performed poorly for a subset of subjects when the color-color target pair was used.

Second, the EnsInt, Swap and VPG models obtained moderate ΔAIC values across most subjects and various conditions, while the EnsInt and Swap models even best fitted several subjects at Lag 1 and 3, when both targets were colors or orientation gratings. Lastly, the VP model exhibited superior and stable performance when the second target was a color item – evident in the color-color and orientation-color target pair conditions. However, its fitness was worse when the second target featured orientation gratings. The VP model was competitive when T2 was color-based (CC/OC), but underperformed when T2 was orientation-based (OO/CO), mirroring the feature- dependent trend.

The narrow range of mean ΔAIC values for each experimental condition (from 0 to 30; refer to Figure 11B) further underscores the slight variances among models at the subject level. The VP model obviously underperformed when the second target was an orientation grating, as indicated by its highest mean ΔAIC value. Conversely, the VP model exhibited a comparable good fitness when the second target was a colored circle. Moreover, when two targets were both colors (CC), the SR model showed worse fitness than other models by presenting a higher mean ΔAIC value across all lags. Generally, the VPG, EnsInt and Swap models exhibited relatively inferior fitting across different experimental conditions, as indicated by their higher mean ΔAIC values. The average model ranking revealed a similar performance pattern (see Figure 11C). Overall, these feature-dependent model comparison results suggest that the performance of a model is influenced by the stimulus features employed in the experiments.

Figure 11

Model comparison results for T2 performance when T1 was correct (T2|T1).



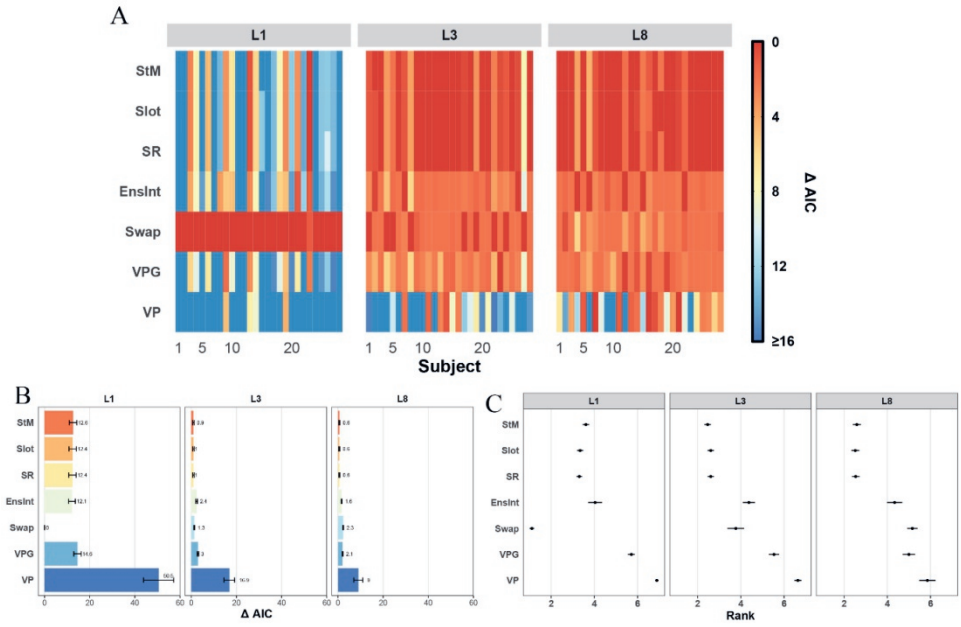
Note. **(A)** Model comparison at the subject level, using the data from Wang et al. The panels in each row present the results with the same lag but different target pairs; the panels in each column present the results with the same target pair but different lags. 'CC' means color-color target pair; 'CO' means color-orientation target pair; 'OC' means orientation-color target pair; 'OO' means orientation-orientation target pair. L1 = Lag 1; L3 = Lag 3; L8 = Lag 8. (**B**) Relative AIC values compared to that of the best-performing model, averaged across all subjects within each condition. (**C**) Average model ranking. Figure conventions follow Figure 2.

Figure 12 illustrates the assessment of these models' fit to T2 data when T1 was incorrect. Because there were insufficient trials for each combination of lag and

target pair, we confined our investigation to T2 performance at each lag. Thereby we can still provide an overview of the models' performance in scenarios where only one item was successfully memorized into working memory. The overall pattern was similar to that seen when T1 was correct. For example, the VP model underperformed compared to the others. Notably, while the Swap model demonstrated superior fitness at Lag 1, these results must be interpreted with caution, due to the combined inclusion of both same- and different-feature target pairs.

Figure 12

Model comparison results for T2 performance when T1 was incorrect.



Note. (**A**) Model comparison at the subject level, using the data from Wang et al. L1 = Lag 1; L3 = Lag 3; L8 = Lag 8. (**B**) Relative AIC values compared to that of the best-performing model, averaged across all subjects at each specific lag. (**C**) Average model ranking at each lag. Figure conventions follow Figure 2.

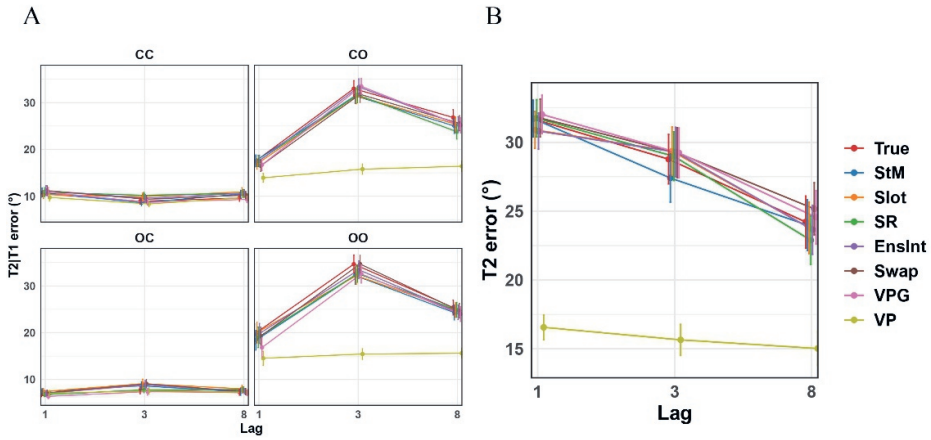
3.4.2. Model Simulation

The results of simulation analysis for the Wang et al. data are depicted in Figure 12. For the T1 correct condition (as shown in Figure 12A), the VPG model did not accurately represent the increased T2 error at Lag 3 when the second target was an orientation grating. Yet, when the second target was a color, the estimated T2 errors obtained from all models and the actual T2 errors clustered closely. It should be noted that there was no attentional blink detected in the experimental

data at Lag 3, when the second target was a color. For the T1 incorrect condition (Figure 12B), a comparison between the simulated and actual data at each lag is possible. Here, the VPG model's estimation of the T2 error was notably less accurate.

Figure 12

Comparison of model simulations and experimental data based on T2 accuracy.



Note. Model simulation results using the data from Wang et al. (**A**) Simulation results in the T1 correct condition. Each panel presents the comparison of the mean T2 error in actual data and in data simulated from seven models, separately for each lag and each target pair condition. 'CC' means color-color target pair; 'CO' means color-orientation target pair; 'OO' means orientation-orientation target pair; 'OC' means orientation-color target pair. True = experimentally observed data. See Method for model abbreviations. (**B**) Simulation results in the T1 incorrect condition. The results were obtained across all target pairs within each specific lag.

4. Discussion

In the current study, we explored visual (WM) representations during AB tasks by systematically comparing a broader set of WM models across multiple datasets. Quantitative assessment of target representations in AB tasks by fitting WM models to continuous reproduction data has been done before, but previous studies have not reached a consensus on interpreting the error distribution of these WM representations for T2, partly due to a lack of systematic comparisons of these models in the AB domain and limited attention to models like the EnsInt and Swap models that consider potentially important nontarget reports. We described comparative fits of seven WM models to four sets of experimental data from three different laboratories. Specifically, we applied MLE for parameter estimation, which allowed us to assess the fitness of these models to the data and then compare

them based on AIC scores. Additionally, we utilized the parameter values from each model to generate simulated data sets, further evaluating the accuracy of these models in describing the experimental data under various conditions.

Across datasets, we found that slot- family models most often win at short lags, supporting predominantly discrete consolidation failures during the AB. Yet, VP/VPG models improve with colors and longer lags, indicating that graded precision reductions emerge when timing/feature content affords partial consolidation. Overall, AB errors are thus mixed: They consist mostly of guesses at short lags, with more low- precision reports at longer lags or with color features. This reconciles prior mixed findings, and from a practical perspective suggests that one's model choice should depend on the lag and feature dimensions being studied.

The three leading models, the StM, Slot and SR models, share a crucial assumption that only a limited number of items can be encoded into WM. In these models' error distributions, when items were not encoded into WM successfully, the corresponding errors follow a uniform distribution indicative of random responses. Our findings showed robust and consistent performance of these models across different data sets, and importantly, their simulations closely reproduced the 'blink' pattern in T2|T1 errors. This pattern of results supports existing WM encoding accounts for the AB phenomenon, where WM consolidation processes are disrupted during the blink period. Specifically, in rapid sequences of stimuli, T2 cannot be consolidated into WM until T1 is completely encoded (Bowman & Wyble, 2007; Chun & Potter, 1995; Jolicœur & Dell'Acqua, 1998; Wyble et al., 2009). These accounts suggest that WM consolidation is slow and capacity limited. In line with this idea, Ricker and Hardman (2017) provided a comprehensive analysis of the relationship between consolidation time and a stable WM representation. They explicitly associated the temporal dynamics of WM consolidation with the AB. They suggested that the duration of consolidation has a direct influence on the probability of a memory item being accessible during reporting.

In addition, the comparison results of the VP and VPG models further supported the importance of including a guess rate component in account for WM representation errors during the AB. First, the VP model generally underperformed at shorter lags (SOAs), indicating a failure to capture impaired T2 representations during blink period. At longer lags (SOAs), when there is sufficient time for both T1 and T2 consolidation, the VP model's performance improved. Second, the VP model displayed enhanced performance under conditions of a weakened AB, such as in Experiment 2A and 2B of Karabay et al. (2022), as well as with color-color and orientation-color target pairs in the datasets of Wang et al. Most importantly, the VPG model, a variant of the VP model that incorporates a guess rate, showed better performance compared to the VP model. The simulation analysis unveiled several issues of the VP model: An underestimation of the response errors, and,

more specifically, an underestimation of the response errors at shorter lags (SOAs) in relation to longer lags (SOAs), demonstrating a failure to accurately capture impaired memory consolidation during the AB. Contrastingly, the VPG model proved to be better, exhibiting a tendency to align with the empirical data across various conditions. These findings align with the results reported in Experiment 3 of Sy et al. (2021)., Our analysis thus suggests that WM errors during the AB are more effectively explained through guessing, as opposed to extremely low precision. This is in keeping with extant literature, which claims that T2 awareness can be discrete during the AB (Asplund et al., 2014; Sy et al., 2021; Wang et al., 2024). However, it is important to note that awareness during the AB can also be gradual, depending on the spatial extent of attention (Karabay et al., 2022).

Upon closer examination of the 'slot' models (the StM, Slot, and SR models), one might argue that the principal divergence lies in their predictions regarding the number of items that can be successfully encoded into WM, also referred to as set size. This is illustrated by the varying guess rates (Pg) for the Slot and SR models, which are determined based on distinct mathematical calculations that take into account the predicted number of available memory slots. To address this, we expanded our analysis to consider both T2|T1 performance, indicative of a set size of two, and T2 performance when T1 was incorrect, as a proxy of a set size of one. By doing so, we can gain insights into model fitness under different memory load conditions. Overall, the StM, Slot, and SR models exhibited similar performance across set sizes, and we could not reliably differentiate them for set sizes of one and two under most conditions. This lack of differentiation could nevertheless also be a consequence of the limited set sizes available in our analyzed data sets (one or two), which are presumably fewer than the number of available visual WM slots as suggested by Cowan (2001). In these analyses, we also noticed that T2 report performance was poorer in the T1 incorrect condition than in the T1 correct condition. We suggest that attentional resources might not be effectively focused in these trials overall, which may explain the poorer performance on T2. In this case, future AB research with set sizes pushing the WM limits will need to be undertaken (e.g., Akyürek et al., 2007) to further distinguish these models' predictions and clarify the relationship between set size and WM consolidation during the AB.

Our study also investigated the performance of models that consider nontarget reports (the EnsInt and Swap models) in the AB domain. These models exhibited distinct performance patterns across different temporal intervals and feature dimensions. The EnsInt model did not show a clear pattern across datasets, making it difficult to definitively ascertain whether the EnsInt model's fitness was impacted by different time intervals. By contrast, the Swap model's performance appeared to be more influenced by the time interval between the two targets, s. For

instance, the Swap model performed better at shorter lags, as evidenced in the model comparison results of Tang et al.'s datasets (see Figure 5 and 6), in the single-stream RSVP paradigm of Karabay et al.'s study (e.g., Experiment 3), and also in the same feature-dimension pairs (e.g., color-color and orientation-orientation) of Wang et al.'s data. These results were in accordance with previous research indicating that temporal target integration and target report order reversals occur frequently at Lag 1 (Akyürek et al., 2012; Karabay & Akyürek, 2019). This, in turn, supports the explanation for Lag 1 sparing (i.e., the lack of an AB at that lag) that is offered by the eSTST model of the AB (Wyble et al., 2009), which holds that both targets are consolidated together when they successively follow each other without intervening distractors. This is particularly relevant in AB tasks where both targets share a common feature-dimension, as the Swap model's prediction of the T2 error distribution can be influenced by the first target. It might thus be reasonable to conclude that the failure of the Swap model at longer lags could be attributed to the weaker influence of T1 on T2 during memory consolidation. Moreover, when analyzing different set sizes, the Swap model displayed better fitness when the set size was one (T1 incorrect condition) compared to its performance when the set size was two (T1 correct condition), as noted in the datasets from Karabay et al. and Wang et al. This is likely due to the swap errors at short lags or SOAs, which result in better performance of the Swap model when T1 is incorrect. Overall, these findings showed that swap errors are present at shorter lags, indicating that T1 and T2 representations partially overlap during consolidation. This pattern implies that AB accounts can be extended by considering the possibility of misbinding between temporally adjacent targets.

Finally, it is important to note a limitation in how the models were assessed. In the current study, model fitness was evaluated using only one criterion, the AIC. Although suitable for the relatively simple models applied here, AIC assumes that all parameters afford equal and independent flexibility. However, cognitive models can sometimes involve underlying parameter correlations. Future research would thus benefit from employing Bayesian model comparison frameworks, such as calculating the Widely Applicable Information Criterion (WAIC).

5. Conclusion

In this study, we explored WM representations during the AB by evaluating seven WM models' fitness against distinct data sets derived from AB tasks. Models positing a limited number of 'storage slots' in WM (StM, Slot, and SR) consistently outperformed other models. . These results suggest that memory representations can be categorized into two distinct types: One representing a complete guess, which occurs when the item was not encoded into WM at all (due to a capacity

limitation or processing limitation), and the other representing the precision with which information is encoded into visual WM. This dichotomy is implemented in the StM, Slot and SR models. Models accounting for long tails in error distributions further confirmed that guesses play a key role in explaining T2 representations during the AB (i.e., the contrast of VPG and VP models). Together, these results align with the theoretical AB models proposing that WM consolidation is disrupted, resulting in no conscious access to T2 during the AB (e.g., Asplund et al., 2014; Wyble et al., 2009).

Moreover, we identified that the lag between targets, the common feature-dimensions shared by targets, and the specific dimension of the target feature (color or orientation) played an important role in model performance. Task conditions thus affect the utility of different models, highlighting the need for careful consideration when selecting a model for a given experimental context. If a research question is centered around the short lags (lag 1-3), the EnsInt and Swap models should be preferred. Indeed, a model allowing both swaps and ensemble integrations should be considered for the short lags. However, models without target interactions should be preferred for later lags (lag 4-8; but see Tang et al., 2020). Future research will be needed to map out the role of attentional factors, such as target feature dimensions, in the WM consolidation process under time constraints. Such studies will help to clarify how overlapping T1-T2 representations and misbinding between targets contribute to memory errors, and to further guide model selection under different task conditions.

Declarations

Acknowledgements We would like to thank Christopher L. Asplund for providing the original data sets from Asplund et al. (2014).

Funding Shuyao Wang was supported by the China Scholarship Council (CSC), grant 201906020179.

Data availability Data generated during the study (Wang et al. data sets), and all the analysis scripts are available on the Open Science Framework at: https://osf.io/zak5f/. The study was not preregistered. The data from Tang et al. (2020) and Karabay et al. (2022) are publicly available through their published articles. The Tang et al. (202) data can be accessed at: https://osf.io/f9g6h. The Karabay et al. (2022) data can be accessed at: https://osf.io/x5dru.

Conflict of interest The authors have no conflict of interest to disclose.

Supplementary Material
A. Further Model fitting and Model Comparison Results

1. Asplund et al. (2014).

Table S1

Model comparison results for T2 performance in the T1 correct condition (T2|T1).

Lag	Model	Mean AIC	Mean ΔAIC	Mean Rank	Mean Log-likelihood
1	StM	1559.77	0.24	2.18	-777.89
	Slot	1559.77	0.24	2.18	-777.89
	SR	1559.77	0.24	2.12	-777.89
	VPG	1561.09	1.56	3.52	-777.55
	VP	1588.21	28.68	5	-792.11
2	StM	1608.82	0.53	2.24	-802.41
	Slot	1608.82	0.53	2.24	-802.41
	SR	1608.82	0.53	2.24	-802.41
	VPG	1609.65	1.36	3.28	-801.83
	VP	1651.48	43.19	5	-823.74
4	StM	1565.80	0.82	2.46	-780.90
	Slot	1565.80	0.82	2.4	-780.90
	SR	1565.80	0.82	2.46	-780.90
	VPG	1565.99	1.02	2.92	-780.00
	VP	1588.11	23.13	4.76	-792.05
8	StM	1490.43	0.69	2.52	-743.21
	Slot	1490.43	0.69	2.52	-743.21
	SR	1490.43	0.69	2.52	-743.21
	VPG	1490.54	0.80	2.8	-742.27
	VP	1504.02	14.29	4.64	-750.01

Note. AIC = Akaike information criterion. See *2.1. Model details* for the model abbreviation. Mean AIC values were obtained from averaging AIC values per model across all subjects, specifically for each lag. Mean ΔAIC values were obtained from averaging the relative AIC values compared to the best fitting model across all subjects, for each lag. For a detailed discussion of how these values were calculated, see *2.6. Model comparison* section of the main text.

Table S2

Model comparison results for T2 performance in the T1 incorrect condition.

Lag	Model	Mean AIC	Mean ΔAIC	Mean Rank	Mean Log-likelihood
1	StM	172.28	0.29	2.12	-84.14
	Slot	172.01	0.02	2.02	-84.00
	SR	172.01	0.02	1.98	-84.00
	VPG	174.39	2.40	4.36	-84.20
	VP	181.53	9.54	4.52	-88.77
2	StM	153.55	0.10	2.12	-74.78
	Slot	153.45	0.00	1.96	-74.73
	SR	153.45	0.00	1.92	-74.73
	VPG	155.76	2.31	4.16	-74.88
	VP	166.70	13.25	4.84	-81.35
4	StM	155.35	0.02	2.08	-75.67
	Slot	155.33	0.00	1.96	-75.67
	SR	155.33	0.00	1.96	-75.67
	VPG	157.49	2.16	4.24	-75.75
	VP	164.00	8.67	4.76	-80.00
8	StM	171.64	0.15	2.2	-83.82
	Slot	171.50	0.01	2.04	-83.75
	SR	171.50	0.01	1.92	-83.75
	VPG	173.71	2.22	4.24	-83.86
	VP	182.49	11.00	4.6	-89.24

Table S3

Maximum-likelihood estimates of the parameters in all models in the T1 correct condition.

		Lag 1		Lag 2		Lag 4		Lag 8	
Model	**Parameter**	**Median**	***SD***	**Median**	***SD***	**Median**	***SD***	**Median**	***SD***
StM	*g*	0.37	0.10	0.45	0.11	0.37	0.12	0.27	0.13
	sd	21.21	3.49	20.69	4.34	20.76	4.37	19.23	4.06
Slot	*capacity K*	1.26	0.21	1.09	0.21	1.27	0.25	1.46	0.27
	sd	21.21	3.49	20.69	4.34	20.76	4.37	19.23	4.06
SR	*capacity K*	1.26	0.21	1.09	0.21	1.27	0.25	1.46	0.27
	sd	19.53	3.16	19.89	3.45	19.56	3.91	16.10	3.72
VPG	*g*	0.33	0.11	0.39	0.14	0.30	0.13	0.21	0.14
	modePrecision	2.42×10^{-3}	8.56×10^{-4}	2.65×10^{-3}	1.45×10^{-3}	2.34×10^{-3}	1.47×10^{-3}	3.5×10^{-3}	1.76×10^{-3}
	sdPrecision	1.20×10^{-3}	5.5×10^{-3}	1.62×10^{-3}	5.96×10^{-3}	3.79×10^{-3}	5.03×10^{-3}	3.81×10^{-3}	4.63×10^{-3}
VP	*modePrecision*	1×10^{-3}	1.98×10^{-11}	1×10^{-3}	5.78×10^{-12}	1×10^{-3}	3.42×10^{-4}	1×10^{-3}	1.6×10^{-3}
	*sd*Precision	4.65×10^{-3}	2.5×10^{-3}	4.62×10^{-3}	2.84×10^{-3}	5.19×10^{-3}	3.49×10^{-3}	8.79×10^{-3}	1.25×10^{-2}

Table S4

Maximum-likelihood estimates of the parameters in all models in the T1 incorrect condition.

		Lag 1		Lag 2		Lag 4		Lag 8	
Model	**Parameter**	**Median**	***SD***	**Median**	***SD***	**Median**	***SD***	**Median**	***SD***
StM	*g*	0.36	0.29	0.49	0.34	0.39	0.29	0.28	0.31
	sd	25.75	33.79	21.18	140.81	22.35	24.61	28.46	21.84
Slot	*capacity K*	1.10	1.40	1.02	0.97	1.21	0.72	1.44	0.68
	sd	21.06	31.48	18.24	29.12	22.30	25.57	19.58	22.05
SR	*capacity K*	1.14	0.78	1.03	1.22	1.21	0.86	1.44	0.92
	sd	23.51	21.10	27.00	75.75	18.64	19.05	19.13	17.65
VPG	*g*	0.50	0.30	0.58	0.31	0.50	0.29	0.31	0.32
	modePrecision	1.88×10^{-3}	4.17	3.56×10^{-3}	6.18	1.66×10^{-3}	0.03	1.86×10^{-3}	1.31
	sdPrecision	1×10^{-3}	33.04	1.06×10^{-3}	27.69	1×10^{-3}	20	1×10^{-3}	20
VP	*modePrecision*	1×10^{-3}	1.1×10^{-3}	1×10^{-3}	1.03×10^{-2}	1×10^{-3}	9.64×10^{-4}	1×10^{-3}	2.76×10^{-3}
	*sd*Precision	3.21×10^{-3}	0.18	3.24×10^{-3}	6.7×10^{-3}	3.54×10^{-3}	20	3.31×10^{-3}	1.51×10^{-2}

2. Tang et al. (2020).

Table S5

Model comparison results for T2 performance in the T1 correct condition (T2|T1).

Experiment	Lag	Model	Mean AIC	Mean ΔAIC	Mean Rank	Mean Log-likelihood
Exp1	**1**	StM	318.28	9.92	3.34	-157.14
		Slot	318.23	9.88	3.07	-157.12
		SR	318.20	9.84	3.00	-157.10
		EnsInt	315.76	7.40	2.93	-154.88
		Swap	309.52	1.17	2.75	-151.76
		VPG	320.86	12.50	5.91	-157.43
		VP	353.49	45.13	7.00	-174.74
	2	StM	509.62	16.89	3.32	-252.81
		Slot	509.35	16.62	2.84	-252.68
		SR	509.34	16.60	2.93	-252.67
		EnsInt	506.71	13.97	3.25	-250.35
		Swap	494.16	1.42	2.93	-244.08
		VPG	512.04	19.30	5.73	-253.02
		VP	575.61	82.87	7.00	-285.80
	3	StM	510.92	12.29	3.14	-253.46
		Slot	510.72	12.09	2.89	-253.36
		SR	510.69	12.07	2.84	-253.35
		EnsInt	507.99	9.36	3.64	-250.99
		Swap	499.56	0.94	2.64	-246.78
		VPG	514.18	15.56	5.86	-254.09
		VP	565.16	66.53	7.00	-280.58
	5	StM	546.46	5.81	2.89	-271.23
		Slot	546.38	5.74	2.64	-271.19
		SR	546.38	5.74	2.66	-271.19
		EnsInt	545.27	4.63	4.30	-269.64
		Swap	541.91	1.27	3.48	-267.96
		VPG	549.03	8.39	5.55	-271.52
		VP	582.04	41.39	6.50	-289.02
	7	StM	498.98	2.64	2.61	-247.49
		Slot	498.90	2.56	2.50	-247.45
		SR	498.83	2.50	2.52	-247.42
		EnsInt	500.10	3.77	4.66	-247.05
		Swap	497.77	1.43	3.80	-245.88
		VPG	501.87	5.53	5.73	-247.93
		VP	525.78	29.45	6.18	-260.89
Exp2	3	StM	1356.37	3.87	2.59	-676.19
		Slot	1356.37	3.87	2.59	-676.19
		SR	1356.37	3.87	2.65	-676.19
		EnsInt	1356.47	3.97	4.13	-675.23
		Swap	1353.60	1.10	3.30	-673.80
		VPG	1360.03	7.53	5.78	-677.02
		VP	1437.18	84.68	6.96	-716.59
	7	StM	1306.75	1.23	2.46	-651.38
		Slot	1306.95	1.44	2.59	-651.48
		SR	1306.57	1.06	2.35	-651.29
		EnsInt	1308.29	2.77	4.70	-651.14
		Swap	1307.78	2.26	4.43	-650.89
		VPG	1311.27	5.75	5.61	-652.63
		VP	1340.81	35.29	5.87	-668.40

Table S6

Model comparison results for T2 performance in the T1 incorrect condition.

Experiment	Lag	Model	Mean AIC	Mean ΔAIC	Mean Ranking	Mean Log-likelihood
Exp1	**1**	StM	769.12	1.68	2.61	-382.56
		Slot	769.08	1.64	2.50	-382.54
		SR	769.06	1.63	2.43	-382.53
		EnsInt	770.26	2.82	4.43	-382.13
		Swap	768.50	1.06	3.39	-381.25
		VPG	771.90	4.46	5.73	-382.95
		VP	847.98	80.54	6.91	-421.99
	2	StM	587.21	2.77	2.93	-291.60
		Slot	587.21	2.77	2.82	-291.60
		SR	587.10	2.66	2.52	-291.55
		EnsInt	586.94	2.50	3.75	-290.47
		Swap	586.24	1.81	3.20	-290.12
		VPG	589.48	5.05	5.77	-291.74
		VP	661.21	76.77	7.00	-328.60
	3	StM	572.66	2.75	2.82	-284.33
		Slot	572.52	2.70	3.37	-284.26
		SR	572.25	2.42	2.55	-284.12
		EnsInt	572.73	2.82	3.13	-283.37
		Swap	572.23	2.32	2.41	-283.11
		VPG	575.15	5.23	2.89	-284.57
		VP	642.13	72.22	3.64	-319.07
	5	StM	521.61	1.09	3.57	-258.81
		Slot	521.55	1.02	3.77	-258.77
		SR	521.44	0.92	2.57	-258.72
		EnsInt	522.22	1.70	5.82	-258.11
		Swap	522.24	1.71	5.48	-258.12
		VPG	524.51	3.99	7.00	-259.26
		VP	573.37	52.84	7.00	-284.68
	7	StM	519.18	0.69	2.61	-257.59
		Slot	519.18	0.69	2.50	-257.59
		SR	519.18	0.69	2.30	-257.59

Table S6 (*continued*)

Experiment	Lag	Model	Mean AIC	Mean ΔAIC	Mean Ranking	Mean Log-likelihood
		EnsInt	520.26	1.77	3.89	-257.13
		Swap	520.49	2.00	4.11	-257.25
		VPG	522.52	4.03	5.91	-258.26
		VP	567.44	48.95	6.68	-281.72
Exp2	**3**	StM	1267.25	8.34	2.45	-631.62
		Slot	1267.13	8.22	2.59	-631.56
		SR	1266.99	8.04	2.39	-631.50
		EnsInt	1265.45	6.53	2.59	-629.72
		Swap	1259.64	0.73	2.25	-626.82
		VPG	1270.05	11.14	2.48	-632.02
		VP	1410.50	151.59	4.05	-703.25
	7	StM	1073.56	0.82	4.17	-534.78
		Slot	1073.56	0.82	4.50	-534.78
		SR	1073.45	0.71	3.74	-534.73
		EnsInt	1074.63	1.88	5.86	-534.31
		Swap	1074.13	1.39	5.83	-534.06
		VPG	1077.55	4.81	6.50	-535.77
		VP	1151.23	78.49	6.61	-573.61

Table S7

Maximum-likelihood estimates of the parameters in all models in the T1 correct condition.

		Exp1										***Exp2***			
		Lag 1		**Lag 2**		**Lag 3**		**Lag 5**		**Lag 7**		**Lag 3**		**Lag 7**	
Model	**Parameter**	**Median**	**SD**	**Median**	**SD**	**Median**	**SD**	**Median**	**SD**	**Median**	**SD**	**Median**	**SD**	**Median**	**SD**
StM	*g*	0.65	0.41	0.83	0.44	0.73	0.43	0.48	0.38	0.19	0.38	0.31	0.34	0.16	0.28
	sd	22.43	19.73	20.94	18.44	20.94	17.14	19.12	15.62	20.52	10.96	21.8	18.11	19.96	10.25
Slot	*capacity K*	0.56	1.47	0.33	1.36	0.5	1.53	1.02	0.94	1.53	1.2	1.38	1.47	1.67	1.40
	sd	21.19	20.32	15.13	21.59	28.24	29.23	18.47	27.64	24.2	25	22.01	18.23	20.58	10.59
SR	*capacity K*	0.78	1.15	1.27	1.19	0.9	1.07	1.22	1.3	1.53	0.72	1.38	0.92	1.67	0.97
	sd	27.03	50.06	35.59	73.62	23.43	50.35	21.27	40.96	20.99	55.96	26.15	39.25	16.43	40.47
EnsInt	*g*	0.26	0.37	2.47×10^{-3}	0.43	0.39	0.38	0.18	0.37	0.15	0.28	0.29	0.3	0.13	0.25
	sd	31.09	47.81	35.49	17.9	28.27	13.82	26.19	21.70	20.27	19.48	33.25	16.18	19.96	13.98
	samples	4.43×10^{-4}	4.59×10^{12}	2.16×10^{-5}	1.24×10^{12}	0.22	7.04×10^{12}	0.94	5.87×10^{12}	10.28	3.78×10^{12}	56.09	6.01×10^{12}	8.23×10^{12}	7.43×10^{12}
Swap	*g*	0.08	0.28	0.07	0.27	0.09	0.36	0.15	0.23	0.05	0.23	0.04	0.25	0.12	0.23
	B	0.41	0.4	0.47	0.37	0.15	0.38	0.04	0.37	1.97×10^{-5}	0.35	0.05	0.27	6.88×10^{-15}	0.22
	sd	25.76	16.15	24.44	52.79	26.73	28.54	23.53	48.27	24.55	11.94	32.20	16.82	19.96	10.78
VPG	*g*	0.92	0.2	0.91	0.16	0.91	0.25	0.69	0.36	0.5	0.33	0.69	0.3	0.33	0.32
	mode-Precision	5.58×10^{-4}	0.7	5.15×10^{-4}	0.42	5.15×10^{-4}	0.03	5.08×10^{-4}	5.63×10^{-4}	5×10^{-4}	2.57×10^{-3}	5×10^{-4}	6.82×10^{-4}	5×10^{-4}	1.61×10^{-4}
	sdPrecision	5×10^{-4}	10.66	7.89×10^{-4}	10.66	6.76×10^{-4}	14.71	5.38×10^{-4}	0.05	6.99×10^{-4}	10.66	5×10^{-4}	0.01	5×10^{-4}	3.6×10^{-4}
VP	*mode-Precision*	5×10^{-4}	1.49×10^{-11}	5×10^{-4}	7.56×10^{-12}	5×10^{-4}	1.1×10^{-11}	5×10^{-4}	8.48×10^{-5}	5×10^{-4}	1.36×10^{-4}	5×10^{-4}	4.97×10^{-12}	5×10^{-4}	1.84×10^{-4}
	*sd*Precision	1.56×10^{-3}	3.05×10^{-4}	1.64×10^{-3}	1.89×10^{-4}	1.57×10^{-3}	2.35×10^{-4}	1.5×10^{-3}	3.37×10^{-4}	1.4×10^{-3}	3.3×10^{-3}	1.5×10^{-3}	2.38×10^{-4}	1.22×10^{-3}	3.82×10^{-4}

Table S8

Maximum-likelihood estimates of the parameters in all models in the T1 incorrect condition.

		Exp1										***Exp2***			
		Lag 1		**Lag 2**		**Lag 3**		**Lag 5**		**Lag 7**		**Lag 3**		**Lag 7**	
Model	**Parameter**	**Median**	**SD**	**Median**	**SD**	**Median**	**SD**	**Median**	**SD**	**Median**	**SD**	**Median**	**SD**	**Median**	**SD**
StM	*g*	0.59	0.38	0.81	0.38	0.46	0.40	0.59	0.37	0.24	0.37	0.65	0.41	0.42	0.34
	sd	18.36	14.81	15.91	21.55	22.47	23.34	17.07	17.2	22.81	45.88	21.72	18.4	20.61	9.13
Slot	*capacity K*	0.81	1.53	0.39	0.89	0.76	1.03	0.83	1.69	1.4	0.97	0.56	0.79	1.16	0.98
	sd	18.86	17.14	18	22.96	21.27	21.15	17.07	18.14	31.77	15.44	24.22	27.62	20.61	9.52
SR	*capacity K*	0.84	1.01	0.68	0.92	1.09	0.95	0.83	1.13	1.45	1.18	0.56	1.22	1.16	0.83
	sd	24.62	93.78	23.82	78.58	26.17	62.94	19.91	12.35	24.84	64.54	19.48	16.13	19.71	10.86
EnsInt	*g*	0.43	0.39	0.76	0.37	0.46	0.40	0.59	0.37	0.19	0.37	0.17	0.41	0.32	0.3
	sd	25.74	20.19	13.38	18.01	20.75	23.22	17.07	16.73	26.72	23.65	25.13	19.88	21.06	16.06
	samples	0.94	2.29×10^{12}	0.01	9.68×10^{11}	0.04	3.5×10^{12}	7.48	2.47×10^{12}	17.12	1.15×10^{13}	0.64	3.68×10^{12}	6.25	4.03×10^{12}
Swap	*g*	3.26×10^{-3}	0.34	0.42	0.38	0.33	0.31	0.38	0.34	0.36	0.37	0.11	0.32	0.35	0.29
	B	0.07	0.37	0.14	0.32	0.06	0.32	0.07	0.15	1.33×10^{-10}	0.06	0.2	0.29	0.03	0.09
	sd	26.65	17.37	23.86	47.13	41.37	43.39	22.98	47.21	21.16	17.82	26.52	15.56	20.61	8.81
VPG	*g*	0.82	0.29	0.85	0.17	0.9	0.24	0.78	0.28	0.59	0.31	0.79	0.27	0.62	0.31
	mode-Precision	5×10^{-4}	1.04×10^{-3}	5.41×10^{-4}	6.54×10^{-4}	5.07×10^{-4}	2.02×10^{-3}	5.07×10^{-4}	0.02	5×10^{-4}	2.58×10^{-4}	5.02×10^{-4}	0.33	5×10^{-4}	1.01×10^{-3}
	sdPrecision	5×10^{-4}	2.68×10^{-3}	5.01×10^{-4}	10.7	5×10^{-4}	6.88×10^{-3}	5.08×10^{-4}	17.56	5.1×10^{-4}	0.02	5.47×10^{-4}	17.22	5×10^{-4}	3.33×10^{-3}
VP	*mode-Precision*	5×10^{-4}	1.33×10^{-11}	5×10^{-4}	1.48×10^{-11}	5×10^{-4}	2.81×10^{-11}	5×10^{-4}	1.38×10^{-11}	5×10^{-4}	4.28×10^{-5}	5×10^{-4}	4.14×10^{-12}	5×10^{-4}	1.57×10^{-4}
	sdPrecision	1.56×10^{-3}	2.16×10^{-4}	1.65×10^{-3}	1.63×10^{-4}	1.56×10^{-3}	3.23×10^{-3}	1.54×10^{-3}	2.17×10^{-3}	1.42×10^{-3}	3.09×10^{-4}	1.61×10^{-3}	3.03×10^{-4}	1.41×10^{-3}	0.01

3. Karabay et al. (2022).

Table S9

Model comparison results for T2 performance in the T1 correct condition (T2|T1).

		Short SOA				Long SOA			
Experiment	**Model**	**Mean AIC**	**Mean ΔAIC**	**Mean Rank**	**Mean Log-likelihood**	**Mean AIC**	**Mean ΔAIC**	**Mean Rank**	**Mean Log-likelihood**
Exp1A	StM	2174.28	0.96	2.26	-1085.14	2269.40	0.51	2.20	-1132.70
	Slot	2174.28	0.96	2.13	-1085.14	2269.40	0.51	2.20	-1132.70
	SR	2174.28	0.96	2.13	-1085.14	2269.40	0.51	2.26	-1132.70
	EnsInt	2176.35	3.03	4.83	-1085.17	2271.39	2.50	4.80	-1132.69
	Swap	2175.36	2.05	4.70	-1084.68	2271.37	2.48	4.89	-1132.68
	VPG	2177.86	4.54	4.96	-1085.93	2272.39	3.50	5.00	-1133.19
	VP	2302.45	129.13	7.00	-1149.22	2329.82	60.93	6.65	-1162.91
Exp1B	StM	2275.15	0.09	2.14	-1135.57	2305.73	0.69	2.33	-1150.86
	Slot	2275.14	0.08	2.07	-1135.57	2305.73	0.69	2.33	-1150.86
	SR	2275.14	0.08	2.07	-1135.57	2305.73	0.69	2.33	-1150.86
	EnsInt	2278.87	3.81	4.93	-1136.43	2307.72	2.68	5.07	-1150.86
	Swap	2277.22	2.16	4.83	-1135.61	2307.70	2.66	5.36	-1150.85
	VPG	2278.69	3.63	4.95	-1136.34	2307.80	2.76	4.52	-1150.90
	VP	2406.58	131.52	7.00	-1201.29	2346.17	41.13	6.05	-1171.08
Exp2A	StM	1826.96	6.94	3.65	-911.48	1851.74	8.50	3.88	-923.87
	Slot	1826.97	6.94	3.71	-911.48	1851.74	8.50	3.88	-923.87
	SR	1826.97	6.94	3.83	-911.48	1851.74	8.50	3.88	-923.87
	EnsInt	1826.64	6.62	4.17	-910.32	1851.78	8.55	5.00	-922.89
	Swap	1828.46	8.43	5.98	-911.23	1853.36	10.13	6.35	-923.68
	VPG	1821.91	1.89	3.46	-907.96	1844.86	1.63	2.73	-919.43
	VP	1824.77	4.75	3.19	-910.39	1846.12	2.88	2.27	-921.06
Exp2B	StM	2386.28	3.58	3.06	-1191.14	2339.42	5.06	3.39	-1167.71
	Slot	2387.35	4.65	3.28	-1191.67	2339.54	5.19	3.61	-1167.77
	SR	2386.33	3.64	3.11	-1191.16	2339.42	5.06	3.44	-1167.71
	EnsInt	2388.24	5.55	5.70	-1191.12	2340.95	6.60	5.61	-1167.47
	Swap	2388.26	5.57	5.74	-1191.13	2341.08	6.73	6.13	-1167.54
	VPG	2384.27	1.57	2.93	-1189.13	2335.63	1.27	2.89	-1164.81
	VP	2389.49	6.80	4.19	-1192.74	2336.28	1.92	2.93	-1166.14
Exp3	StM	1904.31	10.46	2.35	-950.15	1861.28	0.81	2.31	-928.64
	Slot	1904.31	10.46	2.42	-950.15	1861.36	0.89	2.35	-928.68
	SR	1904.31	10.46	2.35	-950.15	1861.83	1.36	2.71	-928.91
	EnsInt	1903.19	9.34	4.35	-948.59	1863.22	2.76	4.79	-928.61
	Swap	1895.25	1.41	3.90	-944.63	1862.67	2.21	4.50	-928.34
	VPG	1908.80	14.95	5.75	-951.40	1865.51	5.05	5.50	-929.76
	VP	2030.28	136.43	6.88	-1013.14	1881.33	20.86	5.83	-938.66
Exp4	StM	1888.70	0.84	2.19	-942.35	1864.14	1.39	2.38	-930.07
	Slot	1888.70	0.84	2.31	-942.35	1864.46	1.70	2.67	-930.23
	SR	1888.70	0.84	2.25	-942.35	1864.14	1.39	2.38	-930.07
	EnsInt	1889.64	1.78	4.29	-941.82	1865.36	2.60	4.60	-929.68
	Swap	1890.29	2.44	4.50	-942.15	1865.66	2.90	4.77	-929.83
	VPG	1891.88	4.02	5.46	-942.94	1866.86	4.10	4.83	-930.43
	VP	1959.16	71.30	7.00	-977.58	1891.04	28.28	6.38	-943.52
Exp5	StM	1442.75	0.55	2.24	-719.38	1458.46	0.06	2.07	-727.23
	Slot	1442.87	0.66	2.28	-719.43	1458.55	0.14	2.22	-727.27
	SR	1442.75	0.55	2.13	-719.38	1458.46	0.06	2.07	-727.23
	EnsInt	1444.21	2.01	4.30	-719.10	1460.39	1.99	4.89	-727.20
	Swap	1444.63	2.43	4.83	-719.32	1460.46	2.05	5.24	-727.23
	VPG	1446.36	4.16	5.48	-720.18	1460.80	2.40	5.13	-727.40
	VP	1511.01	68.81	6.74	-753.51	1495.78	37.38	6.39	-745.89

Table S10

Model comparison results for T2 performance in the T1 incorrect condition.

		Short SOA				Long SOA			
Experiment	**Model**	**Mean AIC**	**Mean ΔAIC**	**Mean Rank**	**Mean Log-likelihood**	**Mean AIC**	**Mean ΔAIC**	**Mean Rank**	**Mean Log-likelihood**
Exp1A	StM	1493.33	1.57	2.54	-744.66	1282.36	1.71	2.67	-639.18
	Slot	1493.32	1.56	2.54	-744.66	1282.15	1.51	2.50	-639.08
	SR	1493.27	1.52	2.48	-744.64	1282.15	1.51	2.43	-639.08
	EnsInt	1495.01	3.25	4.87	-744.50	1283.03	2.38	4.48	-638.51
	Swap	1492.98	1.22	3.13	-743.49	1282.22	1.57	3.83	-638.11
	VPG	1495.30	3.54	5.43	-744.65	1284.42	3.77	5.22	-639.21
	VP	1685.43	193.67	7.00	-840.71	1392.00	111.35	6.87	-694.00
Exp1B	StM	1275.35	1.93	2.67	-635.68	1086.22	0.71	2.21	-541.11
	Slot	1275.35	1.93	2.67	-635.68	1086.23	0.72	2.29	-541.12
	SR	1275.32	1.89	2.52	-635.66	1086.22	0.71	2.21	-541.11
	EnsInt	1275.96	2.54	4.19	-634.98	1088.10	2.59	5.07	-541.05
	Swap	1275.02	1.59	3.33	-634.51	1086.99	1.48	4.17	-540.49
	VPG	1277.92	4.49	5.62	-635.96	1088.80	3.29	5.33	-541.40
	VP	1423.83	150.40	7.00	-709.91	1151.80	66.29	6.71	-573.90
Exp2A	StM	186.56	2.81	2.75	-91.28	169.49	2.05	2.83	-82.75
	Slot	185.61	1.86	2.54	-90.80	169.49	2.05	2.60	-82.75
	SR	185.61	2.76	2.56	-90.80	169.49	2.05	2.54	-82.75
	EnsInt	187.22	3.47	4.10	-90.61	169.41	1.97	3.90	-81.70
	Swap	186.49	2.74	4.13	-90.25	169.86	2.42	4.52	-81.93
	VPG	188.71	4.95	5.92	-91.35	171.48	4.04	6.08	-82.74
	VP	199.17	15.42	6.00	-97.58	180.99	13.55	5.54	-88.49
Exp2B	StM	276.10	5.65	2.83	-136.05	204.01	2.70	2.87	-100.01
	Slot	276.10	5.51	2.78	-136.05	203.81	2.70	2.87	-99.90
	SR	276.10	5.70	2.98	-136.05	204.01	2.50	2.67	-100.01
	EnsInt	276.46	6.00	4.41	-135.23	203.74	2.43	4.06	-98.87
	Swap	271.14	0.69	2.44	-132.57	203.24	1.93	3.50	-98.62
	VPG	278.23	7.78	6.11	-136.11	206.12	4.81	6.15	-100.06
	VP	288.74	18.29	6.44	-142.37	211.83	10.52	5.89	-103.92
Exp3	StM	789.38	0.64	2.31	-392.69	673.82	1.08	2.31	-334.91
	Slot	789.38	0.64	2.31	-392.69	673.64	0.90	2.17	-334.82
	SR	789.38	0.64	2.25	-392.69	673.64	0.90	2.06	-334.82
	EnsInt	791.22	2.48	4.65	-392.61	674.61	1.87	4.52	-334.31
	Swap	790.13	1.39	3.77	-392.07	675.54	2.80	4.73	-334.77
	VPG	792.02	3.27	5.79	-393.01	676.47	3.73	5.92	-335.23
	VP	875.99	87.25	6.92	-436.00	726.31	53.56	6.29	-361.15
Exp4	StM	856.76	1.06	2.42	-426.38	802.15	1.61	2.31	-399.08
	Slot	856.76	1.06	2.54	-426.38	802.15	1.61	2.38	-399.08
	SR	856.75	1.05	2.38	-426.37	802.15	1.61	2.44	-399.08
	EnsInt	858.20	2.51	4.77	-426.10	804.06	3.52	4.98	-399.03
	Swap	856.90	1.20	3.40	-425.45	801.62	1.08	3.35	-397.81
	VPG	859.53	3.84	5.50	-426.77	805.14	4.60	5.58	-399.57
	VP	908.58	52.88	7.00	-452.29	834.36	33.82	6.96	-415.18
Exp5	StM	740.58	2.78	2.35	-368.29	693.13	4.45	2.74	-344.56
	Slot	740.53	2.78	2.37	-368.26	692.98	4.30	2.54	-344.49
	SR	740.57	2.72	2.15	-368.28	692.91	4.23	2.37	-344.45
	EnsInt	741.38	3.58	4.63	-367.69	692.84	4.16	4.00	-343.42
	Swap	739.43	1.63	4.37	-366.71	691.13	2.45	4.26	-342.56
	VPG	742.56	4.76	5.39	-368.28	695.19	6.51	5.52	-344.59
	VP	810.13	72.33	6.74	-403.06	751.32	62.64	6.57	-373.66

Table S11

Maximum-likelihood estimates of the parameters in all models in the T1 correct condition.

		Exp1A				***Exp1B***				***Exp2A***				***Exp2B***			
		Short SOA		**Long SOA**		**Short SOA**		**Long SOA**		**Short SOA**		**Long SOA**		**Short SOA**		**Long SOA**	
Model	**Parameter**	**Median**	**SD**	**Median**	**SD**	**Median**	**SD**	**Median**	**SD**	**Median**	**SD**	**Median**	**SD**	**Median**	**SD**	**Median**	**SD**
StM	*g*	0.36	0.3	0.31	0.18	0.56	0.25	0.35	0.18	0.06	0.11	0.06	0.10	0.09	0.11	0.06	0.05
	sd	22.53	16.78	18.25	6.97	18.16	9.57	15.17	4.41	18.61	4.38	17.79	3.30	23.20	4.88	20.53	3.22
Slot	*capacity K*	1.27	1.44	1.37	0.35	0.88	0.51	1.30	0.35	1.88	0.23	1.88	0.24	1.81	0.41	1.87	0.26
	sd	22.53	16.78	18.25	6.97	18.16	10.05	15.17	4.41	18.61	4.42	17.79	3.30	23.20	4.88	20.53	3.25
SR	*capacity K*	1.27	1.02	1.37	0.35	0.88	0.51	1.3	0.35	1.88	0.23	1.88	0.27	1.81	0.22	1.87	0.11
	sd	22.74	11.69	16.33	6.78	18.76	8.44	13.68	4.23	13.79	3.34	13.11	2.50	17.30	4.39	15.09	2.61
EnsInt	*g*	0.4	0.31	0.31	0.18	0.56	0.27	0.35	0.18	0.06	0.11	0.06	0.10	0.09	0.11	0.06	0.06
	sd	22.53	14.8	18.25	6.97	19.26	18.86	15.17	4.41	18.49	4.35	17.81	3.24	23.20	4.89	20.53	3.26
	samples	7.82×10^{12}	8.13×10^{12}	6.39×10^{12}	5.93×10^{12}	5.96×10^{12}	6.9×10^{12}	6.86×10^{12}	8.16×10^{12}	3.07	1.84×10^{12}	3.15	5.06×10^{11}	2.12×10^{12}	3.35×10^{12}	9.15×10^{11}	2.43×10^{12}
Swap	*g*	0.36	0.28	0.31	0.18	0.53	0.26	0.31	0.18	0.06	0.09	0.05	0.08	0.09	0.11	0.06	0.06
	B	2.02×10^{-15}	0.05	2.97×10^{-15}	0.01	2.89×10^{-15}	5.33×10^{-3}	2.31×10^{-15}	5.06×10^{-3}	5.05×10^{-15}	0.02	9.64×10^{-15}	0.02	3.59×10^{-15}	1.28×10^{-3}	5.84×10^{-15}	3.44×10^{-3}
	sd	22.53	16.86	18.25	6.96	18.54	13.15	15.17	4.41	18.69	4.2	17.89	3.25	23.2	4.88	20.53	3.23
VPG	*g*	0.68	0.23	0.38	0.22	0.63	0.22	0.23	0.21	0.03	0.1	5.4×10^{-3}	0.1	0.06	0.1	0.03	0.04
	mode-Precision	5×10^{-4}	3.04×10^{-3}	5×10^{-4}	1.23×10^{-4}	5×10^{-4}	6.57×10^{-4}	5.27×10^{-4}	2.88×10^{-4}	4.34×10^{-3}	1.73×10^{-3}	4.75×10^{-3}	2.26×10^{-3}	2.31×10^{-3}	1.07×10^{-3}	3.23×10^{-3}	1.09×10^{-3}
	sdPrecision	6.69×10^{-4}	10.42	5.01×10^{-4}	7.72×10^{-4}	5×10^{-4}	6.11×10^{-4}	5.01×10^{-4}	2.84×10^{-3}	4.38×10^{-3}	3.39×10^{-2}	4.9×10^{-3}	8.86×10^{-3}	1.92×10^{-3}	2.02×10^{-3}	2.82×10^{-3}	2.04×10^{-3}
VP	*mode-Precision*	5×10^{-4}	4.13×10^{-12}	5×10^{-4}	4.78×10^{-5}	5×10^{-4}	3.8×10^{-12}	5×10^{-4}	4.06×10^{-5}	4.61×10^{-3}	1.81×10^{-3}	4.85×10^{-3}	2.48×10^{-3}	2.21×10^{-3}	1.29×10^{-3}	3.39×10^{-3}	1.39×10^{-3}
	*sd*Precision	1.55×10^{-3}	1.4×10^{-4}	1.46×10^{-3}	3.7×10^{-4}	1.51×10^{-3}	1.59×10^{-4}	1.5×10^{-3}	1.84×10^{-3}	6.73×10^{-3}	6.27×10^{-3}	6.93×10^{-3}	8.51×10^{-3}	4.71×10^{-3}	2.91×10^{-3}	4.27×10^{-3}	3.34×10^{-3}

Table S11 *(continued)*

		Exp3				*Exp4*				*Exp5*			
		Short SOA		**Long SOA**		**Short SOA**		**Long SOA**		**Short SOA**		**Long SOA**	
Model	**Parameter**	**Median**	**SD**	**Median**	**SD**	**Median**	**SD**	**Median**	**SD**	**Median**	**SD**	**Median**	**SD**
StM	*g*	0.55	0.29	0.15	0.16	0.41	0.21	0.24	0.16	0.32	0.3	0.32	0.23
	sd	17.65	13.67	18.45	6.18	16.13	7.59	15.77	4.67	18.14	13.58	16.93	6.39
Slot	*capacity K*	0.9	0.59	1.70	0.56	1.18	0.44	1.53	0.45	1.35	1.2	1.36	1.44
	sd	17.65	13.67	18.45	6.17	16.13	7.59	15.77	4.94	18.14	13.45	17.08	6.37
SR	*capacity K*	0.9	0.62	1.70	0.83	1.18	0.46	1.53	0.61	1.35	0.78	1.36	0.47
	sd	18.85	11.51	15.34	5.65	16.08	5.46	13.56	3.57	15.89	10.24	15.54	5.09
EnsInt	*g*	0.37	0.29	0.15	0.16	0.41	0.20	0.24	0.16	0.32	0.3	0.32	0.23
	sd	21.38	15.34	18.45	6.18	16.00	7.18	15.77	4.11	18.02	13.9	16.93	6.39
	samples	2.65×10^{12}	1.09×10^{13}	6.41×10^{12}	8.49×10^{12}	5.12×10^{12}	6.55×10^{12}	5.51×10^{12}	5.92×10^{12}	4.69×10^{12}	7.77×10^{12}	5.28×10^{12}	1.05×10^{13}
Swap	*g*	0.41	0.24	0.14	0.16	0.41	0.21	0.23	0.16	0.32	0.29	0.32	0.19
	B	1.69×10^{-12}	0.17	5.99×10^{-15}	0.02	5.73×10^{-15}	0.05	5.29×10^{-15}	0.03	3.57×10^{-15}	0.07	3.04×10^{-15}	0.01
	sd	18.32	11.66	18.45	6.15	16.13	6.73	16.08	4.52	18.51	13	16.93	7.23
VPG	*g*	0.66	0.28	0.14	0.19	0.44	0.20	0.21	0.16	0.61	0.3	0.36	0.23
	mode-Precision	5×10^{-4}	0.36	5×10^{-4}	2.58×10^{-4}	5×10^{-4}	2.1×10^{-4}	5×10^{-4}	1.66×10^{-4}	5×10^{-4}	0.82	5×10^{-4}	1.61×10^{-4}
	sdPrecision	5×10^{-4}	14.12	5×10^{-4}	2.39×10^{-4}	5.15×10^{-4}	1.04×10^{-3}	5.16×10^{-4}	1.56×10^{-3}	5.09×10^{-4}	10.43	5.01×10^{-4}	0.02
	mode-Precision	5×10^{-4}	2.58×10^{-4}	5×10^{-4}	2.02×10^{-4}	5×10^{-4}	8.05×10^{-12}	5×10^{-4}	6.64×10^{-5}	5×10^{-4}	5.85×10^{-5}	5×10^{-4}	1.02×10^{-4}
VP	*mode-sdPrecision*	1.54×10^{-3}	4.22×10^{-4}	1.08×10^{-3}	1.24×10^{-3}	1.5×10^{-3}	1.9×10^{-4}	1.5×10^{-3}	1.04×10^{-3}	1.45×10^{-3}	5.96×10^{-4}	1.48×10^{-3}	5.15×10^{-4}

Table S12

Maximum-likelihood estimates of the parameters in all models in the T1 incorrect condition.

		Exp1A				***Exp1B***				***Exp2A***				***Exp2B***			
		Short SOA		**Long SOA**		**Short SOA**		**Long SOA**		**Short SOA**		**Long SOA**		**Short SOA**		**Long SOA**	
Model	**Parameter**	**Median**	**SD**	**Median**	**SD**	**Median**	**SD**	**Median**	**SD**	**Median**	**SD**	**Median**	**SD**	**Median**	**SD**	**Median**	**SD**
StM	*g*	0.89	0.22	0.71	0.26	0.88	0.25	0.54	0.24	0.29	0.26	0.21	0.26	0.46	0.25	0.30	0.25
	sd	14.44	11.99	13.76	10.74	15.91	8.06	13.67	8.09	15.98	22.54	16.35	26.11	20.66	15.65	20.22	12.22
Slot	*capacity K*	0.15	0.26	0.56	0.47	0.23	0.5	0.93	0.51	1.42	0.90	1.58	1.49	1.08	0.76	1.39	0.81
	sd	11.44	11.72	13.12	8.01	16.18	34.64	13.67	8.14	15.08	8.20	16.35	26.11	20.66	15.65	17.61	12.91
SR	*capacity K*	0.21	0.43	0.56	0.47	0.24	0.53	0.93	0.49	1.42	0.92	1.58	0.80	1.20	0.62	1.39	0.62
	sd	22.33	35.28	15.15	10.53	20.74	57.87	14.39	7.45	13.95	8.02	13.41	20.44	21.65	17.79	17.86	10.19
EnsInt	*g*	0.8	0.41	0.64	0.3	0.69	0.39	0.53	0.24	0.29	0.28	0.28	0.30	0.32	0.24	0.29	0.29
	sd	22.25	22.79	15.72	14.13	16.27	28.57	14.16	11.1	15.13	12.29	13.43	9.30	22.02	25.40	17.61	14.80
			1.29×		1.35×		1.26×	6.78×	3.21×		1.33×		3.52×		1.42×		2.81×
	samples	0.47	10^{12}	10.42	10^{12}	1.65	10^{13}	10^{11}	10^{12}	0.51	10^{12}	0.56	10^{12}	0.82	10^{12}	1.04	10^{12}
Swap												1.09×					
	g	0.72	0.34	0.47	0.27	0.69	0.33	0.48	0.23	0.14	0.22	10^{-10}	0.19	0.13	0.17	0.12	0.22
										2.25×							
	B	0.05	0.28	0.04	0.23	0.02	0.17	0.02	0.06	10^{-8}	0.13	0.04	0.15	0.16	0.18	0.09	0.10
	sd	17.36	18.91	16.31	14.21	16.27	66.22	14.49	7.14	15.92	22.18	18.01	24.58	24.70	15.22	20.09	11.45
VPG	*g*	0.94	0.12	0.75	0.26	0.87	0.2	0.55	0.25	0.28	0.29	0.26	0.30	0.38	0.25	0.29	0.25
	mode-	6.01×		7.39×		5.55×	2.55×	5×	1.63×	4.61×		3.65×		1.47×	4.71×	2.28×	
	Precision	10^{-4}	1.28	10^{-4}	0.02	10^{-4}	10^{-3}	10^{-4}	10^{-3}	10^{-3}	0.90	10^{-3}	0.01	10^{-3}	10^{-3}	10^{-3}	0.08
		5.02×		5×		5×	3.9×	6.07×	8.24×	1×		1×				1×	
	sdPrecision	10^{-4}	14.38	10^{-4}	10.47	10^{-4}	10^{-3}	10^{-4}	10^{-3}	10^{-3}	19.61	10^{-3}	0.01	1×10^{-3}	0.03	10^{-3}	26.69
VP	*mode-*	5×	5.35×	5×	8.88×	5×	6.14×	5×	1.55×	1×		1×	3.34×		2.76×	1×	3.48×
	Precision	10^{-4}	10^{-12}	10^{-4}	10^{-11}	10^{-4}	10^{-12}	10^{-4}	10^{-11}	10^{-3}	0.04	10^{-3}	10^{-3}	1×10^{-3}	10^{-3}	10^{-3}	10^{-3}
		1.64×	1.04×	1.66×	3.15×	1.64×	2.11×	1.65×	4.53×	4.56×		4.49×		3.71×		3.52×	
	*sd*Precision	10^{-3}	10^{-4}	10^{-3}	10^{-4}	10^{-3}	10^{-4}	10^{-3}	10^{-4}	10^{-3}	0.32	10^{-3}	0.01	10^{-3}	0.01	10^{-3}	0.03

Table S12 *(continued)*

		Exp3				*Exp4*				*Exp5*			
		Short SOA		**Long SOA**		**Short SOA**		**Long SOA**		**Short SOA**		**Long SOA**	
Model	**Parameter**	**Median**	**SD**	**Median**	**SD**	**Median**	**SD**	**Median**	**SD**	**Median**	**SD**	**Median**	**SD**
StM	*g*	0.72	0.33	0.43	0.32	0.54	0.25	0.43	0.19	0.61	0.31	0.59	0.3
	sd	15.35	16.54	17.29	10.80	14.55	10.36	15.49	7.21	18.95	13.59	15.24	17.52
Slot	*capacity K*	0.56	0.73	1.13	0.82	0.92	0.53	1.14	0.41	0.72	0.64	0.77	1.64
	sd	13.76	16.75	17.29	12.45	14.55	10.36	15.49	7.21	18.16	26.34	13.41	17.53
SR	*capacity K*	0.56	0.82	1.13	0.95	0.92	0.79	1.14	0.41	0.97	0.75	0.75	1.12
	sd	20.53	12.36	15.54	9.26	16.28	7.75	14.72	5.50	23.33	42.1	15.22	16.46
EnsInt	*g*	0.68	0.33	0.53	0.32	0.51	0.25	0.43	0.19	0.44	0.33	0.59	0.31
	sd	13.76	18.90	13.92	8.12	14.22	10.92	15.51	7.19	22.21	45.71	14.89	13.3
	samples	2.19	8.51×10^{12}	2.12×10^{11}	5.21×10^{12}	3.85×10^{11}	5.11×10^{12}	1.65×10^{12}	5×10^{12}	1.23×10^{12}	6.22×10^{12}	4.27×10^{11}	5.57×10^{12}
Swap	*g*	0.35	0.31	0.3	0.33	0.4	0.24	0.33	0.19	0.44	0.34	0.51	0.31
	B	0.08	0.23	1.14×10^{-10}	0.20	0.05	0.08	0.04	0.09	1.75×10^{-3}	0.25	3.41×10^{-14}	0.29
	sd	25.61	46.16	19.65	13.54	14.61	9.95	15.36	6.91	20.96	59.92	16.00	14.67
VPG	*g*	0.84	0.24	0.49	0.34	0.54	0.19	0.40	0.18	0.75	0.3	0.61	0.29
	mode-Precision	6.35×10^{-4}	0.01	5.67×10^{-4}	0.03	5×10^{-4}	1.22×10^{-3}	5.04×10^{-4}	3.52×10^{-4}	5.04×10^{-4}	5.82×10^{-4}	5.15×10^{-4}	4.05×10^{-3}
	sdPrecision	5.75×10^{-4}	10.2	5×10^{-4}	4.75×10^{-3}	5.25×10^{-4}	0.91	5.11×10^{-4}	0.01	1.07×10^{-3}	0.02	5×10^{-4}	0.02
VP	*mode-Precision*	5×10^{-4}	8.89×10^{-12}	5×10^{-4}	7.49×10^{-4}	5×10^{-4}	9.77×10^{-12}	5×10^{-4}	1.23×10^{-11}	5×10^{-4}	1.99×10^{-11}	5×10^{-4}	1.03×10^{-4}
	mode-sdPrecision	1.62×10^{-3}	2.78×10^{-4}	1.47×10^{-3}	2.35×10^{-3}	1.58×10^{-3}	2.93×10^{-4}	1.52×10^{-3}	4.32×10^{-4}	1.59×10^{-3}	6.02×10^{-4}	1.58×10^{-3}	0.01

4. Wang et al.

Table S13

Model comparison results for T2 performance in the T1 correct condition (T2|T1).

		CC				CO				OC				OO			
Lag	**Model**	**Mean AIC**	**Mean ΔAIC**	**Mean Rank**	**Mean Log-Likeli-hood**	**Mean AIC**	**Mean ΔAIC**	**Mean Rank**	**Mean Log-Likeli-hood**	**Mean AIC**	**Mean ΔAIC**	**Mean Rank**	**Mean Log-Likeli-hood**	**Mean AIC**	**Mean ΔAIC**	**Mean Rank**	**Mean Log-Likeli-hood**
1	StM	277.06	1.25	3.16	-136.53	338.47	0.47	2.36	-167.23	233.70	1.01	3.25	-114.85	124.84	1.29	2.82	-60.42
	Slot	277.06	1.25	2.88	-136.53	338.48	0.48	2.41	-167.24	233.70	1.01	2.43	-114.85	124.73	1.19	2.48	-60.37
	SR	277.98	2.17	3.39	-136.99	338.50	0.50	2.41	-167.25	234.13	1.44	2.75	-115.06	124.84	1.29	2.41	-60.42
	EnsInt	278.17	2.36	4.84	-136.09	340.17	2.17	5.20	-167.09	234.57	1.88	4.79	-114.29	125.37	1.83	4.36	-59.69
	Swap	277.24	1.43	4.30	-135.62	340.47	2.47	5.55	-167.23	235.63	2.94	6.32	-114.82	125.35	1.81	4.61	-59.68
	VPG	278.74	2.93	5.82	-136.37	340.63	2.63	5.75	-167.32	235.24	2.55	5.82	-114.62	127.54	3.99	6.39	-60.77
	VP	277.86	2.05	3.61	-136.93	342.66	4.66	4.32	-169.33	233.16	0.47	2.64	-114.58	127.97	4.42	4.93	-61.98
3	StM	371.72	1.64	3.00	-183.86	371.13	0.44	2.41	-183.57	219.47	1.31	3.07	-107.73	309.69	3.60	2.73	-152.85
	Slot	371.72	1.64	2.79	-183.86	371.03	0.33	2.21	-183.51	219.47	1.31	2.61	-107.73	309.65	3.56	2.48	-152.83
	SR	375.11	5.03	4.36	-185.56	371.05	0.36	2.23	-183.53	220.51	2.35	3.25	-108.25	309.56	3.46	2.29	-152.78
	EnsInt	373.23	3.15	5.30	-183.62	372.61	1.92	4.55	-183.31	220.83	2.67	5.00	-107.41	309.87	3.77	3.86	-151.93
	Swap	373.03	2.95	5.38	-183.52	372.41	1.71	4.13	-183.20	221.32	3.17	5.93	-107.66	308.52	2.43	4.07	-151.26
	VPG	372.37	2.29	4.75	-183.19	373.74	3.05	5.68	-183.87	220.52	2.36	5.18	-107.26	312.17	6.08	5.68	-153.09
	VP	371.08	1.00	2.43	-183.54	397.39	26.70	6.79	-196.70	218.74	0.59	2.96	-107.37	336.39	30.30	6.89	-166.20
8	StM	378.88	1.90	3.07	-187.44	347.09	0.59	2.30	-171.55	220.87	1.29	3.23	-108.43	331.65	1.24	2.23	-163.82
	Slot	378.89	1.91	2.86	-187.44	347.09	0.59	2.30	-171.55	221.25	1.67	2.80	-108.63	331.65	1.24	2.23	-163.82
	SR	380.89	3.92	3.68	-188.45	347.09	0.59	2.25	-171.55	221.10	1.51	3.04	-108.55	331.65	1.24	2.29	-163.82
	EnsInt	380.41	3.43	5.25	-187.20	348.38	1.87	4.39	-171.19	221.87	2.29	4.71	-107.93	333.17	2.76	4.46	-163.58
	Swap	380.28	3.30	5.50	-187.14	348.69	2.18	4.75	-171.34	222.76	3.18	6.50	-108.38	332.16	1.76	4.46	-163.08
	VPG	379.39	2.42	4.96	-186.70	349.22	2.71	5.61	-171.61	222.12	2.54	5.25	-108.06	334.13	3.72	6.11	-164.06
	VP	377.73	0.75	2.68	-186.86	363.37	16.86	6.39	-179.68	220.38	0.79	2.46	-108.19	343.72	13.31	6.21	-169.86

Note. CC = color-color target pair; CO = color-orientation target pair; OC = orientation-color target pair; OO = orientation-orientation target pair. See *2.1. Model details* of the main text for the model abbreviations.

Table S14

Model comparison results for T2 performance in the T1 incorrect condition.

	Lag 1				Lag 3				Lag 8			
Model	**MeanAIC**	**Mean ΔAIC**	**Mean Rank**	**Mean Log-Likelihood**	**MeanAIC**	**Mean ΔAIC**	**Mean Rank**	**Mean Log-Likelihood**	**MeanAIC**	**Mean ΔAIC**	**Mean Rank**	**Mean Log-Likelihood**
StM	614.14	12.62	3.61	-305.068	336.86	0.95	2.46	-166.429	277.62	0.63	2.59	-136.808
Slot	613.96	12.45	3.34	-304.982	336.88	0.97	2.61	-166.44	277.58	0.60	2.52	-136.791
SR	613.87	12.35	3.30	-304.934	336.88	0.97	2.61	-166.44	277.62	0.63	2.54	-136.808
EnsInt	613.65	12.14	4.04	-303.825	338.27	2.36	4.38	-166.135	278.62	1.63	4.34	-136.309
Swap	601.55	0.04	1.11	-297.775	337.24	1.33	3.77	-165.618	279.29	2.31	5.16	-136.645
VPG	616.12	14.61	5.71	-305.061	338.91	3.01	5.54	-166.457	279.04	2.05	5.00	-136.519
VP	652.02	50.51	6.89	-324.01	352.78	16.88	6.64	-174.392	286.00	9.01	5.86	-140.998

Note. For the T1 incorrect condition, analyses were conducted for each specific lag, across all target pairs. See the main text for a more detailed discussion.

Table S15

Maximum-likelihood estimates of the parameters in all models in the T1 correct condition.

		CC						CO					
		Lag 1		Lag 3		Lag 8		Lag 1		Lag 3		Lag 8	
Model	**Parameter**	**Median**	**SD**	**Median**	**SD**	**Median**	**SD**	**Median**	**SD**	**Median**	**SD**	**Median**	**SD**
StM	*g*	0.07	0.11	0.04	0.07	0.06	0.08	0.06	0.14	0.33	0.33	0.29	0.30
	sd	9.13	2.83	8.84	1.71	8.95	1.73	14.61	9.88	17.71	17.29	15.38	6.03
Slot	*capacity K*	1.86	2.36	1.91	1.45	1.88	0.92	1.87	1.17	1.32	1.16	1.41	0.60
	sd	9.13	2.83	8.84	1.71	8.95	1.77	14.88	9.87	15.67	16.82	14.70	8.63
SR	*capacity K*	2.20	1.01	2.61	1.02	2.59	0.83	1.90	0.86	1.32	0.90	1.44	0.78
	sd	6.84	1.98	7.62	1.20	6.99	1.13	11.16	6.81	18.86	11.81	13.13	31.61
EnsInt	*g*	0.07	0.11	0.04	0.07	0.06	0.08	0.09	0.24	0.29	0.34	0.30	0.29
	sd	8.89	2.82	8.73	1.74	8.75	1.69	13.82	6.25	19.74	19.33	13.13	7.78
	samples	4.27	2.24×10^{12}	5.78×10^{11}	3.18×10^{12}	5.06×10^{10}	2×10^{12}	21.42	$2{,}18\times10^{12}$	2.78×10^{11}	4.54×10^{12}	9.25	2.57×10^{12}
Swap	*g*	6.37×10^{-8}	0.09	0.04	0.07	0.02	0.08	0.06	0.12	0.23	0.29	0.27	0.29
	B	0.02	0.05	1.52×10^{-11}	0.02	4.36×10^{-13}	0.02	5.42×10^{-7}	0.07	4.8×10^{-3}	0.13	7.36×10^{-14}	0.04
	sd	9.20	2.37	8.82	1.57	8.95	2.06	14.74	8.46	20.87	16.49	15.22	15.37
VPG	*g*	0.03	0.11	5.85×10^{-6}	0.07	8.16×10^{-4}	0.06	0.07	0.22	0.66	0.26	0.29	0.3
	mode-Precision	1.73×10^{-3}	1.13×10^{-3}	1.97×10^{-3}	1.54×10^{-3}	1.81×10^{-3}	3.82×10^{-3}	6.75×10^{-4}	5.19×10^{-4}	5.22×10^{-4}	0.17	6.24×10^{-4}	7.67×10^{-4}
	sdPrecision	9.38×10^{-4}	0.01	1.1×10^{-3}	0.03	1.8×10^{-3}	0.03	5.01×10^{-4}	6.31×10^{-3}	5×10^{-4}	13.11	5×10^{-4}	8.06×10^{-3}
VP	*mode-Precision*	1.64×10^{-3}	9.67×10^{-4}	2.25×10^{-3}	1.58×10^{-3}	1.97×10^{-3}	2.04×10^{-3}	5.44×10^{-4}	5.21×10^{-4}	5×10^{-4}	1.73×10^{-4}	5×10^{-4}	4.47×10^{-4}
	sdPrecision	2.63×10^{-3}	0.01	3.47×10^{-3}	0.03	3.88×10^{-3}	7.02×10^{-3}	1.12×10^{-3}	5.99×10^{-3}	1.52×10^{-3}	1.15×10^{-3}	1.68×10^{-3}	5.56×10^{-3}

Table S15 *(continued)*

		OC						OO					
		Lag 1		Lag 3		Lag 8		Lag 1		Lag 3		Lag 8	
Model	**Parameter**	**Median**	**SD**	**Median**	**SD**	**Median**	**SD**	**Median**	**SD**	**Median**	**SD**	**Median**	**SD**
StM	*g*	2.05×10^{-14}	0.04	1.12×10^{-13}	0.08	3.24×10^{-14}	0.06	6.28×10^{-14}	0.26	0.51	0.38	0.28	0.30
	sd	7.75	2.62	7.73	2.60	7.43	2.43	15.54	10.26	15.91	41.36	18.56	10.40
Slot	*capacity K*	2.43	2.32	2.05	2.01	2.35	2.35	2.12	1.51	0.99	1.17	1.43	1.67
	sd	7.75	2.62	7.73	2.60	7.43	2.67	15.37	10.61	13.84	25.95	18.56	12.42
SR	*capacity K*	2.76	0.85	2.74	1.00	2.74	0.90	2.05	1.22	1.12	1.01	1.43	0.62
	sd	5.61	1.85	6.14	1.84	5.93	1.86	13.26	6.89	17.77	60.31	15.68	50.19
EnsInt	*g*	1.13×10^{-14}	0.06	0.02	0.08	6.41×10^{-15}	0.06	1.29×10^{-4}	0.22	0.46	0.36	0.28	0.27
	sd	7.75	2.72	7.54	2.54	7.35	2.54	15.93	9.89	19.87	44.40	18.32	7.95
	samples	1.36	1.8×10^{12}	2.09	2.25×10^{12}	14.07	2.78×10^{12}	8.96	8.72×10^{12}	0.47	5.85×10^{12}	6.52×10^{12}	8.99×10^{12}
Swap	*g*	2.37×10^{-9}	0.03	1.45×10^{-5}	0.07	3.04×10^{-8}	0.06	1.93×10^{-9}	0.21	0.29	0.27	0.22	0.22
	B	9.58×10^{-14}	0.03	2.65×10^{-14}	0.02	3.14×10^{-14}	0.01	8.95×10^{-6}	0.23	7.27×10^{-6}	0.32	2.26×10^{-14}	0.25
	sd	7.75	2.42	7.73	2.59	7.46	2.44	14.12	8.90	14.34	44.83	16.16	13.24
VPG	*g*	1.15×10^{-8}	0.03	2.38×10^{-4}	0.05	2.38×10^{-6}	0.04	0.03	0.28	0.69	0.27	0.41	0.31
	mode-Precision	3.05×10^{-3}	5.49×10^{-3}	2.82×10^{-3}	7.39×10^{-3}	2.97×10^{-3}	2.86	6.67×10^{-4}	0.03	6.79×10^{-4}	5.78×10^{-3}	5.08×10^{-4}	1.68×10^{-4}
	sdPrecision	9.36×10^{-4}	3.38×10^{-3}	1.08×10^{-3}	0.03	1.73×10^{-3}	9.45	5.19×10^{-4}	0.1	5×10^{-4}	9.45	5×10^{-4}	6.93×10^{-4}
VP	*mode-Precision*	2.54×10^{-3}	3.27×10^{-3}	2.81×10^{-3}	3.41×10^{-3}	2.96×10^{-3}	1.41	5×10^{-4}	2.13×10^{-4}	5×10^{-4}	2.01×10^{-5}	5×10^{-4}	1.02×10^{-4}
	sdPrecision	9.15×10^{-4}	0.02	2.92×10^{-3}	3.04×10^{-2}	1.74×10^{-3}	9.45	9.6×10^{-4}	5.13×10^{-3}	1.6×10^{-3}	4.77×10^{-4}	1.37×10^{-3}	3.59×10^{-4}

Table S16

Maximum-likelihood estimates of the parameters in all models in the T1 incorrect condition.

		Lag 1		Lag 3		Lag 8	
Model	**Parameter**	**Median**	**SD**	**Median**	**SD**	**Median**	**SD**
StM	*g*	0.54	0.29	0.60	0.26	0.33	0.20
	sd	15.56	9.91	9.64	7.76	10.88	5.11
Slot	*capacity K*	0.93	0.56	0.80	1.37	1.24	0.48
	sd	14.12	36.64	9.64	7.76	10.77	5.47
SR	*capacity K*	0.93	0.56	0.80	0.78	1.33	0.51
	sd	14.12	36.64	11.75	10.20	9.58	3.88
EnsInt	*g*	0.33	0.28	0.55	0.28	0.33	0.20
	sd	18.25	14.46	10.03	10.45	10.08	5.64
	samples	0.97	2.48×10^{12}	8.29	1.83×10^{12}	3.51×10^{11}	5.82×10^{12}
Swap	*g*	0.22	0.18	0.38	0.23	0.26	0.19
	B	0.26	0.13	0.04	0.14	4.87×10^{-14}	0.07
	sd	15.30	6.33	10.69	10.48	11.97	5.29
VPG	*g*	0.57	0.24	0.55	0.24	0.35	0.19
	mode-Precision	5.09×10^{-4}	2.14	1.13×10^{-3}	2.42×10^{-3}	1.15×10^{-3}	5.25×10^{-3}
	sdPrecision	5.68×10^{-4}	9.44	5×10^{-4}	9.45	5×10^{-4}	4.23
VP	*mode-Precision*	5×10^{-4}	2.15×10^{-11}	5×10^{-4}	2.3×10^{-9}	5×10^{-4}	2.69×10^{-4}
	sdPrecision	1.64×10^{-3}	8.26×10^{-4}	1.97×10^{-3}	0.01	2.37×10^{-3}	9.22×10^{-3}

B. Additional analysis for the Ensemble Integration (EnsInt) and Swap models, using the data from Tang et al. (2022).

We performed an extended analysis of the EnsInt and Swap models using the data from Tang et al. (2022), aiming to examine the potential interactions between the target (e.g., T2) and the subsequent mask. Specifically, we introduced three versions for these two models: 1) With-T1. This is the original model discussed in the main text, which accounts for T1 as the sole distractor in the analysis. 2) With-T2mask. This model uniquely considers the subsequent mask as the distractor. 3) With-Both. This model incorporates both T1 and the subsequent mask as the distractors of T2. The methodologies for the model fitting and comparison are consistent with those described in *2. Method* of the main text.

In the analysis of the EnsInt model (Figure S1), we observed different patterns between Experiment 1 and Experiment 2. For Experiment 1, the With-T1 version exhibited the best fitness to the data at shorter lags (Lag 1, 2 and 3), compared to longer lags (Lag 5 and 7). In contrast, the With-T2mask version's performance improved with increasing lag, as indicated at both the subject and group levels. This trend may be attributed to the growing temporal distance between T1 and T2; at longer lags, T2 is more influenced by the subsequent mask than by T1. For Experiment 2, the With-T2mask version showed better fitness both at Lag 3 and Lag 7. Generally, the differences of AIC values are relatively minor (within the range from 0 to 10).

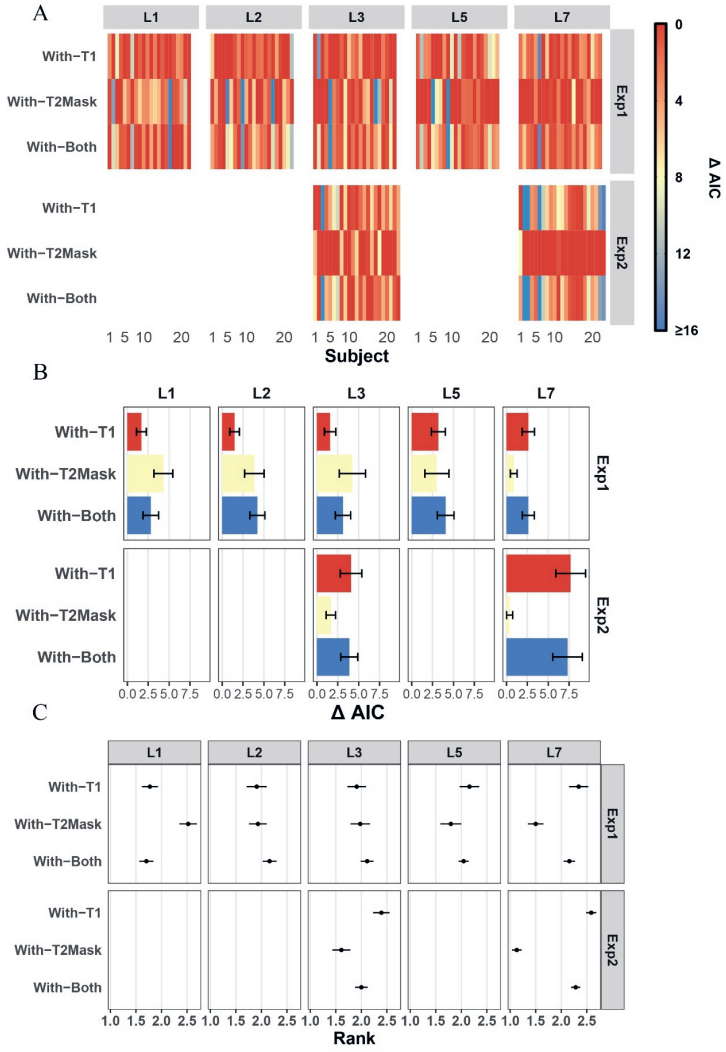
In the analysis of the Swap model (Figure S2), the difference among these three variants were slightly larger, compared to those observed in the EnsInt model. For Experiment 1, it was clearly observed that the With-T1 version consistently showed a superior performance across different lags, although the With-T2mask's fitness improved as lag increased. This suggests that as the time interval between two targets increases, the likelihood of swaps between T2 and its subsequent mask increases. However, despite the observed increase in fitness for the With-T2mask version at longer lags, we still believe that T1 is likely to be a predominant distractor to T2, with regard to potential swap errors. For Experiment 2, the differences among these versions were small at Lag 3. At Lag 7, the With-T2mask showed a slightly better performance than others, which was consistent with the trend observed in the EnsInt model analysis.

Considering the relatively small differences among the variants of both the EnsInt and Swap models, along with the good performance of the With-T1 version of the model, we chose to present this version in the main text for simplicity. It is important to note, however, that our choice did not rule out the potential influence of the subsequent mask's interaction. Unfortunately, due to the design of other datasets, where no identical item types followed T2, we are unable to conduct a similar extended analysis in those cases. Our focus on the With-T1 version is thus a

reflection of both the data available, and our aim to maintain a streamlined presentation.

Figure S1

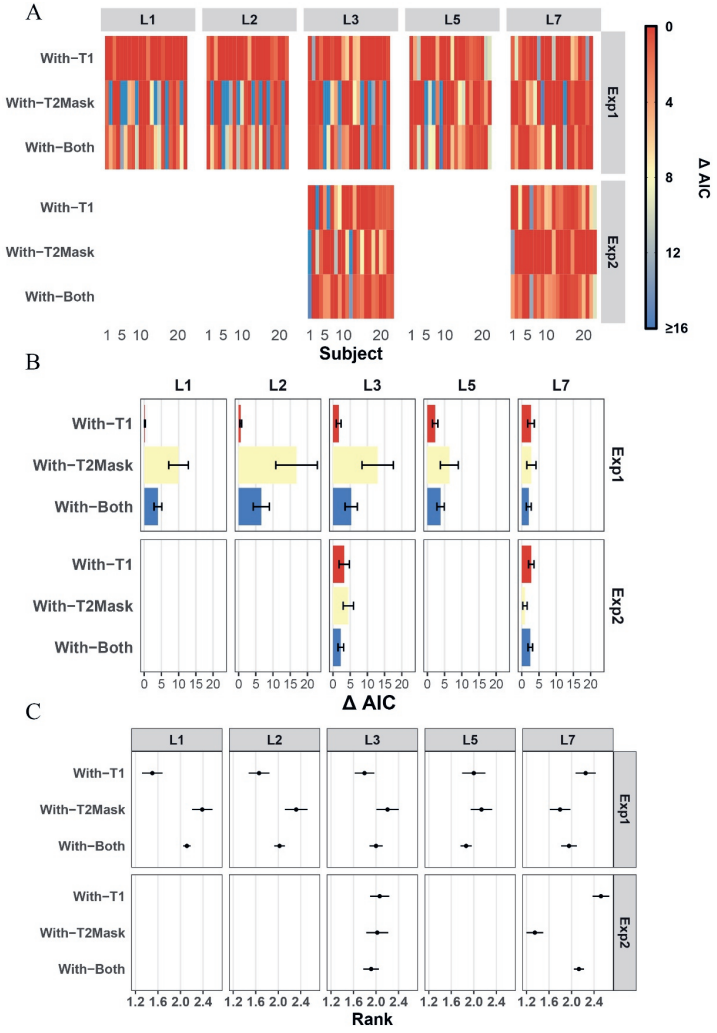
Model comparison results for the EnsInt model and its variants.



Note. With-T1 = only T1 is considered as the distractor. With-T2Mask = only the subsequent mask of T2 is considered as the distractor. With-Both = both T1 and the subsequent mask of T2 are considered as the distractors. L1 = Lag 1; L2 = Lag 2; L3 = Lag 3; L5 = Lag 5; L7 = Lag7. Exp = Experiment. (**A**) Model comparison results at the subject level, using the data from Tang et al. (2020) (**B**) Relative AIC values compared to that of the best-performing model, averaged across all subjects. (**C**) Average model ranking.

Figure S2

Model comparison results for the Swap model and its variants.



Note. (**A**) Model comparison results at the subject level, using the data from Tang et al. (2020) (**B**) Relative AIC values compared to that of the best-performing model, averaged across all subjects. (**C**) Average model ranking. Figure conventions follow Figure S1.

Chapter 3

Visual Awareness under Temporal Constraints

Published as:
Wang, S., Karabay, A., & Akyürek, E. G. (2024). Attentional blur and blink: Effects of adaptive attentional scaling on visual awareness. *Consciousness & Cognition*, *117*, 103627. https://doi.org/10.1016/j.concog.2023.103627

Abstract

Attentional scaling is a crucial mechanism that enables us to flexibly allocate our attention to larger or smaller regions in the visual field. Although previous studies have demonstrated the critical role of attentional scaling in visual processing, its impact on modulating visual awareness is not yet fully understood. This study investigates the adaptive control of attentional scaling and its influence on visual awareness in an attentional blink paradigm. Participants were required to attend to the first target's location, which was manipulated either session-wise, trial-wise, or such that it could be learned across a block of trials. Discrete, all-or-none, awareness was expected when attention was allocated to a narrow area, while gradual awareness was expected when attention was allocated to a larger area. We used mixture modeling to assess second target awareness across these different attentional scales. The results revealed that participants could adaptively control their attentional scale both across stable sessions, and through (implicit) statistical learning in blocks of successive trials. This produced gradual perceptual awareness when the participants adopted a broad attentional scale, causing an attentional "blur". However, trial-wise cues did not allow for attentional scaling, resulting in more discrete target perception overall, and an attentional "blink". We conclude that the attentional scale is to some extent under adaptive control during the attentional blink/blur, where it can produce qualitatively different modes of perceptual awareness.

Keywords: Attentional scale; visual awareness; attentional control; statistical learning

Chapter 3

1. Introduction

The human visual system faces the task of processing a vast and complex visual environment. To deal with this, we rely on selective attention, which allows prioritization and filtering of visual stimuli based on their relevance to the task at hand. One way in which such filtering is achieved is through attentional scaling. Attentional scaling entails controlling the size of the attentional 'zoom lens' across particular regions of the visual field (for a review, see Lawrence et al., 2020b). As the lens metaphor implies, changing its scale (also referred to as scope) will include or exclude stimuli, depending on whether they fall within its perimeter.

The original zoom lens model was proposed by Eriksen and Yeh (1985; also see Eriksen & St. James, 1986), to elucidate the relationship between attentional scale and visual perception. According to the zoom lens model, attentional resources are not distributed over a fixed extent of visual space, but rather to variable sizes, depending on task demands. By adjusting the size of the attentional zoom lens, that is, the spatial scale of attention, the attention system facilitates efficient information processing. Whereas a broad scale of attention enables information processing across a relatively large visual region, narrowing attention allows the limited supply of attentional resources to be concentrated in a small region, which critically results in heightened perceptual ability within that region. Following Eriksen and his colleagues, many studies have provided evidence for the hypothesis that there is a trade-off between the area across which attentional resources are distributed and the processing power within that specific visual area (Barriopedro & Botella, 1998; Castiello & Umiltà, 1990; Greenwood & Parasuraman, 1999, 2004; Turatto et al., 2000).

While these studies have thus confirmed that there is an effect of attentional scaling on visual perception, it is important to underline that this conclusion was largely based on response times recorded during tasks requiring visuospatial information processing. Nonetheless, a handful of studies have delved into the effects of attentional scaling on other aspects of visual processing. For instance, a study conducted by Balz and Hock (1997) found that having a narrow attentional scale improved both response time and spatial resolution. In their study, participants undertook two tasks: Detecting increments either in central dots (a narrow attentional scale) or peripheral dots (a broad attentional scale), and doing a vernier alignment. Just-noticeable-differences (JNDs) were smaller in the latter task in the narrow attention condition, suggesting higher spatial resolution when attention was narrowly focused. Later, Müller et al. (2003) found that the extent of the activated area in visual cortex increased under broad attentional focus compared to narrow attentional focus, whereas the activation magnitude decreased.

In a recent study, Lawrence and colleagues (2020a) went beyond exploring the influence of the distribution of attentional resources on spatial acuity by

investigating its effect on temporal acuity. They utilized both response time and accuracy as measures and manipulated attentional scale by varying the size of a 'global motion inducer', which required participants to spread their attention over the entire inducer area to perceive stimulus movement. After several inducer trials were conducted to set the attentional scale, participants then completed either spatial or temporal gap detection tasks. The results of Lawrence et al.'s study (2020a) showed that a narrow attentional scale improved both spatial and temporal acuity, as indicated by faster response times and higher response accuracy (but see also Goodhew et al., 2016).

1.1. Attentional scaling and visual awareness

Evidence for an even more profound effect of attentional scaling was recently obtained, showing that the nature of awareness also changes with the scale of attention (Karabay et al., 2022; Thiruvasagam & Srinivasan, 2021). When the attentional scale covers only a single location or local-level stimuli (narrow scale), conscious awareness operates in an all-or-none manner. In contrast, conscious awareness exhibits a gradual characteristic if the attentional scale is spread across multiple locations or to global-level stimuli (broad scale). In the study by Thiruvasagam and Srinivasan (2021), hierarchical letters (also called Navon letters; Navon, 2003) were used to alter the attentional scale. The stimuli were big letters or digits, in turn consisting of small letters or digits. They hypothesized that if the task was to report the big letter or digit, participants had to deploy a large scale of spatial attention to process global information. In contrast, reporting the small letters, or digits (local level) required a small attentional scale. Their results indicated the global attentional scale led to a more gradual awareness compared to the local attentional scale.

Evidence from the attentional blink (AB) suggests that scaling is subject to typical dwell time estimates that apply to attentional selection more generally (Karabay et al., 2022). The attentional blink is caused by the selection of a first, briefly presented target stimulus (T1), after which the selection of a subsequent second target (T2) is impaired for up to half a second (Broadbent & Broadbent, 1987; Duncan et al., 1994; Raymond et al., 1992; for a review see Dux & Marois, 2009). Karabay and colleagues (2022) manipulated the scale required to optimally process T1, by having it appear at either a single, predictable location (inducing a narrow scale), or unpredictably at either of two different locations (broad scale)[4]. T1-induced scaling affected the AB, that is, the performance on T2 at short lag.

[4] Karabay et al. (2022) referred to strong and weak gating, for the narrow and broad attentional scale conditions, respectively. Since we are specifically focusing on differences in the extent of attention exclusively, rather than other possible factors (e.g., working memory load or mental fatigue) that might more generally affect gating strength, we will use the scaling terminology in the present paper.

Although overall accuracy was not much changed, mixture modeling showed that the nature of the T2 responses that were given was qualitatively different. Mixture modeling allows for a decomposition of T2 performance into two key components: Memory precision and guess rate (Zhang & Luck, 2008). Specifically, responses are thought to follow a composite distribution, consisting of a von Mises distribution (for continuous circular feature values), centered on the actual target value, and a flat uniform distribution. Responses assigned to the von Mises distribution show evidence of partial target knowledge, with the width of that distribution showing their relative precision. Responses assigned to the uniform distribution do not show evidence of actual target knowledge, that is, they are random guesses, and the height of this distribution thus shows the overall guess rate. By comparing target awareness across short and long temporal lags, Karabay and colleagues (2022) found that the AB causes a full (all-or-none) loss of target information, expressed solely as a higher guess rate, when participants had a narrow attentional scale. However, when they had a broad attentional scale, a gradual loss of target information was observed during the AB, resulting in both higher guess rate and lower precision estimates.

They proposed an adaptive gating hypothesis to explain the occurrence of both gradual and all-or-none awareness of blinked targets during the AB. According to this hypothesis, the attentional gate that determines which input eventually reaches conscious awareness, does not necessarily function in an all-or-none manner. Attentional gating strength follows a sigmoidal function, which modulates the availability of attentional resources. When attentional resources are broadly distributed across the possible locations of T1, attentional resources are diffused. As a compensatory mechanism, attentional gating strength is lower, trying to capture as much target-related information as possible. This lowered gating strength is especially consequential for T2 processing during the AB, allowing its perception to manifest in a more gradual manner. In contrast, when the attentional scale is narrowly concentrated on a single location of T1, cognitive resources are intensely focused on that particular region. This concentrated allocation sets a higher gating strength, ensuring that only targets that have been processed thoroughly are granted access to conscious awareness. As a result, the subsequent T2 awareness exhibits an all-or-none characteristic. Thus, the effects of scaling on temporal attention eventually resemble those found in spatial tasks (e.g., Balz & Hock, 1997; Müller et al., 2003).

1.2. The present study: Adaptive control of attentional scaling

As the studies discussed above also illustrate, the scale of attention can vary based on task demands (Burnett et al., 2013; Eriksen & St. James, 1986; Goodhew et al., 2016; Greenwood & Parasuraman, 1999, 2004; Lawrence et al.,

2020a; Müller et al., 2003). In their model of visual search, Greenwood and Parasuraman (1999; 2004) implemented attentional scaling as a critical component. Specifically, they assumed that attention scales are in response to different sizes of spatial cues. By measuring the response times during feature and conjunction search tasks, the authors concluded that the attentional scale was deployed dynamically according to task demands. According to their model, if the target locations were unpredictable, a broader attention scale is optimal to facilitate the detection over a large region. However, if pre-cues specified the target locations, a constricted attentional focus is more efficient for detecting small targets and enhancing their processing.

However, previous studies have mainly examined the effect of attentional scaling in visual processing in a repeated, blocked fashion (Castiello & Umiltà, 1990; Goodhew et al., 2016; Greenwood & Parasuraman, 2004; Karabay et al., 2022; Poggel et al., 2006). To what extent the attentional scale can be dynamically controlled thus remains an open question. Here, we investigated whether attentional scale changes similarly when it is set at the level of multiple blocks of trials, single blocks of trials, and when it is set on a per-trial basis. We employed an attentional blink task, in which the scale was manipulated by the possible location(s) of T1, and which we measured by the nature of awareness (gradual or discrete) of T2. Critically, we manipulated the scale of attention, such that it was either completely stable across one half of the experiment, largely stable across single blocks of trials, or entirely variable between trials. We expected that if control of the attentional scale is fully adaptive, then even trial-by-trial scaling should be possible. Conversely, if such control is not possible, then only the stable scenario may successfully elicit changes in attentional scale. Of particular interest was the intermediate, block-based condition, in which we tested whether (implicit) "statistical" learning over time might allow scaling.

Extensive research has shown that spatial attention in general can be guided by statistical learning of spatial regularities (for a review, see Theeuwes et al., 2022). In their early studies, Chung and Jiang (1998; 1999) reported that a repeatedly presented visual context, that is, the spatial layout of distractors, facilitated visual search performance compared to a 'novel' context. This facilitation was termed "contextual cueing". Subsequently, other authors examined the role of spatial regularities of distractor as well as target locations in visual search efficiency (Geng & Behrmann, 2002; 2005; Jiang et al., 2013; Wang & Theeuwes, 2018). When targets were presented at high-probability locations, visual search efficiency was enhanced in comparison to when the targets were presented at low-probability locations (Geng & Behrmann, 2002; 2005; Jiang et al., 2013). Moreover, Wang & Theeuwes (2018) demonstrated that high-probability distractor locations led to attentional suppression in that region, resulting in higher target search efficiency.

There is also limited evidence that attentional scaling is subject to this kind of trial-to-trial learning. In a study by Fuggetta and colleagues (Fuggetta et al., 2009), search reaction time was reduced for successive trials in which attentional scale was small, rather than large. However, in this study attentional scale was equated to the size of the search array, which leaves the possibility that this physical change, rather than attention, caused the effect. As in Karabay et al. (2022), attentional scaling in the present study pertained to T1, whereas we measured performance on T2, which was physically the same between conditions, thus avoiding this potential confound.

2. Experiment 1

Experiment 1 examined whether changing the attentional scale for T1 in an attentional blink task would alter visual awareness of T2. In this experiment, the attentional scale was controlled in a session-wise manner, and explicitly cued. In one half of the trials, T1 appeared only at a cued location, thus inducing a narrow attentional scale. In the other half of the trials, T1 location was not cued and not predictable, thus inducing a broad attentional scale. Thereby, this experiment implemented a within-subjects manipulation of the scaling conditions tested by Karabay and colleagues (2022), and we similarly assessed T2 performance by estimating memory precision and guess rate parameters through a standard version of the mixture model (Zhang & Luck, 2008). Changes in the former parameter were considered indicative of gradual target awareness, and changes in the latter as indicative of discrete awareness.

2.1. Method

2.1.1. Participants

Twenty-four undergraduates from the University of Groningen were recruited and awarded course credits for their participation. The number of participants was determined using G-power analysis (α = .05, β = .2; Faul et al., 2007). All participants reported normal or corrected-to-normal vision and gave written informed consent before starting the experiment. One participant was removed from analysis because their average error for T1 or T2|T1 exceeded 2.5 standard deviations above or below the grand mean. The final sample size was thus 23 (mean age = 20.74 years, age range = 18 to 31 years, fourteen females). The study was approved by the ethical committee of the Psychology Department of the University of Groningen (Research code PSY-2122-S-0269).

2.1.2. Apparatus and stimuli

Participants were seated individually in testing cabins with standard office lighting. The experiment was programmed and executed using OpenSesame 3.3 (Mathôt et al., 2012) on a desktop PC running the Microsoft Windows 10 operating system. The stimuli were presented on an LCD monitor (Iiyama Prolite G2773 HS), placed at a viewing distance of approximately 60 cm. The screen was set to 1,920 × 1,080 pixels display resolution, at an 8-bit color depth, and a 100 Hz refresh rate. Responses were collected using a standard USB computer mouse.

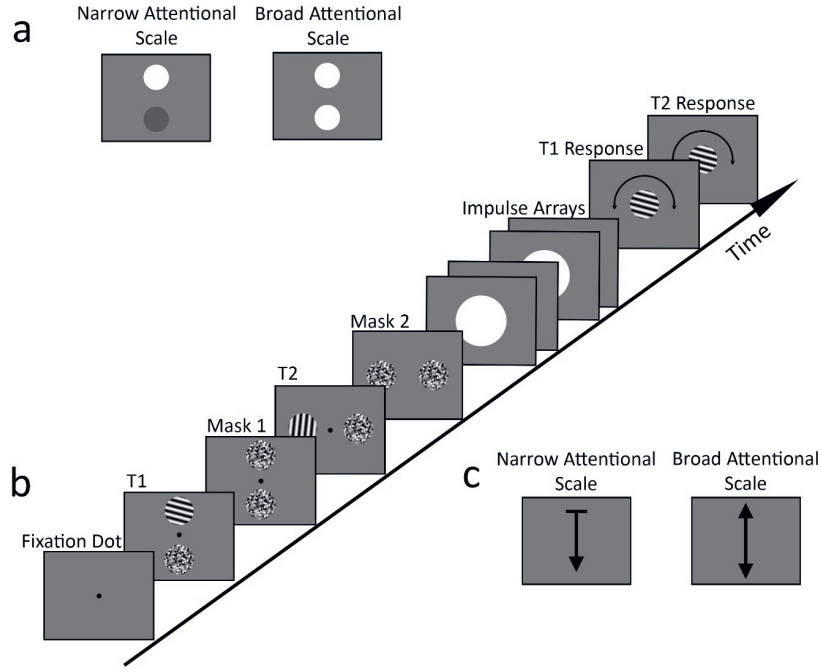
The target stimuli comprised a series of orientation gratings (1.7 cycles/degree, 2.3 degrees of visual angle) with 36 possible orientations. To get these orientations, we started from one degree and increased in steps of five degrees up to 179 degrees. This approach allowed us to evenly distribute the orientations across the full 180-degree spectrum. The orientations were randomly and independently selected for T1 and T2. In the T1 display, two visual stimuli (T1 and its distractor) appeared at a center-to-center distance of 2.8° above or below the fixation dot. In the T2 display, T2 and its distractor appeared at the same distance (2.8°) to the left and right side of fixation. Targets were backward masked by gray-scale mosaic circles of the same size as targets, which were generated as in Karabay et al. (2022). All stimuli were presented on a gray background (RGB 128, 128, 128).

2.1.3. Design and procedure

The design of the experiment is illustrated in Figure 1. Each participant completed two consecutive sessions based on the attentional scale condition, the order of which was counterbalanced between participants. Within each session, targets were separated by either a short or long inter-stimulus interval (ISI; detailed further below). Following 20 practice trials, in each session, there were 10 blocks, containing 20 experimental trials each. Within each session, there were 120 trials with short ISI, and 80 trials with long ISI, as we were primarily interested in the former. In the narrow attentional scale condition, T1 was pre-cued, and either appeared above fixation in the first five blocks, and below fixation in the last five blocks, or vice versa, which was again counterbalanced across participants. In the broad attentional scale condition, T1 location was also evenly distributed, but randomly chosen on each trial and not indicated in advance. In both conditions, a pre-cue display was shown at the start of each single block, which consisted of two filled circles (2.6° of visual angle) that appeared above and below the central fixation dot. The pre-cue remained on screen until participants pressed a key to continue. In the narrow attentional scale session, the pre-cue indicated the location of T1 (above or below fixation) with a white circle, while a dark gray (RGB 96, 96, 96) circle appeared on the other side. In the broad attentional scale session, the two

circles in the pre-cue display were both white, indicating that T1 would appear randomly above or below the fixation.

Figure 1



Note. **(a)** An example of the pre-cues used in Experiment 1, in which the pre-cues appeared at the beginning of each block. **(b)** Schematic of a single trial in Experiment 1. T1 refers to the first target and T2 refers to the second target. The time interval between T1 and T2 was either 250ms (short SOA) or 800ms (long SOA). **(c)** An example of the pre-cues used in Experiment 2, in which the pre-cues appeared at the beginning of each trial.

After the pre-cue, participants needed to press the space bar to start the trials. After a fixation dot was presented for 600-800ms, the T1 display was shown and remained on screen for 90ms, followed by a blank ISI for 10ms. Next, the first mask display, containing two masking circles, was shown with the same spatial arrangement as the T1 display for 90ms. After a short (60ms) or long (610ms) blank ISI, the T2 display was shown for 90ms, in which T2 appeared unpredictably at the left or right of the fixation dot (evenly distributed). After 10ms of ISI, the second mask display was presented on the screen for 90ms. After a delay of 750ms, participants were instructed to reproduce the T1 orientation by rotating an orientation probe (the same as the target stimuli). After an impulse array[5], an

[5] The impulse array had no function and was only included in our current behavioral study to ensure consistency with a future EEG study. The impulse does not affect behavioral performance (Wolff et al.,

identical T2 response display was shown. Finally, at the end of each block, there was a feedback display showing the average accuracy of each target. Participants were allowed to take self-paced breaks between blocks.

2.1.4. Analysis

Since the attentional scale that is applied to T1 affects perceptual awareness of T2 during the AB (Karabay et al., 2022), our primary interest lay with T2 reports at the short SOA, as a function of the attentional scale. Therefore, the final design had three cells: Narrow attentional scale at short SOA, broad attentional scale at short SOA, and long SOA. The long SOA, at which T2 is no longer subject to the AB, thus served as a control condition, and was not further separated into narrow and broad attentional scale conditions. We did not expect effects of scaling on the nature of awareness of T1, for which full attention is always available. However, we still examined T1 error rates (also see the model-based analysis for T1 performance in the Supplementary Material), as they may still give an indication of whether the manipulation of attentional scaling functioned or not, because elevated error rates might be expected in the broad attentional scale condition.

In the analyses, response error was assessed as the angular difference between the target and response value. Participants could make their response anywhere along the 180-degree spectrum. For any angular differences exceeding 90 degrees in one hemisphere, the corresponding difference in the opposite hemisphere was taken, ensuring that all error values remained between -90 and +90 degrees. In addition, as with the majority of traditional AB investigations, we only evaluated T2 performance in cases where the T1 response was accurate (i.e., absolute response error < 22.5°, following Karabay et al., 2022). The logic behind this is that the AB is elicited by the processing of T1, so that if T1 is missed, an AB does not occur, and the T2 response is not informative as such.

Using Bayesian one-way repeated-measures analysis of variance (ANOVA), the variations in T2|T1 response error across all task conditions were determined. We also utilized Bayesian post-hoc testing with a Cauchy prior (center = 0; r = 0.707) to determine where the discrepancies in T2|T1 error arose from. The prior indicates an 80% probability that the effect size falls within the range of -2 to 2 (Gronau et al., 2017). JASP Version 0.16.4.0 (JASP Team, 2022) was used for all of the T2|T1 error analyses. We followed Wetzel et al. (2011) while interpreting Bayes factors. BF_{10} values less than 1 indicate evidence in favor of the null hypothesis, while BF_{10} values greater than 1indicate evidence in favor of the alternative hypothesis. In detail, BF_{10} values between 1 and 3 are considered to provide

2017).

anecdotal evidence, BF_{10} values between 3 and 10 provide substantial evidence, BF_{10} values between 10 and 30 provide strong evidence, BF_{10} values between 30 and 100 provide very strong evidence and BF_{10} values above 100 provide decisive evidence for the model in question.

2.1.5. Mixture modeling

Along with the above measures of overall T2 accuracy, we also analyzed T2|T1 response error by fitting a standard mixture model (Zhang & Luck, 2008). We considered differences in model parameters (guess rate and in particular precision), rather than raw reproduction error most informative about the nature of awareness. Mixture modeling also allows for assessing response patterns across tasks that elicit variable levels of performance (e.g., color vs. orientation memories; Karabay et al., 2022). In the mixture model, participants' response errors fall into two types of distributions: a) a von Mises distribution with zero as its center, capturing responses that reflect (partial) target information in working memory; and b) a uniform distribution over all possible response errors (-90° to +90°), capturing responses that show no evidence that any target information was encoded in working memory. The standard deviation of the von Mises distribution indicates the precision (the inverse of σ) of the remembered target information (i.e., T2), while the height of the uniform distribution represents the probability of a random guessing response (P_g). The model-based analysis was performed using the CatContModel package (Hardman, 2016; version 0.8.0) in the R programming environment (R Core Team, 2022).

There are several steps involved in carrying out this mixture-modeling analysis (for more details, see Hardman et al., 2017; Ricker & Hardman, 2017). To investigate the effect of attentional scaling on T2 awareness, we generated four models by controlling which parameters (P_g and σ) vary across task conditions: (1) A full model where both P_g and σ vary across task conditions; (2) a model with constant precision and varying guess rate, where σ is fixed while P_g is variable; (3) a model with constant guess rate and varying precision, where P_g is fixed while σ is variable; (4) a fully constant model, where both parameters are kept constant across all task conditions. Next, we used a Bayesian hierarchical estimation approach with a Markov chain Monte Carlo (MCMC) sampling technique to obtain posterior distributions of parameters for these four models. The number of iterations separately for each model was set to 10,000, of which the first 1,000 iterations were used as burn-in and removed from the analysis. We then calculated the Watanabe-Akaike information criterion (WAIC) to compare these models. Following the selection of the best model (with the lowest WAIC), we performed Bayesian hypothesis testing on the parameter estimates taken from that model.

2.2. Results

2.2.1. Error

Although T1 error was relatively low (Table 1), T1 error was higher in the broad attentional scaling condition, compared to the narrow attentional scaling condition and/or long SOA. This pattern confirmed that our scaling manipulation had the expected effect on T1 performance. A more detailed summary of T1 performance is included in the Supplementary Materials.

Table 1

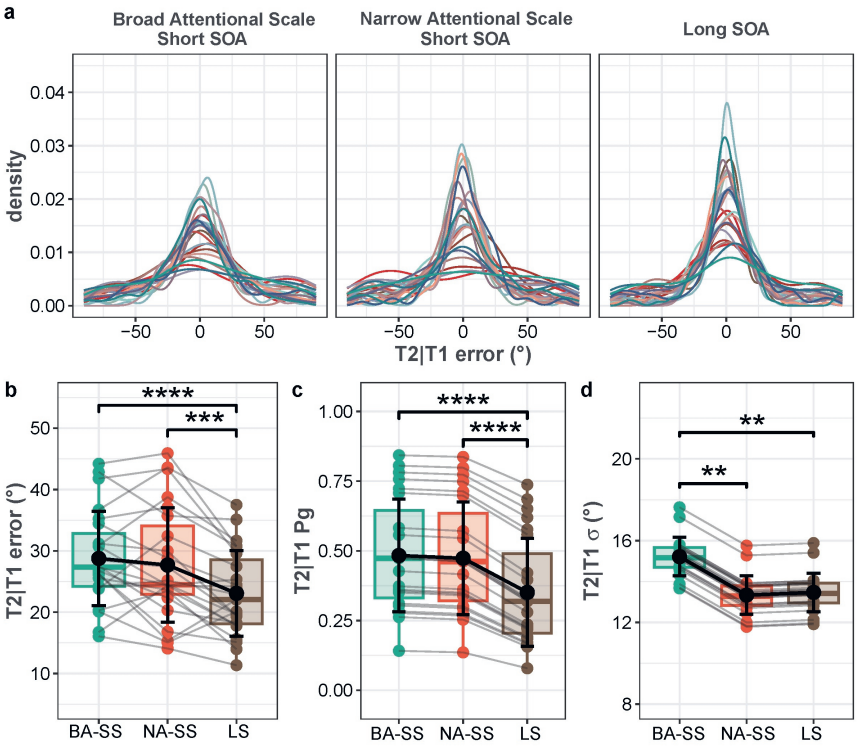
Average T1 error and percentage of trials in which absolute T1 error was smaller than 22.5° for all experiments

Experiment/Task Condition		Mean T1 error (°)		Absolute T1 error < 22.5° (%)	
		Mean	SEM	Mean	SEM
Exp 1					
	BA-SS	20.11	1.26	71.88	2.26
	NA-SS	18.48	1.26	74.28	2.47
	LS	17.69	1.22	75.92	2.44
Exp 2					
	BA-SS	23.05	1.98	66.83	3.55
	NA-SS	20.85	1.90	70.26	3.75
	LS	20.73	2.07	71.06	3.91
Exp 3					
	BA-SS	25.1	1.42	61.45	2.73
	NA-SS	23.39	1.63	65.30	2.91
	LS	22.46	1.38	66.47	2.69

Note. Exp = experiment; BA-SS = the broad attentional scale condition at short SOA; NA-SS = the narrow attentional scale condition at short SOA; LS = the long SOA condition.

The evidence of the main effect of task condition on T2|T1 error was decisive (BF_{10} > 1,000; Figure 2a-b). There was decisive evidence supporting a difference in T2|T1 accuracy between the broad attentional scale at short SOA and the long SOA (BF_{10} > 1,000), and very strong evidence for a difference between the narrow attentional scale at short SOA and the long SOA (BF_{10} = 93.34). The average absolute T2|T1 error was smaller at long SOA (23.07°; see Table 2), compared to the other two conditions at short SOA (28.76° for the broad attentional scale and 27.69° for the narrow attentional scale). The hypothesis testing results between the two attentional scale conditions at short SOA provided strong evidence against a difference in T2|T1 error (BF_{10} = .32).

Figure 2



Note. (**a**) Probability density plots of each participant's T2|T1 error distribution for each task condition. Each line indicates one participant. SOA = stimulus onset asynchrony; Short SOA corresponds to 250ms between T1 and T2, and Long SOA corresponds to 800ms between T1 and T2. (**b**) Absolute T2|T1 error in different task conditions. BA-SS = the broad attentional scale condition at short SOA; NA-SS = the narrow attentional scale condition at short SOA; LS = the long SOA condition. Colored dots represent individual data. Black dots with error bars represent averages with 95% confidence intervals. * represents substantial evidence against the null hypothesis ($3 < BF_{10} < 10$), ** represents strong evidence ($10 < BF_{10} < 30$), *** represents very strong evidence ($30 < BF_{10} < 100$), and **** represents decisive evidence ($BF_{10} > 100$)**.** (**c**) T2|T1 guess rate (*P*) estimates from the Full model, which was the best fitting model. (**d**) T2|T1 σ estimates from the same model.

Table 2

T2|T1 error and parameter (P and σ) estimates from the full model across task conditions for all experiments

Experiment/Task Condition		Error (°)		P_g		σ (°)	
		Mean	SEM	Mean	SEM	Mean	SEM
Exp1							
	BA-SS	28.76	1.61	0.48	0.042	15.22	0.2
	NA-SS	27.69	1.95	0.47	0.042	13.34	0.2
	LS	23.07	1.46	0.35	0.04	13.47	0.2
Exp2							
	BA-SS	31.92	1.87	0.61	0.051	14.07	0.32
	NA-SS	31.96	2.04	0.61	0.051	14.40	0.32
	LS	26.55	1.99	0.43	0.053	14.36	0.32
Exp3-F0							
	BA-SS	34.88	1.39	0.67	0.032	14.38	0.42
	NA-SS	34.21	1.48	0.65	0.033	13.7	0.42
	LS	29.24	1.24	0.52	0.036	13.68	0.42
Exp3-F6							
	BA-SS	34.76	1.44	0.67	0.034	14.54	0.35
	NA-SS	34.21	1.51	0.66	0.034	13.53	0.35
	LS	29.43	1.4	0.52	0.038	13.54	0.35
Exp3-F9							
	BA-SS	34.87	1.37	0.67	0.033	15.04	0.34
	NA-SS	34.09	1.49	0.66	0.033	13.51	0.34
	LS	29.35	1.43	0.52	0.037	13.54	0.34
Exp3-F12							
	BA-SS	34.71	1.38	0.66	0.033	15.54	0.32
	NA-SS	34.72	1.55	0.67	0.033	13.34	0.32
	LS	29.3	1.44	0.52	0.037	13.59	0.32

Note. Exp = experiment; P_g= guess rate; σ = imprecision (the inverse of precision). BA-SS = the broad attentional scale condition at short SOA; NA-SS = the narrow attentional scale condition at short SOA; LS = the long SOA condition. In Experiment 3, F0 = the original data set; F6 = the filtered data set with the first six trials of each block removed; F9 = the filtered data set with the first nine trials of each block removed; F12 = the filtered data set with the first twelve trials of each block removed.

2.2.2. Model-based analysis

For T2|T1 performance, the Full model was the winning model with the lowest WAIC value, indicating that both precision and guess rate varied across task conditions (Table 3). The parameters estimated with the Full model were then analyzed for hypothesis testing. For the parameter P_g, Bayes factors revealed decisive evidence for the alternative hypothesis (BF_{10} > 100), which implies the guess rate varied across different task conditions (Figure 2c). T2|T1 P_g at long SOA ($M_{long\text{-}SOA}$ = .35) was lower compared to the broad attentional scale (M_{broad} = .48, BF_{10} > 1,000), and narrow attentional scale conditions (M_{narrow} = .47, BF_{10} > 1,000) at short SOA. However, no evidence was found favoring the effect of attentional scaling on guess rate of T2|T1 (BF_{10} = .06). For T2|T1 σ, there was substantial evidence in favor of the effect of task condition on T2|T1 σ (BF_{10} = 6.55; Figure 2d). For the Bayesian paired T-test between broad and narrow attentional scale at short

SOA, the results indicated strong evidence (BF_{10} = 21.02) of the main effect of scaling on precision. Additionally, Bayesian test strongly favored that T2|T1 σ was larger in the broad attentional scale condition at short SOA (σ = 15.22°) than in the long SOA condition (σ = 13.47°; BF_{10} = 21.53), while there was no evidence in favor of the difference (BF_{10} = .66) between the narrow attentional scale at short SOA (σ = 13.34°) and the long SOA.

Table 3

WAIC for all possible models in Experiment 1

	T2|T1	
Model	WAIC	ΔWAIC
Full model	**74985.15**	**0.00**
Constant σ	74990.73	5.58
Constant P_g	75025.42	40.27
Constant all	75068.69	83.54

Note. WAIC = Watanabe-Akaike information criterion; *Δ*WAIC = the differences of WAIC from the best model. All parameters were estimated across three task conditions (BA-SS, NA-SS, LS). In the Full model, both P_g and σ could be estimated freely across task conditions. In the Constant σ model, σ was fixed while P_g was variable. In the Constant P_g model, P_g was fixed and σ was estimated as a variable. In the Constant all model, both parameters were fixed across different task conditions. Lower WAIC values indicate a better fit of that model, and the best model has been highlighted with bold font.

3. Experiment 2

Our first experiment demonstrated that changes in the attentional scale set for T1 indeed alter awareness of T2. Thus, there is a degree of adaptive control over attentional scaling. However, the control that was required in the present experiment was limited in that it was stable across entire trial blocks of trials. In Experiment 2 we thus wanted to assess whether fully adaptive, trial-by-trial scaling is also possible.

3.1. Method

3.1.1. Participants

Twenty-eight undergraduates from the University of Groningen were recruited and awarded course credits for participation. All participants reported normal or corrected-to-normal vision, and gave written informed consent before starting the experiment. Two participants were removed from the analysis. One was due to the same exclusion criterion that was applied in Experiment 1, the other was excluded because they did not finish the whole experimental task. The final sample size was thus 26 (mean age = 21.77 years, age range = 19 to 32 years, seventeen females).

3.1.2. Design and procedure

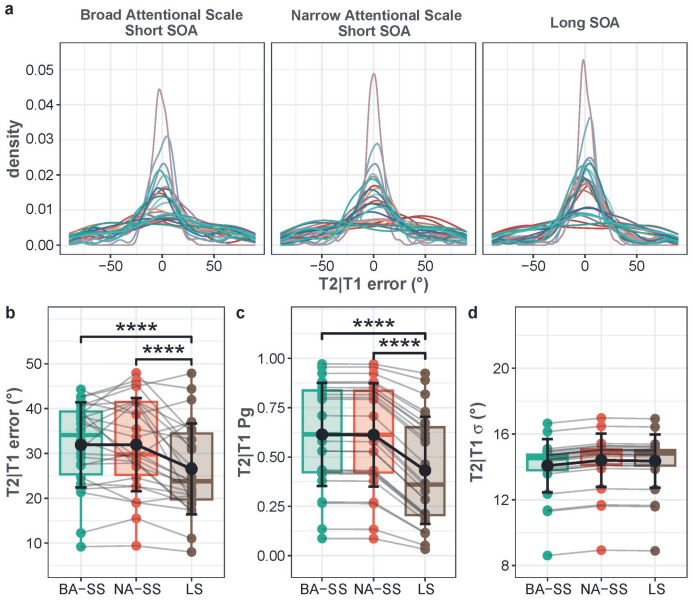
The experimental design and procedure were similar to Experiment 1, except for the following changes. Instead of presenting block-wise cues, T1 locations were cued trial-wise. As shown in Figure 1c, there were two kinds of pre-cue display, either an upward arrow or downward arrow cueing the exact location of T1 (inducing a narrow attentional scale), or both an upward and downward arrow cueing that T1 would appear randomly above or below the fixation dot (inducing a broad attentional scale). The cue display was terminated by a key press, after which the fixation dot appeared. As in Experiment 1, there were 400 trials in total, which were evenly and randomly distributed into 20 blocks.

3.2. Results

3.2.1. Error

Bayesian repeated measures ANOVA revealed decisive evidence for the effect of task condition on T2|T1 error (BF_{10} > 1000; Figures 3a-b). Specifically, the average T2|T1 error decreased from the short SOAs (31.92° with broad attentional scale and 31.96° with narrow attentional scale) to the long SOA (26.55°; $BF_{10\text{-all}}$ > 1000). For the comparison between the broad and narrow attentional scale at short SOA, BF_{10} values (.21) indicated substantial evidence favoring the null hypothesis that there was no difference between conditions.

Figure 3



Note. (**a**) Probability density plots of each participant's T2|T1 error distribution for each task condition. (**b**) Absolute T2|T1 error in different task conditions. (**c**) T2|T1 guess rate (P_g) estimates from the Full model. (**d**) T2|T1 σ estimates from the Full model. Figure conventions follow Figure 2.

3.2.2 Model-based analysis

According to the WAIC values, the best fitting model for T2|T1 performance was the Constant σ model (Table 4). However, the hypothesis testing results derived from the Full model were consistent with those of the Constant σ model. Therefore, to provide a comprehensive view of parameter estimates and ensure uniformity in presenting results across various experiments, we have chosen to detail the analysis using the Full model. Analysis results for the best model are given in the Supplementary Materials. We observed decisive evidence for the effect of task condition on T2|T1 guess rate (BF_{10} > 1,000). As seen in Figure 3c, the Bayesian factors ($BF_{10\text{-}all}$ > 1,000) revealed more guess responses at short SOA (.61 for both broad and narrow attentional scale conditions) than at long SOA (.43). Conversely, BF_{10} was .06 in the comparison between broad and narrow attentional scale at short SOA, showing evidence against a difference. Furthermore, in contrast to the effect on T2|T1 P_g, task condition had no effect on T2|T1 σ (BF_{10} = 0.11; Figure 3d), indicating that T2 awareness did not change in a gradual manner, but only in an all-or-none manner in Experiment 2.

Table 4

WAIC for all possible models in Experiment 2

	T2|T1	
Model	WAIC	ΔWAIC
Full model	79999.90	3.44
Constant σ	**79996.46**	**0.00**
Constant P_g	80113.88	117.42
Constant all	80132.63	136.18

Note. WAIC = Watanabe-Akaike information criterion; *Δ*WAIC = the differences of WAIC from the best model. Table conventions follow Table 3.

4. Experiment 3

As was evident from the results of Experiment 1 and 2, the size of the attentional scale could be controlled in blocks of trials, but not in a trial-by-trial manner. It may therefore be assumed that adjustment of the attentional scale takes time, which may be lacking from one trial to the next. Hence, in Experiment 3, we further tested the degree to which the attentional scale can be adjusted over time. Similar to statistical learning of spatial regularities, we hypothesized that the scale needed for T1 could be implicitly controlled due to statistical learning of T1 locations across successive stable trial sequences (Chun & Jiang, 1999; Jiang et al., 2013; Wang et al., 2019; Wang & Theeuwes, 2018), and thereafter have its effect on the nature of T2 awareness.

4.1. Method

4.1.1. Participants

Thirty-two undergraduates from the University of Groningen were recruited in exchange for course credits. All participants reported normal or corrected-to-normal vision and gave written informed consent before starting the experiment. One participant was removed according to the same exclusion criterion as in Experiment 1. The final sample size was 31 (mean age = 19.38 years, age range = 17 to 22 years, twenty-four females).

4.1.2. Design and procedure

The experimental design and procedure were similar to Experiment 1, except for the following changes. First, there was no pre-cue during the whole task. Each trial started with a fixation dot appearing for 600-800ms. Second, for each participant, there was a high-probability T1 location in the narrow attentional scale condition. Specifically, for participants with even numbers, the high-probability T1 location was above, while for participants with odd numbers, the high-probability T1 location was below fixation. Third, Experiment 3 consisted of 10 experimental

blocks of 40 trials each. For half of these blocks, forming the narrow attentional scale condition, T1 was more frequently (90%) displayed at the high-probability location than the other one. For the other half of these blocks, forming the broad attentional scale condition, the two T1 locations (above and below) had the same probability (50%). The order of the blocks was randomized.

4.1.3. Analysis

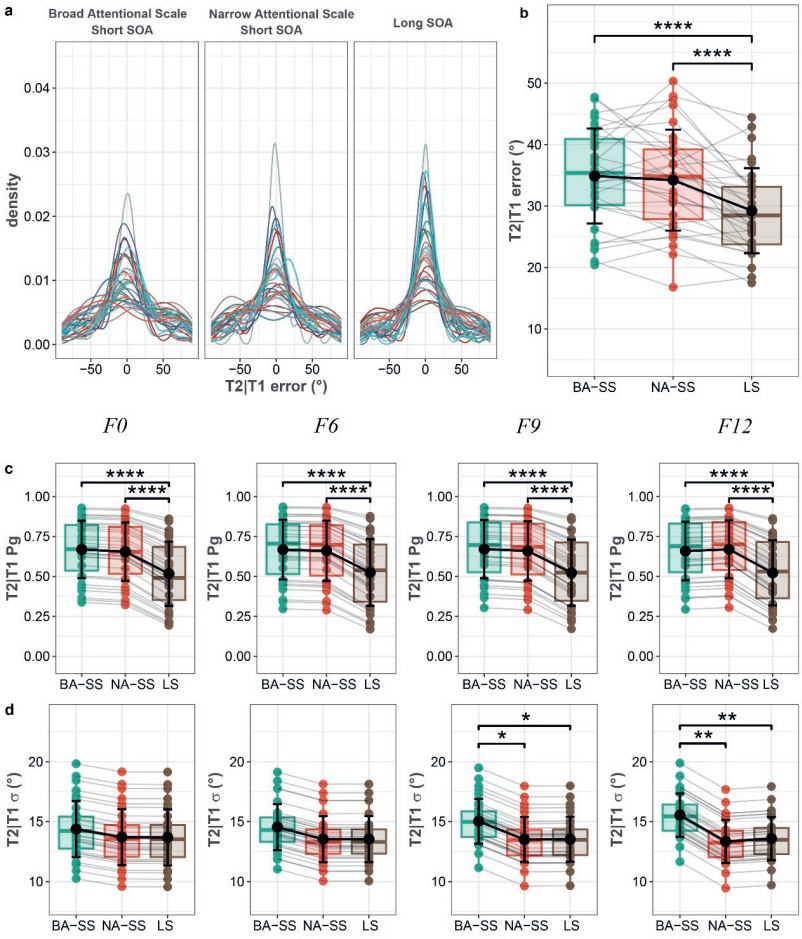
The analysis was similar to that in Experiments 1 and 2, except for the following: Besides the analyses on the data set which included all trials (*F0*), we also carried out the model-based analysis for three other filtered data sets. Since participants had to learn about the probable T1 location without explicit cuing, it is reasonable to assume that participants would need time to do so. Given the randomized order of the blocks, there was variability in the sequence with which participants encountered the different attentional scale conditions. This sequencing could, in principle, introduce transient effects at the beginning of a block, especially if participants were adjusting from one attentional scale condition to another, and the learning of the appropriate T1 locations could thus take some time to develop. To capture these effects, we opted to remove a set number of trials from the beginning of each block. This decision was guided by preliminary analyses which indicated that this approach would best capture the core effects of interest. As a result, we obtained three filtered data sets, labeled as *F6*, *F9*, and *F12,* representing that the first six, nine and twelve trials were filtered out, separately for each block. The analysis method and procedure were otherwise identical for all the data sets.

4.2. Results

4.2.1. Error

Consistent with the results of the first and second experiments, decisive evidence showed that there was a main effect of task condition on T2|T1 response error (Figure 4). Looking at the direct comparison between the broad attentional scale at short SOA and the long SOA, the average T2|T1 error decreased from 34.88° to 29.24° (BF_{10} > 1,000). The same pattern was also observed when comparing the narrow attentional scale at short SOA (average T2|T1 error = 34.21°) and the long SOA (BF_{10} > 1,000). Bayesian testing revealed strong evidence against a T2|T1 error difference between the broad and narrow attentional scale conditions at short SOA (BF_{10} = .25).

Figure 4



Note. (**a**) Probability density plots of each participant's T2|T1 error distribution for each task condition. (**b**) Absolute T2|T1 error. **(c)** T2|T1 guess rate (P_g) estimates for the data set including all trials *(F0)*, for the data set in which the first six trials of each block were filtered out (*F6*), for the data set in which the first nine trials of each block were filtered out (*F9*), and for the data set in which the first twelve trials of each block were filtered out (*F12*). **(d)** T2|T1 σ estimates for the *F0, F6, F9* and *F12* data sets separately. All parameters shown in this figure are based on the Full model. Figure conventions follow Figure 2.

4.2.2. Model-based analysis

With the *F0* and *F6* data sets, we observed a similar pattern of model comparison results as in Experiment 2 (Table 5). The Full model displayed a small divergence in WAIC value compared to the winning model, the Constant *σ*. In detail, the Full model's WAIC value was 2.09 higher for *F0*, and 3.23 higher for *F6*, than the Constant *σ* model. However, when we removed more first trials from each

block (*F9* and *F12*), the Full model became the best fit. As hypothesis testing results were almost identical for the best fitting model and the Full model across the *Fo* and *F6* data sets, we focus here on the Full model results to maintain consistency (see Supplementary for the best fitting model analysis with *Fo* and *F6* data sets).

For the *Fo* data set, task condition had a main effect on the T2|T1 guess rate (BF_{10} > 1,000; Figure 4). Pairwise comparison yielded decisive evidence (BFs_{10} > 1,000) when contrasting both broad and narrow attentional scales at short SOA against the long SOA. This pattern also emerged in T2|T1 P_g analysis across *F6*, *F9*, and *F12* data sets. Conversely, the T2|T1 σ analysis revealed divergence across the four data sets. For the *Fo* and *F6* data sets, there was no effect of task condition on T2|T1 σ (BF_{10} = 0.28 and 0.52, respectively). When comparing the broad attentional scale at short SOA and the long SOA, both data sets revealed anecdotal evidence in favor of the alternative hypothesis, suggesting a difference between the two conditions (BF_{10} = 1.5 for *Fo* and 2.39 for *F6*). Moreover, the analysis with *F6* data set showed the average T2|T1 σ was 14.54° in the broad attentional scale condition, and slightly reduced to 13.53° in the narrow attentional scale condition (BF_{10} = 1.53). There was no evidence favoring the differences of T2|T1 σ between broad attentional scale (σ_{broad} = 14.38°) and narrow attentional scale at short SOA (σ_{narrow} = 13.7°, BF_{10} = 0.91). When the first nine trials from each block (*F9*) were removed, anecdotal evidence supported a task condition effect on T2|T1 σ (BF_{10} = 1.43). It should be noted that there was substantial evidence (BF_{10} = 7.74) favoring a difference between the broad attentional scale and the long SOA condition, with T2|T1 σ averaging 15.04° in the former condition and decreasing to 13.54° in the latter. Average T2|T1 σ in the narrow attentional scale condition (13.51°) was also less than in the broad attentional scale condition (BF_{10} = 3.25). Lastly, in the analysis of the *F12* data set, we observed substantial evidence favoring the effect of task condition on precision (BF_{10} = 6.06). In paired comparison hypothesis testing, strong evidence was observed not only for the comparison between the broad attentional scale at short SOA and the long SOA (BF_{10} = 13.34), but also for the comparison between the two different scales at short SOA (BF_{10} = 11.48). Specifically, T2|T1 σ averaged higher with broad attentional scale (15.54°) than narrow (σ_{narrow} = 13.34°), and was also higher than the T2|T1 σ at long SOA ($\sigma_{long\text{-}SOA}$ = 13.59°).

Table 5

WAIC for all possible models in Experiment 3

	F0		*F6*		*F9*		*F12*	
Model	WAIC	ΔWAIC	WAIC	ΔWAIC	WAIC	ΔWAIC	WAIC	ΔWAIC
Full model	90808.89	2.09	77715.17	3.23	**70813.43**	**0.00**	**64080.94**	**0.00**
Constant σ	**90806.80**	**0.00**	**77711.93**	**0.00**	70814.18	0.75	64084.20	3.26
Constant P_g	90873.19	66.38	77765.38	53.44	70861.24	47.81	64125.96	45.02
Constant all	90897.43	90.62	77787.62	75.69	70888.60	75.16	64151.63	70.69

Note. *F0* refers to the data set including all trials. *F6* refers to the filtered data set in which the first six trials of each block were removed. *F9* refers to the filtered data set in which the first nine trials of each block were removed. *F12* refers to the filtered data set in which the first twelve trials of each block were removed. Table conventions follow Table 3.

5. General Discussion

We carried out three experiments to investigate adaptive control of attentional scaling and its impact on visual awareness during the attentional blink phenomenon. In Experiment 1, we manipulated the attentional scale by varying the possible location of T1 within multiple blocks of trials. In one half of the experiment, T1 location was constant and pre-cued with 100% validity. In the other half, T1 location varied unpredictably. In the former condition, participants should adopt a narrow attentional scale, while they should adopt a broad scale in the latter condition. We expected this change in scale to be expressed in a change in T2 precision between the two conditions (Karabay et al., 2022), and this was indeed what we found. In Experiment 2, a trial-by-trial paradigm was implemented, in which T1 locations varied from trial to trial, but were also validly pre-cued in one half of the trials. Participants seemed to be unable to use these cues to change their attentional scale, as we did not find evidence for a change in T2 precision. Model comparisons further revealed evidence of predominantly discrete T2 awareness, with the Constant σ model showing the best fit, which suggested that the participants might have defaulted to a narrow attentional scale. In Experiment 3, we introduced semi-constant T1 locations (fixed or variable) in single blocks of trials, hypothesizing that participants would learn these regularities and adjust their attentional scale accordingly. We indeed observed the expected precision effect, but only reliably after the first 9-12 trials within each block had been shown, and learning had taken place. Overall, our study thus revealed that attentional scale, as indexed by a change in T2 precision, can be adaptively adjusted during the AB, albeit not on a trial-by-trial level.

5.1. The dynamics of attentional scaling

The result obtained from Experiment 1 is in line with previous work on attentional scaling, which suggested that keeping stimulus (location) probability stable is a key component in adjusting the attentional scale to a particular size, and

maintaining that for a period of time (Balz & Hock, 1997; Goodhew et al., 2016; Hubner, 2000; Lawrence et al., 2020a; Müller et al., 2003; Turatto et al., 2000). The outcome of Experiment 1 also dovetailed with that of Experiment 2, which showed that explicit cues did not lead to changes in the attentional scale on a trial-by-trial basis. It thus seems that voluntary, or endogenous control over the scale of attention has a relatively slow time course. In the two-stage theory of attentional focusing proposed by Turatto et al. (2000), attention is automatically directed to any stimulus that suddenly appears, which is followed by a "top-down" effort to maintain the extent of attentional focus. This suggests that attentional control involves a time-consuming, sequential process, which may explain why trial-to-trial variability does not seem to lend itself to an effective adjustment of attentional scale.

In spite of this apparent attentional sloth, Experiment 3 showed that participants were able to adjust their attentional scale within 9-12 trials. Once we filtered out the first 9 trials from each block, we observed evidence favoring the hypothesis that there was a difference in T2 precision between the broad scale at short SOA and the long SOA, suggesting that the nature of T2 awareness during the AB changed. Moreover, as we filtered out the first 12 trials, we observed further evidence for an effect of attentional scaling on T2 precision: T2 precision varied between the broad and narrow scales at short SOA. Experiment 3 thus suggested that attentional scaling can be adaptively controlled through statistical learning of spatial regularities. Our results are consistent with previous studies that investigated the role of statistical learning in the control of spatial attention (e.g., Awh et al., 2012; Failing & Theeuwes, 2018; Theeuwes, 2018). The time course of this endogenous control process also seems compatible with prior research (Egeth, 2018; Lawrence et al., 2020a).

5.2. Attentional scaling and perceptual awareness during the attentional blink

In our study we capitalized on the previously reported effect that when the time interval between two targets is short, attentional scaling for T1 affects perception of T2 (Karabay et al., 2022). In terms of the AB, which we investigated by comparing performance between short and long lags, our study confirms that the loss of T2 information can occur in both a gradual and an all-or-none manner, depending on whether the attentional scale is spread over a large or small area. While Karabay et al. (2022) established these distinct forms of information loss by comparing across temporal lags, our direct comparison within the short lag isolates how spatial scale modulates the nature of this loss. In the broad scale condition, the AB takes the shape of an attentional "blur", in which T2 information is partially lost in relatively many trials. In the narrow scale condition, the AB is a proper blink,

causing a complete loss of T2 information in some trials, but preservation in others. These findings are consistent with recent studies (Karabay et al., 2022; Sy et al., 2021), supporting the notion that visual awareness during the AB can be both gradual and discrete. This offers a nuanced perspective on the debate about the nature of awareness during the AB, with some studies suggesting a discrete emergence of awareness (Asplund et al., 2014; Sergent & Dehaene, 2004; Vul et al., 2009), while others argue that awareness emerges gradually (Nieuwenhuis & de Kleijn, 2011; Overgaard et al., 2006). The present results furthermore suggest that it is possible to exert a degree of adaptive control over target awareness during the AB.

Because effects of attentional scaling on T2 are observed only at short SOAs between targets, both in the current study, as well as in previous work (Karabay et al., 2022), one might hypothesize that attentional scaling itself is subject to the AB. For instance, one account might be derived from the influential eSTST model of the AB (Bowman & Wyble, 2007; Wyble et al., 2009), which suggests that attentional deployment is regulated competitively through both target excitation and working memory suppression. During the AB, when T1 is being encoded into working memory as a distinct episode, attentional allocation to subsequent events (T2) is suppressed to prevent interference with the encoding process of T1. This means that T2 is likely to be missed or delayed in perception due to the suppression of attention caused by the ongoing T1 encoding. From this perspective, it is reasonable to assume that the attentional scaling process during the blink could also be suppressed. Hence, the specific attentional scale induced for accurate T1 identification would be sustained for T2 processing when the interval between targets falls inside the AB.

However, the present results cast some doubt on the necessity of this assumption. Given that several successive trials seem to be needed in order to change one's attentional scale, it seems likely that the necessary time is simply lacking within the course of a single trial. The lack of an effect of scaling at longer SOAs between targets might alternatively be accounted for by the comparative level of attentional resources that are available. The AB that is in effect at short SOA may provide the circumstance in which the scaling effect on target report emerges. As participants struggle to report T2 correctly, they are caught between two fires: A narrow, focal attention mode, which is able to process target identities quite well, but which runs the risk of over-engaging in T1 processing and losing T2 altogether, and a broad, diffuse mode that is less likely to run this risk, but which reduces the comparative quality of the target representations. By contrast, at longer SOAs, there might be enough attentional resources to spare to process T2 well, regardless of the scale that is in effect on the current trial.

Although our main interest was the consequences of attentional scaling on the perception of T2, we may also consider why T1 seemed to show a different pattern of effects. For instance, T1 guess rate varied as a function of the attentional scale in all experiments reported here, while T1 precision was unaffected. There may be two reasons for these differences. First, the qualitatively different allocation of attention to T1 and T2 may play a role. T1 enjoys the full availability of attention, and participants can detect it quite well, in spite of a degree of sensory difficulty due to masking. Conversely, T2 has to be processed when attention is still engaged by T1, which limits the availability of attention, and which is expressed in the AB (Broadbent & Broadbent, 1987; Duncan et al., 1994; Raymond et al., 1992). In terms of Rensink's (2015) attentional taxonomy, we might assume that the biggest challenge to processing T1 lies with attentional "orientation", involving sampling and filtering functions. Conversely, the processing of T2 is further compounded by T1-induced delays in attentional "integration", involving primarily binding and individuating in the context of RSVP. We might hypothesize then that the added attentional 'duress' experienced with T2 might allow the expression of gradual and/or discrete awareness on T2 only. Second, it is conceivable that certain manipulations of attentional scaling, such as the trial-wise cues in Experiment 2, might initially induce a shift in the attentional locus for T1, which may subsequently not extend to a longer-term adjustment of the attentional scale. Thereby, different effects on T1 and T2 might have arisen.

6. Conclusion

Our findings offer new insights into the adaptive control of attentional scaling during the AB. We found that attentional scaling can be modulated adaptively, although not at the level of individual (cued) trials. We observed commensurate effects on target report during the AB, where a broad attentional scale resulted in an attentional blur, that is, gradual target awareness. We also observed that when control of attentional scaling was not possible, participants seemed to revert to a narrow attentional scale, leading to all-or-none awareness, which is typically found in classic RSVP AB paradigms. Finally, our findings provide support for previous claims that conscious awareness can emerge in both a discrete and gradual manner during the AB, highlighting the importance of considering attentional control when investigating the nature of awareness.

Acknowledgments

We are most grateful to Wouter Kruijne for coining the term "attentional blur".

SUPPLEMENTARY MATERIAL

1. T1 analysis across experiments.

Table S1

T1 errors and parameter (P and σ) estimates from the full model across task conditions for all experiments

Experiment/Task Condition		Error (°)		P_g		σ (°)	
		Mean	SEM	Mean	SEM	Mean	SEM
Exp1							
	BA-SS	20.11	1.26	0.24	0.031	13.67	0.47
	NA-SS	18.48	1.26	0.19	0.028	13.83	0.47
	LS	17.69	1.22	0.19	0.027	13.29	0.47
Exp2							
	BA-SS	23.05	1.98	0.35	0.056	13.37	0.38
	NA-SS	20.85	1.90	0.29	0.054	12.75	0.38
	LS	20.73	2.07	0.27	0.054	13.19	0.38
Exp3-F0							
	BA-SS	25.1	1.42	0.37	0.041	14.87	0.41
	NA-SS	23.39	1.63	0.31	0.040	14.49	0.41
	LS	22.46	1.38	0.31	0.040	14.22	0.41
Exp3-F6							
	BA-SS	24.87	1.40	0.37	0.041	14.97	0.40
	NA-SS	22.98	1.64	0.31	0.040	14.65	0.40
	LS	22.35	1.43	0.31	0.040	14.16	0.40
Exp3-F9							
	BA-SS	24.95	1.39	0.38	0.041	15.06	0.40
	NA-SS	22.92	1.61	0.31	0.040	14.64	0.40
	LS	22.35	1.47	0.31	0.040	14.19	0.40
Exp3-F12							
	BA-SS	24.99	1.41	0.37	0.041	14.98	0.39
	NA-SS	22.87	1.60	0.31	0.040	14.57	0.39
	LS	22.38	1.51	0.31	0.041	14.05	0.39

Note. Exp = experiment; P_g= guess rate; σ = imprecision (the inverse of precision). BA-SS = the broad attentional scale condition at short SOA; NA-SS = the narrow attentional scale condition at short SOA; LS = the long SOA condition. In Experiment 3, F0 = the original data set; F6 = the filtered data set with the first six trials of each block removed; F9 = the filtered data set with the first nine trials of each block removed; F12 = the filtered data set with the first twelve trials of each block removed.

Table S2

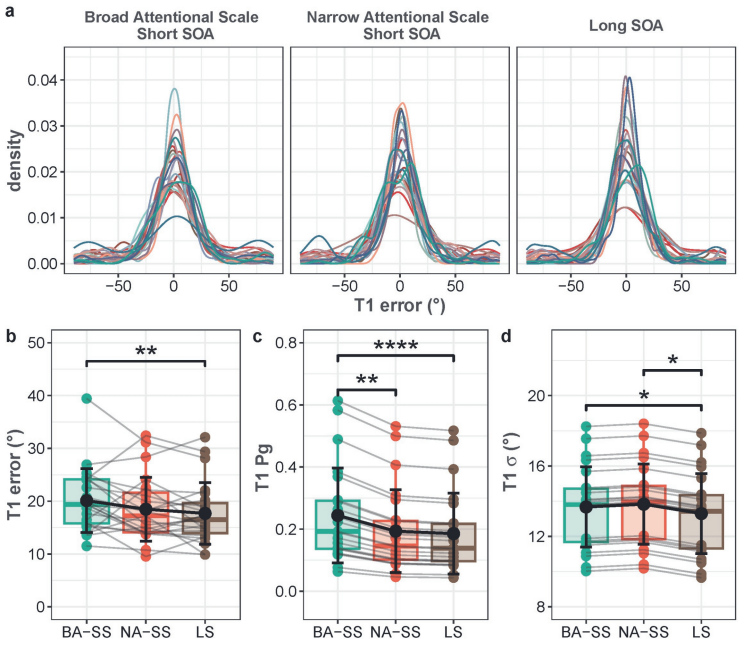
WAIC for all possible models for T1 performance in all experiments

	Exp1		***Exp2***		***Exp3 – F0***		***Exp3 – F6***		***Exp3 – F9***		***Exp3 – F12***	
Model	WAIC	ΔWAIC	WAIC	ΔWAIC	WAIC	ΔWAIC	WAIC	ΔWAIC	WAIC	ΔWAIC	WAIC	ΔWAIC
Full model	95919.42	2.08	**109550.0**	**0.00**	134167.00	0.32	113837.02	0.03	**103795.62**	**0.00**	**93726.73**	**0.00**
Constant σ	**95919.34**	**0.00**	109550.7	0.68	**134166.68**	**0.00**	**113836.99**	**0.00**	103796.99	1.37	93727.22	0.48
Constant P_g	95933.25	15.91	109576.5	26.51	134180.61	13.93	113837.43	10.44	103808.90	13.28	93739.30	12.57
Constant all	95939.80	22.46	109586.6	36.56	134194.04	27.36	113860.55	23.55	103821.74	26.12	93752.49	25.75

Note. WAIC = Watanabe-Akaike information criterion; ΔWAIC = the differences of WAIC from the best model. All parameters were estimated across three task conditions (BA-SS, NA-SS, LS). In the Full model, both P_g and σ could be estimated freely across task conditions. In the Constant σ model, σ was fixed while P_g was variable. In the Constant P_g model, P_g was fixed and σ was estimated as a variable. In the Constant all model, both parameters were fixed across different task conditions. Lower WAIC values indicate a better fit of that model, and the best model has been highlighted with bold font. Table conventions follow Table S1.

1.1. Experiment 1

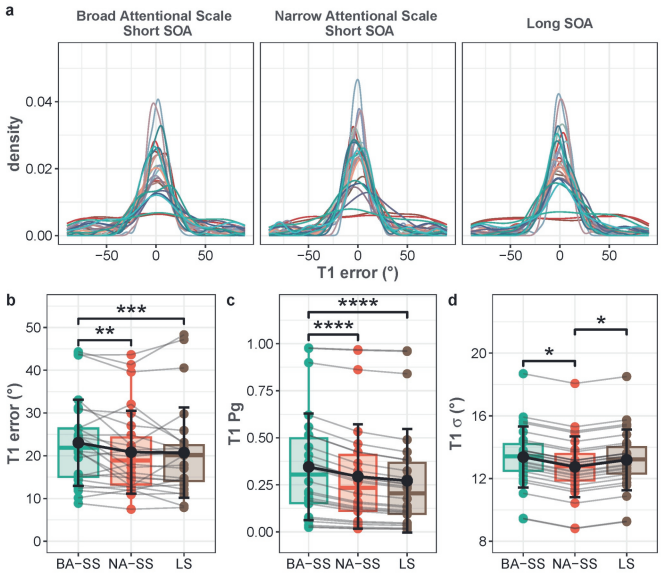
Figure S1



Note. (**a**) Probability density plots of each participant's T1 error distribution for each task condition. Each line indicates one participant. SOA = stimulus onset asynchrony; Short SOA corresponds to 250ms between T1 and T2, and Long SOA corresponds to 800ms between T1 and T2. (**b**) Absolute T1 error in different task conditions.BA-SS = the broad attentional scale condition at short SOA; NA-SS = the narrow attentional scale condition at short SOA; LS = the long SOA condition. Colored dots represent individual data. Black dots with error bars represent averages with 95% confidence intervals. * represents substantial evidence against the null hypothesis ($3 < BF_{10} < 10$), ** represents strong evidence ($10 < BF_{10} < 30$), *** represents very strong evidence ($30 < BF_{10} < 100$), and **** represents decisive evidence ($BF_{10} > 100$). (**c**) T1 guess rate (P) estimates from the Full model. (**d**) T1 σ estimates from the same model.

1.2. Experiment 2

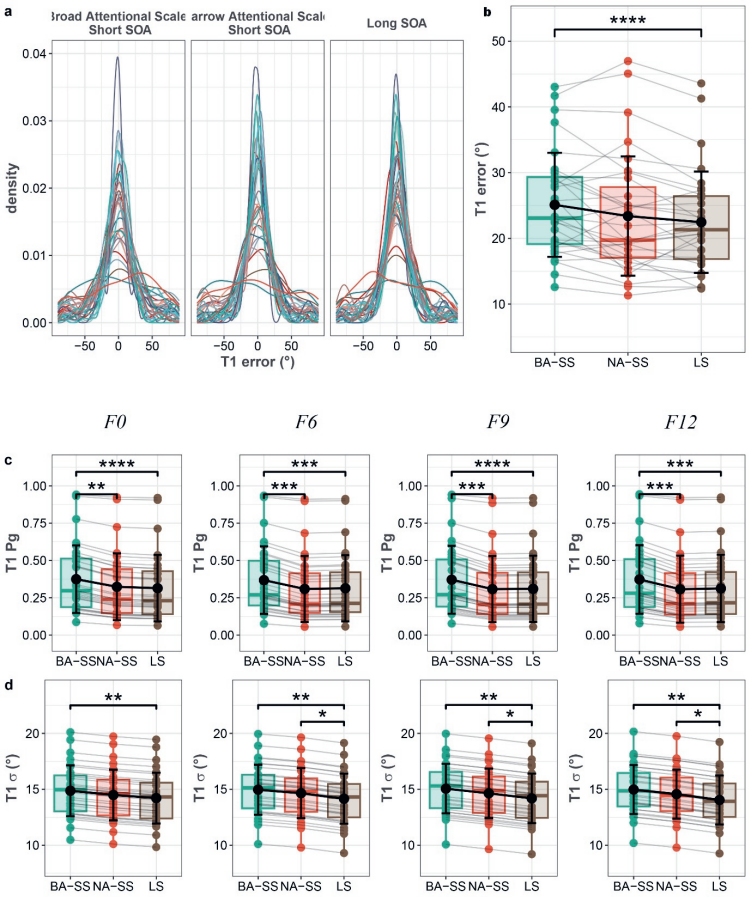
Figure S2



Note. (**a**) Probability density plots of each participant's T1 error distribution for each task condition. (**b**) Absolute T1 error in different task conditions. (**c**) T1 guess rate (P_g) estimates from the Full model. (**d**) T1 σ estimates from the same model. Figure conventions follow Figure S1.

1.3. Experiment 3

Figure S3



Note. (**a**) Probability density plots of each participant's T1 error distribution for each task condition. (**b**) Absolute T1 error in different task conditions. **(c)** T1 guess rate (P_g) estimates for the data set including all trials *(F0)*, for the data set in which the first six trials of each block were filtered out (*F6*), for the data set in which the first nine trials of each block were filtered out (*F9*), and for the data set in which the first twelve trials of each block were filtered out (*F12*). **(d)** T1 σ estimates for the *F0, F6, F9* and *F12* data sets separately. All parameters shown in this figure are based on the Full model. Figure conventions follow Figure S1.

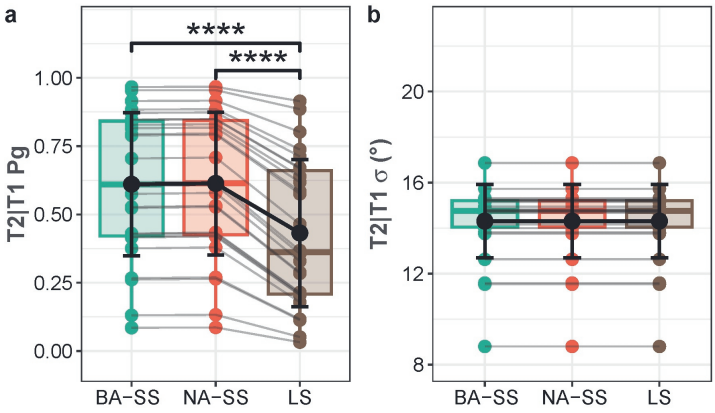
2. Bayesian hypothesis testing on the parameter estimates from the best model of T2|T1 in Experiment 2 and Experiment 3.

2.1. Experiment 2

In Experiment 2, the Constant σ model showed the best fitting performance. However, due to the slight differences between the Constant σ model and the Full model (ΔWAIC = 3.44), we used the Full model in the main analyses to have a full insight of the parameters' value across task conditions. Here, we present hypothesis testing results on guess rate and precision parameters based on the best model, the Constant σ model, for reference.

Decisive evidence was observed in favor of an effect of SOA on T2|T1 guess rate (BF_{10} > 1,000, Figure S4). T2|T1 P_g averaged .66 at both broad attentional and narrow attentional scale conditions at short SOA and decreased to .41 at the long SOA condition (BFs_{10} > 1,000).

Figure S4



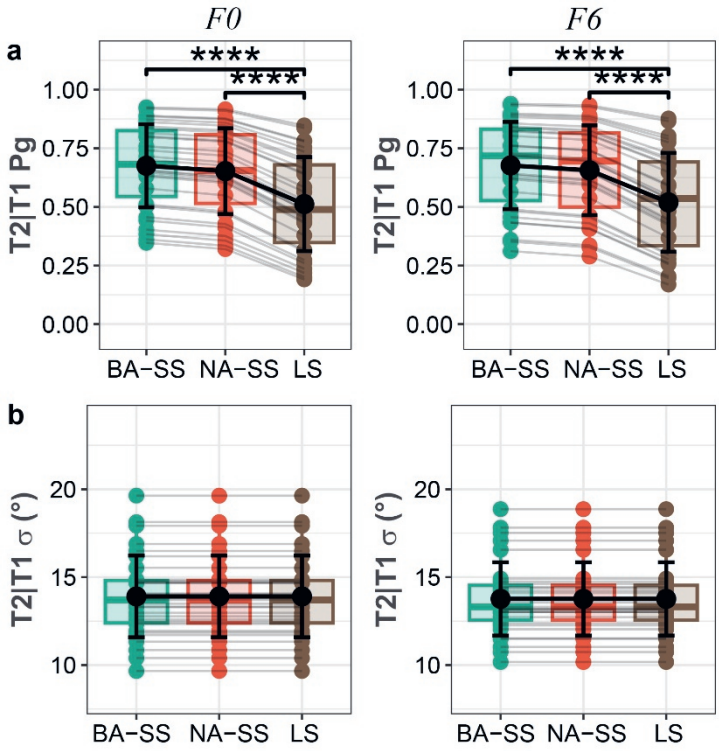
Note. T2|T1 hypothesis testing results with the parameter estimates from the best model, the Constant σ model, in Experiment 2. (**a**) T2|T1 guess rate (P_g) estimates. (**b**) T2|T1 σ estimates. Figure conventions follow Figure S1.

2.2. Experiment 3.

Similar to Experiment 2, the Constant σ model performed best for the *F0* and *F6* data sets. Here, we present hypothesis testing on parameters obtained from the winning model, the Constant σ model, for *F0* and *F6*. It should be noted that for the *F9* and *F12* data sets, the winning model is the Full model. For *F0* and *F6* data sets, decisive evidence was observed favoring of the effect of task condition on guess rate (BFs_{10} > 1,000, Figure S5). When contrasting the broad attentional scale or the narrow attentional scale at short SOA against the long SOA, the hypothesis

testing results provided decisive evidence supporting the differences of guess rate (BFs_{10} > 1,000). However, for the comparison between broad and narrow attentional scales at short SOA, Bayesian factors (BFs_{10} < 1) supported the null hypothesis, which means no statistical differences of the guess rate between these two attentional scales.

Figure S5



Note. T2|T1 hypothesis testing results with parameter estimates from the best model in Experiment 3, for *Fo* and *F6* data sets. (**a**) T2|T1 guess rate estimates. (**b**) T2|T1 σ estimates. Figure conventions follow Figure S1 and S3.

Chapter 4

Covert Recognition under Temporal Constraints

Published as:
Wang, S., van der Mijn, W. R., Karabay, A., & Akyürek, E. G. (2026). Multimodal detection of concealed information in rapid serial visual presentation using EEG and pupillometry. *Neuropsychologia*, *225*, 109418. https://doi.org/10.1016/j.neuropsychologia.2026.109418

Abstract

Concealed Information Tests (CITs) aim to detect recognition of critical information that individuals attempt to hide, typically using physiological markers. Although previous CIT studies have combined several autonomic indicators such as heart rate and pupil change, it is still unclear whether adding neural measures to pupillometry can capture complementary aspects of recognition and attentional control. To investigate this, we examined whether electroencephalography (EEG) and pupillometry jointly provide reliable markers of concealed information in a rapid serial visual presentation (RSVP) paradigm, which constrains strategic processing and emphasizes rapid recognition. Participants viewed streams of faces containing a critical probe—either a personally familiar (parent's) face or an unfamiliar face—while performing a sex-based target detection task. EEG and pupil size were recorded concurrently, focusing on four measures: ERP amplitude at Pz, theta-band (4–8 Hz) power, absolute pupil size, and pupil size change. At the group level, all measures differentiated probes from controls, reflecting attentional orienting and recognition. At the individual level, detection varied across modalities. To integrate evidence, we applied Fisher's method to combine p-values across measures. Although overall detection did not substantially improve, combined inference compensated for limitations of single measures.

***Keywords**:* concealed information test; rapid serial visual presentation; electroencephalography; pupillometry

1. Introduction

As a scientifically grounded approach for detecting deception, the Concealed Information Test (CIT) has attracted considerable attention within the domain of cognitive psychology and psychophysiology (Ben-Shakhar & Elaad, 2003; Verschuere et al., 2011). The CIT was originally introduced as the Guilty Knowledge Test by Lykken (Lykken, 1959, 1960), who first demonstrated that autonomic nervous system (ANS) responses (e.g., galvanic skin response) could reliably differentiate between crime-relevant (e.g., murder weapon details) and neutral information. In a typical CIT paradigm, participants are presented with different types of stimuli: probe items, which carry meaningful or personally significant information for knowledgeable individuals, and control items, which are neural alternatives within the same category. The underlying assumption is that only individuals with specific knowledge will recognize the probe, and as a result exhibit different responses (physiological or behavioral) compared to the control items.

The dominant theoretical account for the CIT effect is the orienting response (OR). ORs are automatic physiological responses and attentional reactions triggered by novel, salient, or personally significant stimuli (Sokolov, 1963). Within the CIT context, the probe acts as a significant stimulus only for knowledgeable individuals, thereby eliciting enhanced ORs compared to neutral (control) items. Empirical studies have provided evidence for this view, demonstrating larger physiological responses to probes among informed participants (Gati & Ben-Shakhar, 1990; Lykken, 1974; Verschuere et al., 2004). Consistent with the automatic nature of the OR, the recognition of personally familiar faces is considered a highly automatic process, and remains detectable even when participants explicitly attempt to conceal their recognition (Dalski et al., 2022; Wiese et al., 2019; 2022; Young& Burton, 2018).

A variety of physiological indicators have been used in CIT studies, mainly reflecting autonomic arousal, including skin conductance, heart rate, respiration, and pupillometry (see Gamer, 2011 for a review). In addition to these autonomic measures, central nervous system (CNS) indices such as electroencephalography (EEG) and functional magnetic resonance imaging have also been employed in CIT research (Farwell & Donchin, 1991; Rosenfeld et al., 2004; Ganis et al., 2003), providing further insights into the cognitive processes underlying concealed information detection. However, the combined use of CNS and ANS signals to identify multimodal physiological markers that are sensitive to recognition processes and effective in the CIT paradigm, has rarely been attempted.

Among EEG markers, the P300 component has received particular attention in CIT research. This positive deflection, typically peaking around 300 ms after stimulus onset, is widely interpreted as reflecting attentional allocation,

stimulus evaluation, and context updating in working memory (Polich, 2007; Squires et al., 1975). These processes are critical when a stimulus violates expectations or carries motivational relevance, as is the case for concealed information. The P300 is reliably larger for probe items than for control items, indicating the detection of salient or personally significant information (for a recent review, see Rosenfeld, 2020). A meta-analysis by Meijer et al. (2014) demonstrated that the P300 not only distinguishes probes from controls with high reliability but also outperforms autonomic measures such as skin conductance, respiration, and heart rate in terms of effect size. This strong performance underscores the theoretical and practical importance of P300 as an index of recognition and attentional engagement in CIT paradigms.

Beyond the P300, previous research on EEG oscillations has shown the link between theta oscillations (4-8 Hz) and several cognitive functions that are likely engaged during concealed information detection. Specifically, increases in theta power over medial frontal sites are consistently observed during conflict monitoring and cognitive control, processes that help participants manage competing responses and maintain task goals (Cavanagh et al., 2010; Cavanagh & Frank, 2014; Cohen & Donner, 2013; Nigbur et al., 2011). Theta activity has also been linked to successful memory encoding and retrieval (Klimesch et al., 1997), and to target image recognition in RSVP (Meng et al., 2012). Furthermore, theta responses have been shown to mark the detection of famous faces in RSVP paradigms (Alsufyani et al., 2019).

From a practical perspective, in spite of the effectiveness in CITs of physiological measures, such as autonomic measures and the P300, a continuing concern is the test's vulnerability to countermeasures – intentional strategies employed by 'suspects' (often knowledgeable individuals in lab studies) to manipulate their physiological reactions. Such strategies may involve suppressing physiological reactions to probe items or artificially enhancing responses to neutral items. Participants may purposefully attempt to direct their attention to control items, for instance. Prior findings have shown that these techniques can diminish the detection accuracy across both autonomic indicators and central nervous measures such as the P300 (Honts et al., 1996; Mertens & Allen, 2008; Rosenfeld et al., 2004).

To address the problem of countermeasures, recent research has explored the implementation of Rapid Serial Visual Presentation (RSVP; Broadbent & Broadbent, 1987) into the CIT framework. In RSVP, stimuli are presented in rapid succession at a fixed spatial location, typically at a rate of 10 items per second. This rapid speed imposes temporal constraints and high cognitive demands, reducing the opportunity for individuals to exert top-down control on their responses, thereby limiting the effect of countermeasures. Bowman et al. (2013, 2014) were

the first to integrate RSVP into the CIT. Using participants' real names as probe stimuli, they demonstrated that salient items evoked stronger P300 responses than irrelevant ones – even when participants attempted countermeasures. Chen et al. (2023) recently showed that pupil dilation within RSVP could also discriminate concealed information to some extent, offering a non-invasive and low-cost alternative to EEG. However, pupil-based detection was less sensitive than ERP-based detection at the individual level.

Most prior research on concealed information testing, including RSVP-based designs (Bowman et al., 2013, 2014; Chen et al., 2023), has relied on single measures of either CNS or ANS activity. Although this could be sufficient, in principle, to obtain an index of a particular cognitive process, such as an OR, the advantage of using multiple measures is that they have the potential to capture different processes simultaneously (e.g., recognition-induced emotion and attentional orienting), as well as different outcomes or aspects of the same process (e.g., enhanced perceptual processing and encoding into working memory as a consequence of attentional orienting). A small body of work has explored the combined use of multiple physiological signals, though primarily within traditional CIT paradigms. For example, Gamer et al. (2008) found that integrating skin conductance responses, respiration line length, and heart rate enhanced classification accuracy beyond that achieved by any single measure. A few studies have attempted to combine CNS and ANS indices, although with mixed findings. Ambach et al. (2010) reported that combining P300 amplitudes with skin conductance responses improved detection accuracy at the individual level. In contrast, other studies have reported limited sensitivity of the P300 component in differentiating probe from irrelevant items, when combined with automatic measures, potentially due to task-specific parameters such as long inter-stimulus intervals (ISIs) that may have weakened the P300 response (Gamer & Berti, 2010; Matsuda et al., 2009).

To our knowledge, no prior study has examined the combined use of CNS and ANS within an RSVP-based CIT paradigm. The present study was designed to further explore the feasibility and effectiveness of this approach using a multimodal physiological framework. We recorded two types of physiological signals: EEG and pupil size. From the EEG data, we considered in particular ERP amplitudes at the Pz electrode to target the P300 component, as well as theta-band (4-8 Hz) power across midline electrodes (Fz, Cz, Pz; Cavanagh et al., 2010; Cohen & Donner, 2013). From the pupillometry data, we analyzed both absolute pupil size and pupil size change over time (see Chen et al., 2023; 2025).

The EEG measures were selected based on their established sensitivity in cognitive processing in RSVP paradigms and their effectiveness in detecting concealed information, as reviewed above. Pupillometry was included as a

complementary measure for both theoretical and practical reasons. Pupil size has been shown to reflect cognitive processes relevant to CIT, including attention, arousal, and recognition. Its utility has been demonstrated in prior CIT studies (e.g., Bradley & Janisse, 1981; Chen et al., 2023; Lubow & Fein, 1996; Seymour et al., 2013). Moreover, pupil dilation has been linked to the processing of motivationally significant stimuli, often in parallel with enhanced P3 amplitudes (Nieuwenhuis et al., 2011). Additionally, pupil size change – calculated as the sample-to-sample difference in pupil diameter – captures the rapid fluctuations in the pupil response, making it well suited to track transient attentional shifts and cognitive effort in the fast-paced RSVP paradigm. All of these processes could potentially play a role in CIT. Finally, from a practical perspective, pupil size can be recorded non-invasively, offering a low-cost alternative to EEG.

In addition to analyzing each measure separately, we applied Fisher's method to combine individual-level p-values across central (EEG) and autonomic (pupillometry) modalities, following the procedures established by Bowman and colleagues (2013, 2014). We specifically aimed to investigate whether combining these signals provides added value beyond single measures when recognition occurs under rapid, attention-constraining conditions. Based on prior findings, we expected that single measures would differentiate probes from controls at both group and individual levels. More importantly, we predicted that combining evidence across central and autonomic measures would enhance individual-level detection compared to any single measure.

2. Method

2.1. Participants

Twenty-three undergraduates (nineteen females; mean age = 22.5 years) participated in this study. The sample size is comparable to previous CIT studies, which typically included around 15-25 participants (Bowman et al., 2013; Matsuda et al., 2009; Rosenfeld et al., 2006). Furthermore, the main analysis in the present study focused on individual-level effects, aiming to assess whether concealed knowledge can be detected within each participant. Therefore, this sample size was considered to be sufficient. All participants reported having normal or corrected-to-normal vision. Participants received 10 euro as compensation. The study was conducted in accordance with the Declaration of Helsinki (2013) and approved by the ethics committee at the University of Groningen (approval code PSY-2223-S-0280). Written informed consent was obtained from each participant prior to the experiment.

2.2 Apparatus and Stimuli

The experiment was designed and controlled using OpenSesame (v3.3.14) (Mathôt et al., 2012), and conducted in a dimly lit, sound-attenuated laboratory cabin. The program was run on a computer with a Windows 10 operating system. Stimuli were displayed on a 27″ LCD Iiyama PL2773H monitor with a refresh rate of 100 Hz and a resolution of 1920×1080 pixels.

Participants were seated in a stable position, with their heads secured using a chin rest and a forehead support to minimize movement. The viewing distance between the participant's eyes and the monitor was 60 cm. All stimuli were displayed at the center of the screen against a dark background (HEX #808080). A white fixation dot, subtending a visual angle of 0.12° x 0.12°, was presented to maintain participants' visual focus during the experiment.

All face stimuli, except for the personally familiar faces, were selected from the "10k US Adult Faces Database" (Bainbridge et al., 2013). Demographic and other attribute labels were available for 2,222 faces from this database. For the current study, 915 faces were selected that had no facial hair, faced the camera head-on, had a happy or neutral expression, had an image quality that was rated larger than 1 (rated 0-5), and whose age was rated as 2, 3, or 4 (on a 1-5 scale, where 1 = <20 years, 2 = 20 - 30 years, 3 = 30 - 45 years, 4 = 45 - 60 years, 5 = >60 years). This selection was made to prevent personally familiar faces from standing out due to age-related salience. Personally familiar face images were obtained from each participant, who were instructed to provide a photograph of either their mother or father facing the camera head-on.

In order to reduce eye movement and pupil activity as much as possible, all selected and provided face images were standardized using the "Face Processor" python package (van der Mijn, 2023). This application detected the position of the eyes and nose of each face and repositioned the image so that the eyes were level on the horizontal axis, and the center point of the triangle eyes-nose was aligned with the center of the image. Face images were cropped into an elliptical shape with standardized dimensions of 100 pixels in height and 70 pixels in width, which also excluded the ears for all faces. Then, the images were converted to greyscale, and normalized to an average intensity of 128 (on a scale of 0-255).

EEG signals were recorded using a TMSI REFA 32 system, equipped with 26 electrodes placed following the standard 10-20 system, at a sampling rate of 1000 Hz. Impedances were kept below 10 kΩ. EEG was referenced online against the average of all electrodes. The Fpz electrode served as ground. To facilitate offline re-referencing, two electrodes were positioned on the left and right mastoids. To monitor eye movements and blinks, electrooculography (EOG) data was simultaneously recorded using electrodes placed at four locations: above and below the left eye, and at the outer canthi of both eyes. The EEG data acquisition was managed using OpenViBE software (Renard et al., 2010).

Pupil sizes were continuously monitored and collected using an EyeLink eye-tracking system (SR Research), sampling at a frequency of 1000 Hz. Prior to the experiment, a standard 9-point calibration procedure was carried out to ensure accurate tracking of pupil size throughout the experiment.

2.3. Experimental Procedure

The sequence of a single trial is illustrated in Figure 1. During each trial, a stream of face images (14 stimuli in total) was presented. Following a previous RSVP-CIT study from our lab (Chen et al., 2025), the stimulus onset asynchrony (SOA) was set to 125 ms and the inter stimulus interval (ISI) was set to16 ms. The majority of the stream (13 out of 14) consisted of random selected distractors. One critical stimulus was randomly inserted at the fifth, sixth, seventh, or eighth position in the sequence. As shown in Figure 1, the inserted critical stimulus in a given trial could be one of the following four types: 1) Target face, a face of the opposite sex to the other faces. which served as the behavioral detection target; 2) Probe face, whose identity determined the type of the experimental block, either being a personally familiar face or an unfamiliar face; 3) Distractor face, a distractor face that varied across trials; 4) Fixed control face, a face selected from the same pool as the distractors and kept constant within the block, presented equally often as the probe to control for presentation frequency. Note that to prevent gender from acting as a confound, the 13 distractor faces, the fixed control face, and the probe stimulus (whether familiar or unfamiliar) were always the same sex as the parent image provided by the participant. Only the target face was a randomly selected face of the opposite sex.

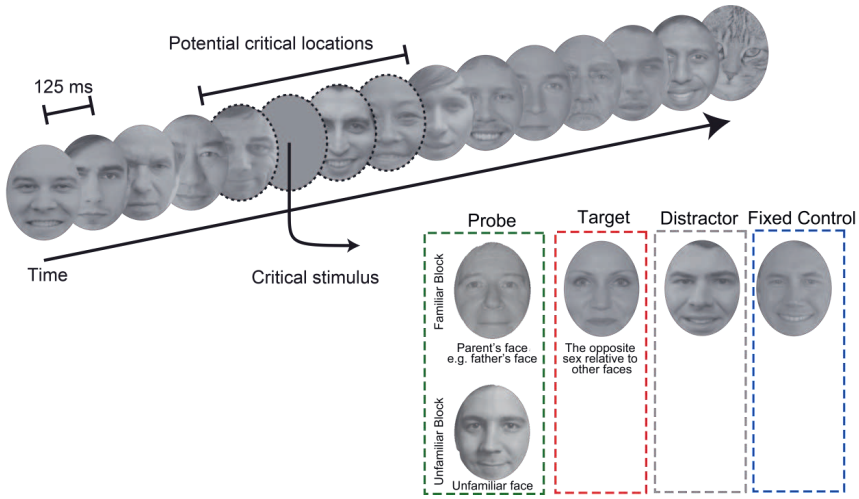
The experiment consisted of a block-level factor (Familiarity) and a trial-level factor (Stimulus type). There were 14 separate blocks in total, each containing 20 trials. The type of block was determined by the identity of the Probe face used throughout that block. In the seven “Familiar” blocks, the Probe was the participant’s personally familiar face. In the other seven “Unfamiliar” blocks, the probe was an unfamiliar face, which was randomly selected from the distractor subset at the start of the experiment. The 14 blocks were presented in a fully randomized order for each participant. This design ensured that sequence-related effects, such as fatigue or practice, did not systematically bias the physiological responses.

At the end of each trial, participants were asked to indicate whether they had seen a face of the opposite sex, that is, the target (“Did you see a female/male face?”). Correct responses were rewarded with 10 points, while incorrect responses would deduct 10 points. Additionally, in order to ensure attention throughout the entire RSVP, the final stimulus would be either a dog or a cat face, which was counterbalanced over participants. Participants’ scores would increase or decrease

another 5 points based on their answer to the question “Did you see a dog or a cat?”. All two-choice responses were given using the “c” and “m” keys.

Figure 1

Trial sequence example



Note. Trial sequence illustrating the possible types and positions of the critical stimulus within a trial. The probe face represents either a personally familiar face or an unfamiliar face, depending on the block type. In this example, the personally familiar face is represented by the participants’ father’s face (the actual image shown here was taken from the image database, for reasons of privacy). The distractors and the fixed control face were gender-matched to the probe. The target face was of the opposite sex, here a female face, to serve as the behavioral detection goal. Only one critical face appeared per trial.

2.4. Data Analysis

Open-practices statement. All data and analysis scripts used in this paper are publicly available on the Open Science Framework (https://osf.io/fpcgu/). The study was not pre-registered.

2.4.1. Data Preprocessing

EEG Preprocessing. EEG data were processed offline using the Python package *eeg_eyetracking_parser* (Mathôt et al., 2023), which integrates functions from the MNE-Python library. Initially, raw EEG signals were re-referenced to the mastoid electrodes. Muscle artifacts were automatically detected by identifying activity in the 110-140 Hz high-frequency range that exceeded a z-score threshold of 5. The data were then band-pass filtered between 0.1 and 40 Hz to remove slow drifts and high-frequency noise, and subsequently downsampled to 250 Hz. Bad EEG channels were detected and rejected using the RANSAC algorithm

implemented in the *autoreject.Ransac*. To identify and remove ocular artifacts, we first created vertical and horizontal EOG channels by computing bipolar differences between electrodes placed above and below the left eye (vertical EOG), and between electrodes placed near the left and right temples (horizontal EOG). Independent Component Analysis (ICA) was then performed on a high-pass filtered copy of the EEG data (1Hz), using the 'picard' algorithm implemented in *mne.preprocessing.ICA*. Components related to blinks and eye movements were identified based on their strong correlation with the EOG channels, which were then removed from the data.

For ERP analysis, data were epoched time-locked to the onset of the critical stimulus, using a window from -100 ms to 1000 ms. A baseline correction was applied using the pre-stimulus interval (-100 to 0 ms). Bad epochs were identified and excluded using the *autoreject.Autoreject* procedure.

Additional Preprocessing for Time-frequency Analyses. EEG data were prepared for time-frequency analysis to specifically examine activity within the theta-band. Epochs were defined using the same time window (-100 to 1000 ms relative to stimulus onset). Spectral power in the theta band (4-8 Hz, in 2 Hz steps) was computed using Morlet wavelet convolution with a two-cycle kernel. The resulting time-frequency data were cropped to a 0-1000 ms post-stimulus window and downsampled by a factor of 16 (from 1000 Hz). To allow for between-subject comparisons, the power values were z-transformed within each participant.

Pupil-size Preprocessing. Pupil data were preprocessed following the procedures described by Mathôt and Vilotijević (2022). Missing or invalid samples were interpolated using the blink reconstruction function from Eyelinkparser (see *datamatrix.series.blinkconstruct*). Each pupil trace was baseline-corrected by subtracting the mean pupil diameter during the 50 ms preceding target onset. Signals were then downsampled to 25 Hz. Given the relatively slow dynamics of the pupil response, this sampling rate provided sufficient temporal resolution while enhancing computational efficiency and visualization quality.

In addition to analyzing absolute pupil size, we computed pupil size change to capture the dynamic fluctuations. We calculated the difference between consecutive time points in the preprocessed pupil traces. The resulting variable represents the sample-to-sample change in pupil diameter. To reduce high-frequency noise, we applied a moving average smoothing filter with a 240 ms window.

2.4.2. Group-level Univariate Analyses

In the initial stage of analysis, we assessed whether physiological responses to probe and control stimuli differed at the group level across two experimental conditions: familiar and unfamiliar. Based on prior findings (Bowman et al., 2013,

2014; Chen et al., 2023), we expected stronger responses to familiar probes compared to control stimuli, while no reliable difference was hypothesized between unfamiliar probes and controls.

We focused on four variables: ERP signals at the Pz electrode, theta-band power across the Fz, Pz, and Cz electrodes, absolute pupil size, and pupil size change. For each condition, we applied a cluster-based permutation test (CBPT) on the group-level to identify continuous time windows where significant differences were present between probe and control trials.

Analyses were carried out using the *time_series_test* library (Mathot & Vilotijevic, 2022), following their approach of applying single-trial linear mixed-effects models. The ERP signals at Pz, z-scored theta band power, pupil size, and pupil size change served as single measures. Trials level (probe or control) was treated as a fixed effect with by-participant random intercepts and slopes. Clusters were identified using a significance threshold of $p < .05$, and the absolute sum of z-scores within each cluster was used as the test statistic. Each test was run with 1,000 iterations.

2.4.3. Individual-level Univariate Analyses

Individual-level analyses were performed using single-trial data through region of interest (ROI) analyses (Brooks et al., 2016; Poldrack, 2007). For each subject and measure, we defined a time window based on the maximum response observed in target-present trials. Specifically, ERP signals at Pz and theta band power were analyzed using a 200-ms window, while a longer 400-ms window was used for pupil size and pupil size change due to their slower temporal dynamics (Chen et al., 2023). Within these individual-specific windows, we calculated the mean value of each physiological measure for every single trial. These single-trial values were then used as the data points for independent-sample t-tests to compare probe and control levels for each participant. This approach used one-tailed t-tests with an alpha level of 0.05. By defining a single ROI per participant based on target trials, this approach reduced the need to make multiple comparisons.

2.4.4 Combining Significance Analysis (Fisher's Method)

To increase detection sensitivity by aggregating evidence across multiple physiological measures, we applied Fisher's combined probability test at the individual level. This approach integrates the results of separate univariate analyses into a single joint test, allowing for the identification of participants who may have consistent but subthreshold effects across the measures taken.

For each participant, we combined the one-tailed p-values from three univariate tests: ERP amplitudes at Pz, z-scored theta-band power, and pupil size change. Absolute pupil size was excluded from this analysis due to its correlation

with pupil size change, which might be inconsistent with the assumption of statistical independence of Fisher's method.

The combined test statistics were calculated using the standard Fisher formula:

$$X^2_{2k} = -2\sum_i^k \ln(p_i),$$

where p_i represents the one-tailed p-value from the ith test. k equals three here, representing the number of tests being combined. X^2 follows a chi-squared distribution with $2k$ degrees of freedom. To avoid computational errors, p-values equal to zero were replaced with the smallest legitimate value (0.001). The resulting combined p-value reflects the overall strength of evidence for probe-control differences across all three measures. Participants with a combined p-value below .05 were classified as detected.

3. Results

3.1. Task Performance

Accuracy was calculated across all trial types, with correct responses defined as "yes" for target trials and "no" for probe, control, and distractor trials. The overall mean accuracy was 75.8%, exceeding the chance level of 50%. Specifically, participants correctly detected targets on 72.8% of target-present trials and correctly rejected non-targets on 77.8% of target-absent trials. At the individual level, all participants achieved an overall accuracy of at least 64.6% in this target/no-target detection task. Furthermore, the mean end-of-stream task accuracy across all trials was 94.6%. These accuracy levels indicate that participants followed task instructions and remained attentive throughout the experiment.

3.2. Group-level Univariate Analyses[6]

Figure 2 illustrates the grand-average ERP waveforms at Pz for each trial type in both the familiar and unfamiliar conditions. In both conditions, ERP responses to target faces significantly differed from control faces. Specifically, in the familiar condition (Figure 2a), target faces elicited significant greater amplitudes compared to control faces during the interval from 456 to 1000 ms (p < 0.001). Similarly, in the unfamiliar condition (Figure 2b), target faces differed significantly from control faces between 492 and 960 ms (p < 0.001).

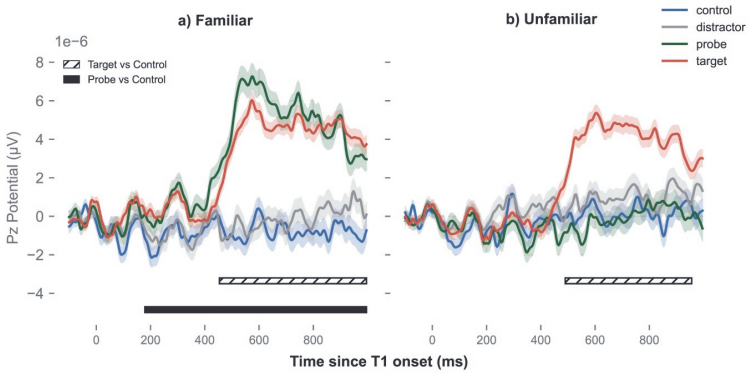
Critically, the ERP amplitudes to probe faces significantly differed from control faces only in the familiar condition (180–1000 ms, p < 0.001; Figure 2a). In

[6] Supplementary group-level comparisons between target and familiar probe trials across all modalities are provided in the Appendix for reference.

contrast, there were no significant differences observed between ERP waveforms for unfamiliar probe and control faces (Figure 2b).

Figure 2

Grand average ERP waveforms at the Pz electrode



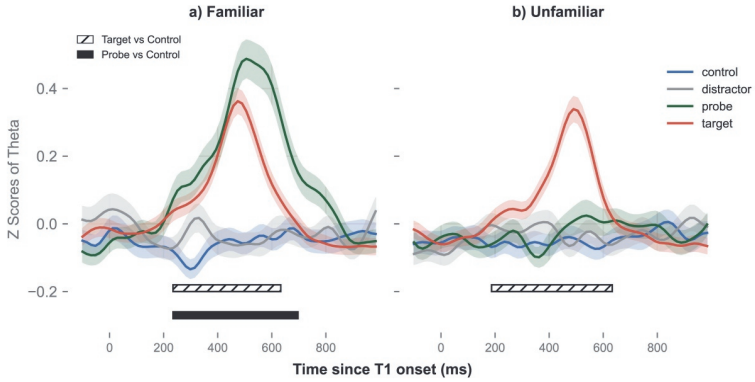
Note. Grand-average ERP waveforms for the a) familiar and b) unfamiliar conditions. Lines represent mean potential over time (in μV), time-locked to the onset of the critical item, plotted separately for target (red), probe (green), distractor (grey) and control (blue) trials. Shaded regions indicate ±1 SEM across participants. Horizontal bars indicate time windows where a significant cluster ($p < .05$) was detected by the group-level cluster-based permutation test (hatched bar for target vs. control, solid black bar for probe vs. control).

The results from the CBPT demonstrated that theta-band power exhibited significant differences between personally familiar faces and control faces (240–709 ms, $p < 0.001$; Figure 3a). Additionally, target faces also elicited significantly greater theta-band responses than control faces in the familiar condition (240–644 ms, $p < 0.001$).

In the unfamiliar condition (Figure 3b), however, significant differences in the theta-band power were observed only between target and control faces (191–644 ms, $p < 0.001$), with no significant difference detected between unfamiliar probe and control stimuli.

Figure 3

Average z-scores on theta waves

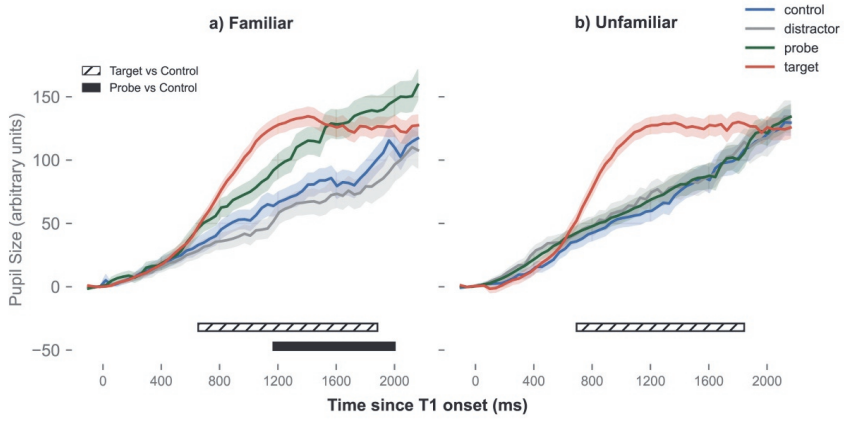


Note. Average Theta-band power (z-scored) over time for the a) familiar and b) unfamiliar conditions. Formatting and statistical conventions match those in Figure 2.

As depicted in Figure 4, pupil responses to target faces were significantly greater compared to control faces in both familiar (667 – 1918 ms, $p < 0.001$) and unfamiliar conditions (707–1877 ms, $p < 0.001$). Notably, pupil responses to familiar (probe) faces significantly exceeded those to control faces (1191–2039 ms, $p = 0.013$).

Figure 4

Average pupil traces



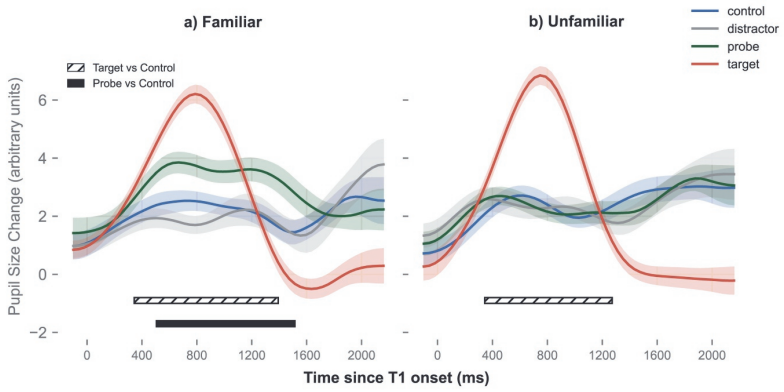
Note. Average pupil traces over time for a) familiar and b) unfamiliar conditions. Plotting format and statistical markings are consistent with Figure 1.

Figure 5 illustrates the time course of pupil size change in the familiar and unfamiliar conditions. In both conditions, the pupil size change in response to

target faces was significantly greater than that to the control faces, with significant clusters observed from 344 to 1393 ms in the familiar condition and from 344 to 1272 ms in the unfamiliar condition (both $p < 0.001$). Moreover, the pupil size change in response to the personally familiar faces was significantly greater than that to the control faces, occurring from 505 to 1514 ms ($p < 0.001$).

Figure 5

Average pupil size change



Note. Pupil size changes for a) familiar and b) unfamiliar conditions. Plotting format and statistical markings are consistent with Figure 1.

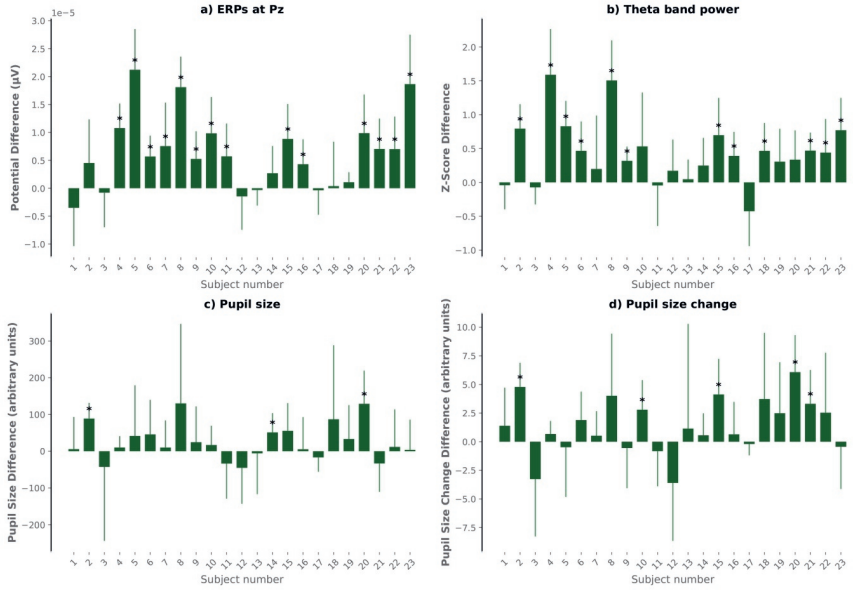
3.3. Individual-level Univariate Analyses

Individual-level analyses were performed exclusively for the comparison between familiar probe (personally familiar faces) and control faces, that is, only using the trials from familiar condition. This selection was guided by the group-level results, which indicated that only familiar faces elicited reliably different physiological responses compared to control faces. For each subject, the response difference was computed as the sum of the sample-by-sample differences between familiar and control trials within the predefined ROI, determined based on the response in target trials.

The results of these analyses are summarized in Figure 6. ERP amplitudes at Pz exhibited the highest detection rate, with 14 out of 23 participants (60.9%) showing statistically significant differences between familiar probe and control stimuli. Theta-band power showed significant differences in 12 participants, resulting in a 52.2% detection rate. However, detection rates for pupil-based measures were considerably lower: 3 participants (13.0%) showed significant differences between familiar and control stimuli in absolute pupil size, and 5 participants (21.7%) in pupil size change.

Figure 6

Individual-level ROI-based analysis in the familiar condition

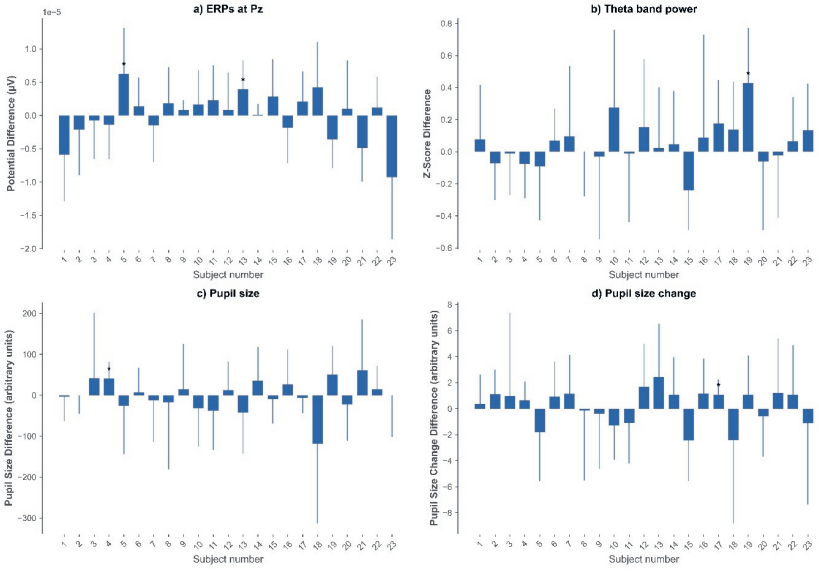


Note. Individual probe-control differences for each subject in the familiar condition, based on ROI-based t-tests for each subject and each dependent measurement. Each panel shows results for each measurement: a) ERP amplitudes at Pz, b) theta-band power, c) pupil size and d) pupil size change. Bars represent the mean difference between probe and control trials within each participant's selected ROI time window. Error bars indicate ±1 SEM across trials. Asterisks denote participants with statistically significant differences (p <.05, one-tailed).

Additionally, we applied the same individual-level analysis to the unfamiliar block. The detection rate was low across all measures. Specifically, significant effects (i.e., false alarms) were observed in only 2 out of 23 participants for ERPs at Pz. For theta power, pupil size, and pupil size change, significant effects were observed in only 1 of 23 participants (Figure 7).

Figure 7

Individual-level ROI-based analyses in the unfamiliar condition



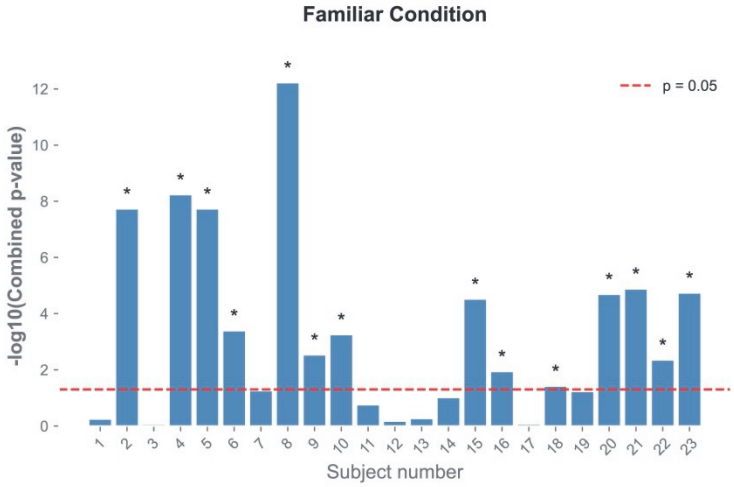
Note. Figure conventions follow Figure 6.

3.4. Multivariate Analysis (Fisher's Method)

Figure 8 shows the p-values obtained for each participant using Fisher's method, based on individual-level univariate analyses of three measures: ERP amplitudes at Pz, theta-band power and pupil size change. In total, 14 out of 23 (60.9%) showed combined *p*-values below the .05 threshold. Several additional participants (e.g., subjects 7, 14 and 19) had combined *p*-values near .05, suggesting marginal effects although not reaching conventional significance.

Figure 8

Combined significance per participant

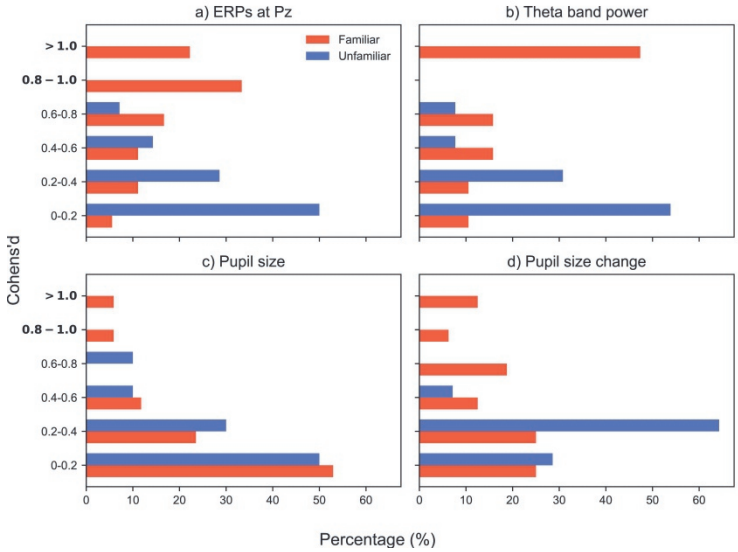


Note. Combined significance values from Fisher's method, separately for each participant in the familiar condition. Bars represent -log10 of the combined *p*-value across ERP signals (Pz), theta band power, and pupil size change. The red dashed line marks the significance threshold (p = .05). Asterisks indicate participants with significant combined effects.

Figure 9 illustrates the distribution of effect sizes (Cohen's *d*) from the individual-level comparisons between probe and control trials, across all four measures, for both familiar and unfamiliar conditions. Effect sizes were binned into six ranges: 0 to 0.2, 0.2 to 0.4, 0.4 to 0.6, 0.6 to 0.8, 0.8 to 1.0 and > 1. For ERP signals in the familiar condition, over 50% of participants showed large effect sizes (d > 0.8) and more than 70% showed medium-to-large effects (d > 0.6). For theta-band power, the proportion was slightly lower, with approximately 50% of the participants showing large effects and over 60% reaching medium-to-large thresholds (0.6). However, pupil-based measures yielded generally smaller effects. Specifically, for pupil size, around 10% of participants showed large effect size (d > 0.8) in the familiar condition whereas none exceeded d = 0.8 in the unfamiliar condition. For pupil size change, over 30% participants showed medium-to-large effects (d > 0.6) and about 20% showed large effects in the familiar condition. No participants showed effect sizes larger than 0.6 in the unfamiliar condition.

Figure 9

Effect size (Cohen's d) distribution

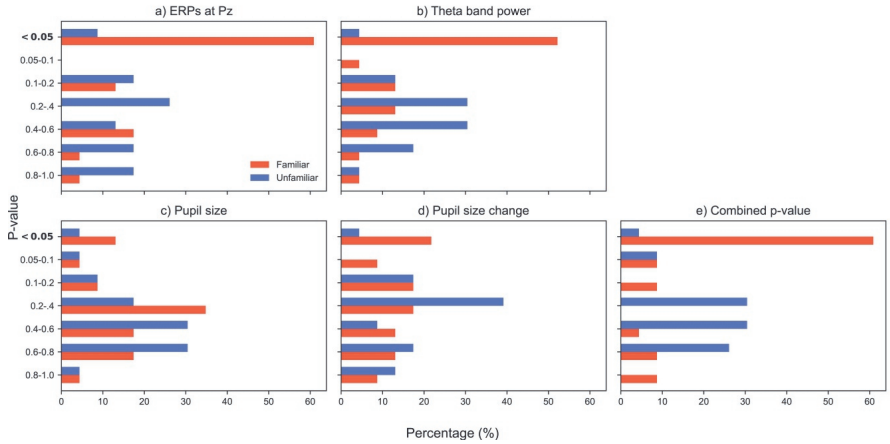


Note. Distribution of individual effect sizes (Cohen's *d*) for each dependent measurement in the familiar (red) and unfamiliar (blue) conditions. Each panel corresponds to a different measurement: a) ERP amplitudes at Pz, b) theta band power, c) pupil size, and d) pupil size change. Bars represent the proportion of participants whose probe-control effect sizes fall into each bin.

Figure 10 shows the distribution of *p*-values from both the individual-level univariate analyses and multivariate analyses. *p*-values were binned into the following ranges: <0.05, 0.05-0.1, 0.1-0.2, 0.2-0.4, 0.4-0.6, 0.6-0.8, and 0.8-1. In the familiar condition, ERP amplitudes and theta-band power measures showed *p*-values below .05 in a substantial proportion of participants, consistent with high detection rates reported earlier. The distribution of *p*-values of pupil-based measures were relatively flat, with most values falling above the .05 threshold, in both conditions. However, a higher proportion of participants reached the threshold for significance ($p < .05$) in the familiar condition compared to the unfamiliar condition. This indicates that pupil size and pupil size change were sensitive to personally familiar faces, albeit with lower overall detection rates. The combined *p*-value distribution showed a distinct separation between personally familiar stimuli and unfamiliar stimuli, indicating improved detection effectiveness when integrating across multiple measures.

Figure 10

p-value distribution



Note. Distribution of p-values from individual ROI-based t-tests for each dependent measurement in the familiar (red) and unfamiliar (blue) conditions. Panels a-d correspond to the same measurements as in Figure 8. Bars represent the proportion of participants whose probe > control p-values fall into each bin.

4. Discussion

4.1. Summary

This study evaluated the effectiveness of multiple physiological signals – ERP amplitude at electrode at Pz (targeting the P300), theta-band power, pupillary responses (pupil size and pupil size change) – in detecting concealed information in an RSVP paradigm. At the group level, all four measures successfully differentiated personally familiar stimuli from neutral control items. However, substantial differences emerged at the individual level: ERP amplitudes demonstrated the highest detection sensitivity (14 out of 23 participants; 60.9%), followed by theta-band power (12 out of 23 participants; 52.2%). In contrast, pupil size (3 out of 23 participants; 13.0%) and pupil size change (5 out of 23 participants; 21.7%) showed notably lower detection rates. By contrast, false alarms in the unfamiliar condition were obtained for only 2 participants on the P300, and 1 participant for each of the other measures, indicating that the univariate detection rates are unlikely to reflect chance. These results underscore that while pupillometry is sensitive at the group level, it may be less robust for individual-level detection under RSVP conditions. Moreover, the combined inference using Fisher's method yielded significant combined p-values for 14 out of 23 participants.

4.2. ERP and Theta-Band Power (CNS Measures)

A significant ERP amplitude difference at Pz was observed between personal familiar and control faces from approximately 180 to 1000 ms post-stimulus. Within this window, both probe and target conditions elicited a prominent positive peak, followed by a late positive slow wave. This pattern aligns with previous CIT studies showing enhanced P300 amplitudes in response to concealed information, such as personally familiar faces (Lefebvre et al., 2007) or self-relevant autobiographical items (Rosenfeld et al., 2004, 2006). The P300 component has been linked to the engagement of cognitive resources for evaluating task-relevant or self-relevant stimuli, reflecting a process of attention allocation, stimulus recognition, and working memory updating (Polich, 2007; Squires et al., 1975). In the context of concealed information detection, an enhanced P300 is thought to reflect the automatic and meaningful recognition of critical items, even when explicit behavioral responses are absent. Interestingly, the probe stimuli in the current study elicited a prominent P3 component with an amplitude comparable to that of the target stimuli. This contrasts with findings from recent RSVP studies which reported weaker P3 responses relative to targets (Alsufyani et al., 2019; Hajilou, 2020). Those studies utilized either famous faces (Alsufyani et al., 2019) or lecturers' faces as personally familiar stimuli (Hajilou, 2020). This discrepancy likely reflects qualitative differences in stimulus familiarity. The participant-provided images in our study represented highly personal familiarity, thereby eliciting a robust neural response similar in magnitude to the target.

The extended positivity beyond the typical P300 window observed for both probe and target stimuli may reflect sustained cognitive engagement to task-relevant or self-salient information. This interpretation is consistent with prior findings on the late positive potential (LPP), a component associated with sustained attention to motivationally significant events (Hajcak et al., 2010; Schupp et al., 2000).

At the individual level, ERP amplitude at electrode Pz successfully discriminated concealed information in 14 out of 23 participants (60.9%). Although substantial, this detection rate is somewhat lower than near-perfect levels that have been previously reported (e.g., Bowman et al., 2013; Rosenfeld et al., 2004, 2006). However, our findings are broadly consistent with recent work specifically examining familiar face recognition within RSVP paradigms, which reported comparable individual-level sensitivity for ERP analyses (e.g., 8 out of 14 significant participants; Hajilou, 2020). This suggests that the RSVP format alone may not explain the discrepancy. A likely reason could be the stimulus characteristics. Specifically, it is more difficult to process complex facial stimuli compared to simple text or words in a rapid visual stream. Furthermore, in our study, the familiar faces were processed for uniformity and thereby visually

degraded, potentially reducing their recognizability. As a result, participants may have failed to detect the familiar face on some trials, thereby reducing the likelihood of eliciting a differential neural response.

Significant enhancement in theta-band power was observed for personally familiar stimuli within a 240 – 640 ms time window. This finding aligns with prior studies suggesting that theta oscillations support a range of cognitive functions, including cognitive control, working memory maintenance, and internal attention regulation (Alsufyani et al., 2019; Cavanagh & Frank, 2014; Kahana et al., 2001; Tesche & Karhu, 2000). In the context of our RSVP-based CIT, the increase in theta-band power likely reflects the engagement of cognitive control to resolve attentional conflict. Personally familiar faces, although not task-relevant, may have briefly captured attention due to their self-significance. Participants likely needed to reorient attention and refocus on the target detection task.

At the individual level, theta-band power discriminated concealed information in 12 out of 23 participants (52.2%). Although slightly lower than the ERP-based detection rate, theta-band measures may still be considered useful in CIT for familiar faces, particularly under temporal constraints.

4.3. Pupillometry (ANS Measure)

The present study revealed a robust group-level effect in pupil dilation: Participants showed significantly greater dilation in response to personally familiar stimuli compared to control items. This finding is consistent with previous CIT research demonstrating that pupil size is a reliable physiological marker of concealed information (Chen et al., 2023; Dionisio et al., 2001; Lubow & Fein, 1996).

Early research demonstrated that pupil size increases with cognitive load and attentional demands (Kahneman & Beatty, 1966), and subsequent studies linked pupil dilation to the allocation of cognitive resources under varying task demands (Cabestrero et al., 2009). Querino et al. (2015) further suggested that pupil responses can differentiate between automatic and controlled processes, with significantly greater dilation during controlled, effortful processing. In our RSVP-based CIT paradigm, the sudden appearance of a personally familiar face (e.g., a parent's face) is likely to trigger automatic attentional capture. Participants must actively redirect attention toward the ongoing rapid stream. The observed pupil dilation in response to personally familiar stimuli may thus reflect the cognitive effort required to resolve this attentional conflict and sustain goal-directed processing under temporally constrained conditions.

Pupil dilation has also been linked to phasic activity in the locus coeruleus–norepinephrine (LC-NE) system, which plays a central role in modulating attentional engagement and arousal (Alnæs et al., 2014; Gilzenrat et al., 2010;

Nieuwenhuis et al., 2011). According to adaptive gain theory, this system modulates attentional focus based on stimulus salience, with pupil dilation serving as an index of enhanced neural gain. In the current study, personally familiar stimuli likely triggered such a phasic response, consistent with their motivational and cognitive salience.

Despite the robust group-level effects observed in pupillary responses, the individual-level detection rates in the current study were relatively low. This finding is consistent with Chen et al. (2023), who also reported limited single-subject classification accuracy using pupil-based measures under an RSVP-CIT paradigm. This limitation can partly be attributed to the structure of RSVP paradigms. Because pupil size changes relative slowly over time, the rapid presentation of stimuli in RSVP can cause responses to temporally adjacent items to overlap. This makes it difficult to associate changes in pupil size with a specific stimulus, such as the probe, thereby reducing the accuracy of single-trial classification. Group-level analyses can benefit from averaging across participants, which reduces random noise and reveals consistent patterns in the data. However, individual-level classification requires stable differentiation of probe versus control items within each participant. The inherently low signal-to-noise ratio of pupil-based measures, combined with inter-individual variability in autonomic responses, may further limit their reliability under temporally demanding conditions.

By contrast, some earlier studies employing slower-paced CIT designs (e.g., Bradely & Janisse, 1981; Dionisio et al., 2001; Seymour et al., 2013) reported higher individual detection rates using pupil-based measures. However, the findings across these studies remain mixed, and differences in task design and classification methodology further complicate direct comparison. Taken together, these results indicate that while pupil dilation is promising for individual detection in CIT, its effectiveness is highly constrained by methodological factors – particularly the stimulus pacing and signal isolation.

4.4. Combined Inference across Multiple Physiological Measures

Previous efforts have emphasized the potential of combining central and autonomic physiological signals to improve detection accuracy in CIT (Ambach et al., 2010; Gamer & Berti, 2010). From this perspective, we evaluated whether integrating ERP amplitude, theta-band power, and pupil size change would enhance individual-level detection in an RSVP-based CIT.

Using Fisher's method for *p*-value combination, we identified fourteen out of twenty-three participants with significant joint responses. Although this detection accuracy is not beyond the one obtained from ERP amplitude alone, it captured several distinct individuals who were not reliably detected by any single

measure. For example, subjects 2 and 18 were successfully identified through the combined inference. Although their ERP responses were not significantly different between probe and control faces, they showed significant differences in either theta or pupil measures. This finding illustrates how combining modalities can compensate for weak effects in one domain by leveraging strong signals in another. In contrast, subjects 7 and 11 exhibited a significant P300 effect but lacked strong responses in other two signals, resulting in a non-significant combined *p*-value. Subject 14 exhibited a significant effect in absolute pupil size only, yet similarly failed to reach significance in the combined measure. Notably, these three subjects showed near-significant combined *p*-values. This outcome reflects a limitation of unweighted *p*-value combination methods: Strong evidence in one modality can be diluted when other modalities contribute less consistent information.

4.5. Limitations and Future Directions

One may argue that different stimulus sources for familiar and unfamiliar faces could introduce systematic bias. To minimize this risk, all images used in our study underwent identical standardization processes. Although residual differences cannot be entirely ruled out, the combination of rigorous stimulus normalization and the very rapid presentation rate makes it highly unlikely that systematic image properties, rather than genuine recognition, accounted for the observed neural effects. Future research may further address this point by presenting familiar images from one participant as unfamiliar stimuli for others, which would provide an additional control for any remaining sources of bias.

An additional limitation of the present study is the relatively low detection rate at the individual level, particularly for pupillary measures. While robust group-level effects were observed across modalities, achieving reliable individual detection remains challenging. In particular, the short ISIs in RSVP paradigms, while well suited EEG data to track rapid neural responses, likely limited the effectiveness of slower-developing signals such as pupil dilation. Extending the ISI may enhance the detection efficiency of autonomic responses; however, prior research suggests that longer ISIs can reduce the sensitivity of P300 component (Matsuda et al., 2009; Gamer & Berti, 2020). These findings illustrate the trade-off between optimizing experimental timing for CNS and ANS measures. Another risk of resorting to a slower pace of presentation is that it might open the door for effective countermeasures, which the RSVP method aims to achieve.

It is noteworthy that although EEG data in current and previous studies (Bowman et al., 2013, 2014) achieved high detection rates in CIT, it's still challenging to translate this approach to real-world settings. For example, in laboratory settings, the analysis of EEG data often requires averaging across many repetitions to enhance the signal-to-noise ratio. However, practical applications

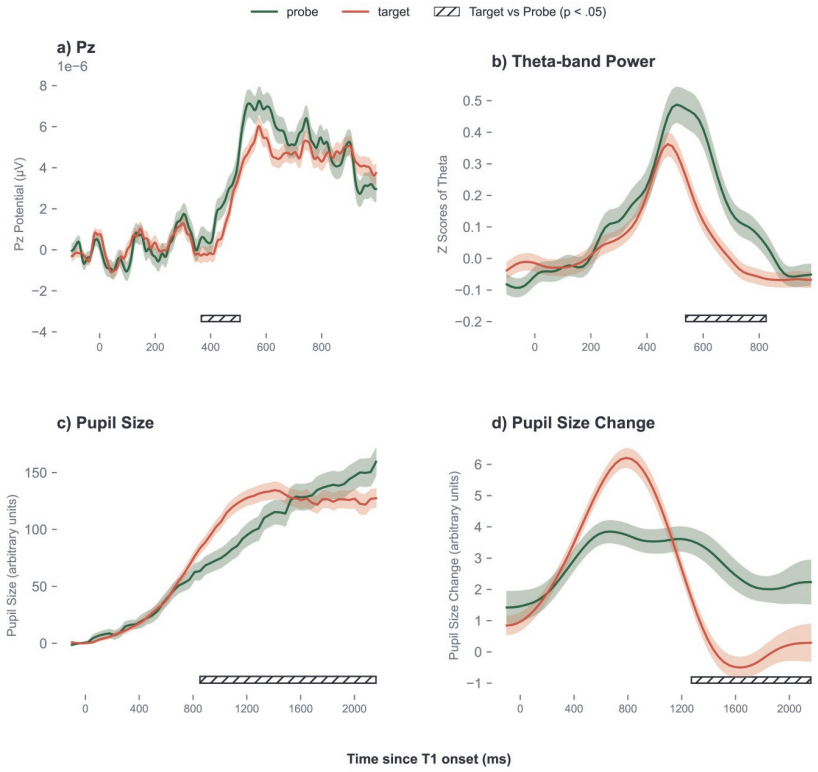
require high accuracy from relatively few trials. Our findings offer empirical support for a potential multimodal solution to this limitation. As discussed in previous section, the combined inference successfully identified individuals who were missed by single measures. This demonstrates that integrating multiple physiological signals can compensate for the inherent instability in single-trial data. However, the modest overall improvement in combined detection reflects the limitations of our current integration approach. Future work might explore alternative integration strategies and analysis algorithms to help transition this technology into realistic environments.

Appendix

To supplement the primary analysis, we compared target and probe trials within the familiar condition (Figure A1). The cluster-based permutation test (CBPT) revealed a significant difference at Pz during the 368 – 508 ms interval (p = 0.013). Regarding time-frequency results, a significant difference in theta-band power was observed between 540 and 828 ms (p < .001). For pupil metrics, target and familiar probe trials differed significantly in both mean pupil size (860–2180 ms, p = .02) and pupil size change (1260–2140 ms, p < .001).

Figure A1

Group-level comparisons between Target and Probe trials in the familiar condition.



Note. (a) ERP waveforms at the Pz electrode (in μV); (b) Theta-band power; (c) Mean pupil size; and (d) Pupil size change. Lines represent group-level means time-locked to the onset of the critical item, plotted for target (red) and probe (green) trials. Shaded regions indicate ±1 SEM across participants. Horizontal bars at the bottom of each panel indicate time windows where a significant cluster (p < .05) was detected for the target vs. familiar probe comparison using cluster-based permutation test.

Chapter 5
General Discussion

A fundamental challenge for the human cognitive system is to preserve distinct representations from a rapid, continuous sensory system. This dissertation set out to examine how key cognitive processes, including WM consolidation, conscious perception, and stimulus recognition, face this challenge under temporal constraints using the RSVP paradigm. This work investigated the dynamic allocation of limited resources that determines what information gains access to consciousness, and what is lost. To this end, three empirical studies were conducted to address different facets of this resource regulation. First, we investigated the nature of WM consolidation failures when resources are limited across time, by testing the suitability of different computational models of WM in accounting for the target representations during the AB. Second, we examined whether top-down spatial attention configurations can be flexibly adjusted under temporal constraints, and how such flexibility affects the nature of conscious perception – specifically, whether awareness emerges in a graded or discrete manner under varying attentional configurations. Finally, we explored how internal memory representations can covertly guide attention under temporal constraints, even in the absence of overt report. Across studies, we show that the system regulates information flow via reactive gating, proactive spatial scaling, and memory- driven priority signals. In this final chapter, I provide an overview of these findings, and discuss their implications for attention, working memory, and consciousness.

The Discrete Nature of Working Memory Encoding Limitations

The classical AB paradigm provides a window through which we can examine how limited cognitive resources are allocated across time. One of the central questions concerns which cognitive processes are disrupted and thereby lead to the failure to report T2. Although accounts diverge on the precise locus of this disruption, a widely held view is that WM consolidation is impaired during the AB (Chun & Potter, 1995; Jolicœur & Dell'Acqua, 1998,1999; Wyble et al., 2009). Yet, the precise nature of this encoding limitation remains unclear. Does it reflect a complete encoding failure, in which T2 never gains access to WM on a subset of trials, or does it reflect degraded encoding, such that target representations enter WM but with insufficient precision for accurate report?

In **Chapter 2**, multiple WM models were systematically compared across AB datasets and experimental conditions. The results consistently favored models that include a guessing component, such as the Standard Mixture model, the Slot model, and the Slots plus Resources model. These models assume that not all items can be encoded into WM. Items that fail to be encoded produce random responses, represented by the uniform component of the error distribution. In contrast, Variable Precision (VP) models – assuming that all items are encoded but with

variable levels of precision – generally performed worse, especially at short stimulus-onset asynchronies where the blink occurs. A VP variant that incorporated a guessing parameter (VPG model) provided a better fit than the standard VP model, supporting the view that all-or-none encoding is a central aspect of WM consolidation under temporal constraints. This aligns with behavioral evidence that, within the blink window, access probability (guessing) changes while precision is comparatively stable (Asplund et al., 2014; Sergent & Dehaene, 2004).

It is worth noting that improvements in the VP-family fits did occur, but under specific conditions – notably when the blink was attenuated (e.g., at longer stimulus-onset asynchronies or when T2 was defined by color). Our data suggest that when temporal separation or feature configuration eases the bottleneck, variability in representational precision becomes more visible. Within the core blink window, however, performance is best explained by failures of encoding rather than gradual loss of precision.

An additional insight came from the performance of the Swap model at lag-1 condition. The model provided a markedly better fit at lag 1, consistent with empirical findings that order confusions between T1 and T2 are more likely when the targets are temporally adjacent and share overlapping features (Akyürek et al., 2012; Karabay & Akyürek, 2019). The success of the Swap model at lag 1 supports the interpretation that lag-1 sparing reflects not only preserved consolidation but also increased vulnerability to target confusions, as described in the eSTST framework (Wyble et al., 2009; 2011).

Overall, these model-based results suggest that under strong temporal constraints (e.g., within blink window), errors are best explained by encoding failures rather than reduced precision. These findings support a discrete- access account, in which limited attentional resources are temporarily fully occupied and only become available again after a brief interval. This is also consistent with the explanation in the eSTST model (Wyble et al., 2009, 2011), which proposes the time-dependent attentional gating mechanism. In this framework, attention is enhanced by T1 but then temporarily suppressed, limiting its availability for T2. In our findings, when temporal demands are relaxed (e.g., at longer lags), representational variability becomes more apparent. Moreover, at lag 1, misbinding and order confusions provide an additional source of error.

Within this modeling framework, the guess parameter serves as an index of discrete access during the blink, whereas precision reflects the quality of representations once access has been achieved. This separation sets up the next question addressed in Chapter 3: can top-down control of attentional scale shift these parameters – reducing guessing and/or altering precision – and there by change the form of conscious access during the AB?

The Spatiotemporal Configuration of Consciousness

The preceding section (Chapter 2) investigated WM consolidation in the traditional AB paradigm, where awareness of T2 has often been described as discrete and all-or-none. This view is supported by those studies which show a discrete emergence and complete loss of awareness (Asplund et al., 2014; Sergent & Dehaene, 2004; Vul et al., 2009). However, other findings indicate that awareness during the AB does not always align with this dichotomous view. Under certain conditions, awareness can emerge in a more graded fashion (Karabay et al., 2022; Nieuwenhuis & de Kleijn, 2011; Overgaard et al., 2006; Sy et al., 2021).

In **Chapter 3**, we addressed this issue by examining whether manipulations of attentional scale could modulate the nature of awareness experienced for T2 during the AB. In our study, the logic was that if attentional scale can be flexibly adjusted, then the nature of T2 consciousness should change accordingly: a narrow scale would be expected to produce discrete, all-or-none access, whereas a broad scale would lead to a more gradual emergence of awareness. Across three experiments, we tested this prediction with mixture modeling of continuous report data, focusing on how lag and attentional scale jointly affect guessing and precision of T2 representations. At the behavioral level, T2 report accuracy was consistently lower at short than long lags, indicating that conscious perception of T2 was absent on a subset of trials. Mixture modeling confirmed this pattern: in all three experiments, guess rates increased at short relative to long lags, indicating discrete loss of awareness during the AB.

The critical question was whether attentional scale could alter the quality of awareness when T2 was consciously perceived. In Experiment 1, the attentional scale was manipulated block-wise. At short lags, guess rates did not differ between narrow and broad conditions, but precision was lower under broad attentional scale. Comparing broad attention at short with the long-lag baseline, both guess rate and precision changed, indicating a higher probability of complete failures as well as less precise T2 representations. By contrast, narrow attention at short lag differed from the long-lag baseline only in guess rate, with precision remaining unchanged. This dissociation indicates that while the AB is fundamentally associated with discrete loss of awareness, broad attentional scale additionally produces a graded deterioration in representational quality. These findings align with Karabay et al. (2022), who showed that attentional focus can influence both the visibility and fidelity of T2 during the AB.

In Experiment 2, we attempted to induce attentional scaling with trial-wise cues. As in Experiment 1, guess rates were higher at short lags relative to long lags, but precision did not vary across attentional scales. We interpret this as evidence that trial-wise cues were insufficient to reliably modulate the attentional scale, consistent with prior claims that endogenous scaling requires stability and time to

be effectively implemented (Lawrence et al., 2020; Turatto et al., 2000). Also, participants' limited ability to adjust spatial focus on a trial-by-trial basis suggests that spatial attention needs time to scale and is not readily adjusted on a trial- by- trial basis (Hayden & Gallant, 2005).

In Experiment 3, semi-constant T1 locations (fixed or variable) were introduced within a single block, enabling participants to gradually learn these regularities and adjust their attentional scale accordingly. The precision effect emerged reliably only after 9 trials within a block, once learning had taken place. After learning, the pattern of results for broad versus narrow attentional scale at short lags, and for comparisons with the long-lag baseline, mirrored those observed in Experiment 1. This further suggests that attentional scale can be adaptively adjusted during the AB, but such adjustments depend on accumulated exposure rather than immediate, trial-by-trial control. Moreover, the findings from Experiment 3 also supports the view that the deployment of spatial attention can be modulated through statistical learning (Awh et al., 2012; Failing & Theeuwes, 2018).

Model comparison results were consistent with the parameter patterns observed in the empirical data. In Experiment 1 and 3, the full mixture model, which allows both guessing rate (P_g) and precision (σ) to vary across conditions, provided the best fit. By contrast, in Experiment 2 the constant σ model fit best. Overall, these results point to two forms of awareness loss that emerged in our study (**Chapter 3**). We conceptualized the gradual loss of awareness, reflected in reduced σ when T2 was consciously perceived, as attentional *blur*. This complements the classical notion of the attentional *blink*, which denotes a discrete loss of awareness marked by increased guessing rates at short lags. At short lags, broad attentional focus reduced the precision of T2 reports compared to narrow focus, leading to a 'blurred' T2. Relative to the long-lag baseline, narrow attentional focus was characterized primarily by increased guessing rate, corresponding to the typical AB, whereas broad attention was characterized by both increased guessing and reduced precision, reflecting the coexistence of blink and blur. Furthermore, the findings from these empirical experiments together indicate that proactive control can affect conscious access under temporal constraints. This is aligned with a recent study that observed a stronger interaction between spatial and temporal attention under higher task demands (Palmieri & Carrasco, 2024).

Another important concern is why the influence of attentional scale was observed only at short lags and not at longer intervals. Short lags impose strong temporal constraints, which limit the attentional resources available for processing successive targets. In this situation, struggling to report two targets correctly, participants are caught between two alternatives. A narrow, focal attentional model supports relatively high-fidelity processing of target identities but carries the risk of

over-engaging with T1 and losing T2 altogether. A broader, more diffuse mode reduces this risk by distributing attention more widely, yet it does so at the cost of lower T2 representational precision. At longer lags, temporal constraints are relaxed and resources are sufficient to support T2 report regardless of attentional scale, so these trade-offs between blink and blur are largely attenuated.

The distinct patterns for T1 and T2 further support this interpretation. Across experiments, T1 guessing varied with attentional scale whereas the precision remained unchanged. As the first target in the sequence, T1 is processed with relatively full attentional resources and thus presumably without a trade-off in allocation. In this situation, awareness tends to be all-or-none: participants either detect T1 or fail to report it, which is expressed in guessing but not in precision. By contrast, T2 must be processed while T1 is still being encoded during the blink time window, which constrains the available resources. Under this condition, both discrete and gradual loss of awareness can be expressed for T2.

Finally, the findings of this chapter complement those of **Chapter 2**. **Chapter 2** demonstrated that the WM consolidation is disrupted during the AB, making a guessing component a necessary, but not a sufficient, feature of T2 performance. The present results indicate that such failures of awareness can emerge in two forms: a discrete, all-or-none loss of access when attention is focused on a narrow area, and a gradual degradation of representational precision when attention is broadly distributed. Together, these findings suggest that the consciousness during the AB is not characterized by a single mode, but by a dual pattern influenced by both consolidation limits and attentional configuration.

Covert Recognition in RSVP

Chapter 4 extended the investigation to the interaction between external constraints and internal representations using the RSVP-CIT paradigm. **Chapter 4** examined covert recognition using an RSVP-CIT paradigm. While this design has its practical value for detecting concealed information, it also reflects how temporal attention is influenced by internal representations. Personally familiar information can automatically capture attention when it appears as a probe in RSVP streams. This allowed us to investigate how memory-driven attentional deployment can be detected through physiological signals under temporal constraints. To this end, we measured multiple physiological indicators including ERP amplitudes at the Pz electrode (targeting P300 component), theta-band power, and pupillary responses (pupil size and pupil size change).

We applied a cluster-based permutation test on the group level and found that all physiological indicators successfully distinguished familiar probes from neutral control stimuli, in line with previous CIT findings (Bowman et al., 2013, 2014; Chen et al., 2023; Rosenfeld et al., 2004, 2006). To interpret these effects, it

is useful to consider the cognitive processes that each measure reflects. The P300 component is closely related to the evaluation of salient stimuli and the updating of WM (Polich, 2007; Squires et al., 1975). Increases in theta-band power are linked to cognitive control and the regulation of internal attention (Cavanagh & Frank, 2014; Kahana et al., 2001). Furthermore, pupil dilation has been tied to activity in the locus coeruleus-norepinephrine system, which modulates arousal and attentional engagement (Gilzenrat et al., 2010; Nieuwenhuis et al., 2011). In the present RSVP-CIT context, personally familiar faces, although task-irrelevant, are likely to trigger automatic attentional capture due to their self-significance. This initial attentional capture creates a conflict with the ongoing goal of detecting targets in the rapid stream. Under temporal pressure, participants must therefore reorient attention and reallocate resources to sustain task performance. These processes are reflected in the physiological signals we observed.

At the individual level, however, detection sensitivity diverged. To control multiple comparisons, we applied region-of-interest analyses for each physiological measure. ERP achieved the highest detection rate, identifying covert recognition in more than half of the participants. Theta-band power provided somewhat lower but still substantial detection, whereas pupil-based measures provided only limited single-subject classification. One possible explanation for this divergence concerns the strengths and limitations of using RSVP in a CIT paradigm. On the one hand, rapid presentation minimizes opportunity for top-down control, reducing the likelihood that participants can deploy countermeasures to affect the responses to concealed information. On the other hand, the same temporal structure makes it difficult for slower-developing signals, such as pupil dilation, to be isolated from adjacent events. Group-level averaging can mitigate this limitation by reducing noise, but reliable individual-level detection requires stable probe-control differentiation within each participant. Earlier studies using slower-paced CIT designs have reported higher detection rates with pupil-based measures (Bradley & Janisse, 1981; Dionisio et al., 2001; Seymour et al., 2013), which is consistent with this interpretation. In comparison, central nervous system measures such as ERP and theta oscillations occur within a few hundred milliseconds and are therefore better aligned with the temporal structure of RSVP. The divergent performance across measures thus likely reflects differences in how well each physiological system aligns with the time scale of the task.

In sum, the present findings demonstrate that covert recognition can be detected under RSVP using multiple physiological measures, even when overt report is not required. ERP and theta-band signals proved more reliable for individual-level detection than pupillometry, yet each modality provides a distinct perspective on recognition processes under temporal constraints. These results not only show the availability of the RSVP-CIT for concealed information testing, but

also further illustrate the interaction between internal memory and temporal attention, in line with recent theoretical frameworks that suggests that attention flexibly shifts between perceptual and mnemonic domains (Che et al., 2024; Gresch et al., 2024; Nobre & Gresch, 2025).

Future Perspectives

While the current work has elucidated the interactions between perception, attention and memory within the RSVP paradigm, most analyses relied on comparing performance across discrete temporal slots (e.g., short vs. long lags). However, this discrete approach captures the outcomes of processing limits but may fail to characterize the continuous process of how these limits emerge and dissipate. Therefore, one direction of the future research is to investigate how these processing stages (such as working memory consolidation) unfold under varying temporal pressures. For instance, does the visual system dynamically adjust its processing speed to match the external input? Addressing these questions will require developing theoretical and computational models that explicitly capture the time-dependent nature of information processing in the visual system.

Moreover, the neural mechanisms underlying visual cognition under temporal constraints require precise mapping. While our behavioral data suggest a flexible resource allocation, the neural signature of this mechanism remains to be fully identified. High-temporal-resolution neuroimaging, such as EEG or MEG, is therefore essential to track how information is dynamically prioritized, encoded, and maintained across successive moments.

Finally, most current paradigms rely on simplified and static visual displays. Extending research to more naturalistic and dynamic environments is crucial for understanding how temporal constraints influence visual cognition in real-world settings. To this end, future studies could consider the integration of other sensory modalities and the demands of longer, sustained tasks. Such approaches will help clarify how temporal constraints shape visual cognitive processing dynamically.

Conclusion

This dissertation investigated the mechanisms of visual cognition under temporal constraints. By combining computational modeling, behavioral psychophysics, and physiological measures, we aimed to explore how the visual cognition system adapts under time pressure. Our findings demonstrate that cognitive bottlenecks typically appear in a discrete, all-or-none manner when resources are limited across time, although this pattern is not always rigid. We further found that the nature of conscious access – whether discrete or graded – can be dynamically influenced by the proactive configuration of spatial attention.

This also suggests an interaction between the spatial aspect of attention and its temporal resolution. Moreover, we found that internal memory representations can covertly guide attention, capturing processing resources even in the absence of overt report. Taken together, these results suggest that the temporal constraints observed in RSVP are not merely passive structural failures, but reflect active control mechanisms that strategically balance representational precision and conscious access.

References

Akyürek, E. G., & Hommel, B. (2005). Target integration and the attentional blink. *Acta Psychologica*, *119*(3), 305–314. https://doi.org/10.1016/j.actpsy.2005.02.006

Akyürek, E. G., & Wolff, M. J. (2016). Extended temporal integration in rapid serial visual presentation: Attentional control at Lag 1 and beyond. *Acta Psychologica*, *168*, 50-64. https://doi.org/10.1016/j.actpsy.2016.04.009

Akyürek, E. G., Eshuis, S. A. H., Nieuwenstein, M. R., Saija, J. D., Başkent, D., & Hommel, B. (2012). Temporal target integration underlies performance at Lag 1 in the attentional blink. *Journal of Experimental Psychology: Human Perception and Performance*, *38*(6), 1448–1464. https://doi.org/10.1037/a0027610

Akyürek, E. G., Hommel, B., & Jolicoeur, P. (2007). Direct evidence for a role of working memory in the attentional blink. *Memory & Cognition*, *35*(4), 621-627. https://doi.org/10.3758/BF03193300

Akyürek, E. G., Leszczyński, M., & Schubö, A. (2010). The temporal locus of the interaction between working memory consolidation and the attentional blink. *Psychophysiology*, *47*(6), 1134–1141. https://doi.org/10.1111/j.1469-8986.2010.01031.x

Alnæs, D., Sneve, M. H., Espeseth, T., Endestad, T., van de Pavert, S. H., & Laeng, B. (2014). Pupil size signals mental effort deployed during multiple object tracking and predicts brain activity in the dorsal attention network and the locus coeruleus. *Journal of Vision*, *14*(4), 1. https://doi.org/10.1167/14.4.1

Alsufyani, A., Hajilou, O., Zoumpoulaki, A., Filetti, M., Alsufyani, H., Solomon, C. J., Gibson, S. J., Alroobaea, R., & Bowman, H. (2019). Breakthrough percepts of famous faces. *Psychophysiology*, *56*(1), e13279. https://doi.org/10.1111/psyp.13279

Alvarez, G. A., & Cavanagh, P. (2004). The capacity of visual short-term memory is set both by visual information load and by number of objects. *Psychological Science*, *15*(2), 106–111. https://doi.org/10.1111/J.0963-7214.2004.01502006.X

Ambach, W., Bursch, S., Stark, R., & Vaitl, D. (2010). A Concealed Information Test with multimodal measurement. *International Journal of Psychophysiology*, *75*(3), 258-267. https://doi.org/10.1016/j.ijpsycho.2009.12.007

Arnell, K. M. (2006). Visual, auditory, and cross-modality dual-task costs: Electrophysiological evidence for an amodal bottleneck on working memory consolidation. *Perception & Psychophysics*, *68*(3), 447–457. https://doi.org/10.3758/BF03193689

Arnell, K. M., & Jolicœur, P. (1999). The attentional blink across stimulus modalities: Evidence for central processing limitations. *Journal of Experimental Psychology: Human Perception and Performance*, *25*(3), 630–648. https://doi.org/10.1037/0096-1523.25.3.630

Arnell, K. M., & Larson, J. M. (2002). Cross-modality attentional blinks without preparatory task-set switching. *Psychonomic Bulletin & Review*, *9*(3), 497–506. https://doi.org/10.3758/BF03196305

Asplund, C. L., Fougnie, D., Zughni, S., Martin, J. W., & Marois, R. (2014). The attentional blink reveals the probabilistic nature of discrete conscious perception. *Psychological Science,* *25*(3), 824–831. https://doi.org/10.1177/0956797613513810

Awh, E., Barton, B., & Vogel, E. K. (2007). Visual working memory represents a fixed number of items regardless of complexity. *Psychological Science*, *18*(7), 622–628. https://doi.org/10.1111/j.1467-9280.2007.01949.x

Awh, E., Belopolsky, A. V., & Theeuwes, J. (2012). Top-down versus bottom-up attentional control: A failed theoretical dichotomy. *Trends in Cognitive Sciences, 16*(8), 437–443. https://doi.org/10.1016/j.tics.2012.06.010

Baars, B.J. (1989). *A cognitive theory of consciousness*. Cambridge, MA: Cambridge University Press.

Bae, G. Y., Olkkonen, M., Allred, S. R., Wilson, C., & Flombaum, J. I. (2014). Stimulus-specific variability in color working memory with delayed estimation. *Journal of Vision*, *14*(4), 7–7. https://doi.org/10.1167/14.4.7

Bainbridge, W. A., Isola, P., & Oliva, A. (2013). The intrinsic memorability of face photographs. *Journal of Experimental Psychology: General*, *142*(4), 1323–1334. https://doi.org/10.1037/a0033872

Balz, G. W., & Hock, H. S. (1997). The effect of attentional spread on spatial resolution. *Vision Research,* *37*(11), 1499–1510. https://doi.org/10.1016/S0042-6989(96)00296-9

Barriopedro, M. I., & Botella, J. (1998). New evidence for the zoom lens model using the RSVP technique. *Perception & Psychophysics, 60*(8), 1406–1414. https://doi.org/10.3758/BF03208001

Bays, P. M., Catalao, R. F. G., & Husain, M. (2009). The precision of visual working memory is set by allocation of a shared resource. *Journal of Vision*, *9*(10), 1–11. https://doi.org/10.1167/9.10.7

Ben-Shakhar, G. (2011). Countermeasures. In B. Verschuere, G. Ben-Shakhar, & E. Meijer (Eds.), *Memory detection: Theory and application of the concealed information test* (200–214). Cambridge University Press.

Ben-Shakhar, G., & Elaad, E. (2003). The validity of psychophysiological detection of information with the Guilty Knowledge Test: A meta-analytic review. *Journal of Applied Psychology*, *88*(1), 131–151. https://doi.org/10.1037/0021-9010.88.1.131

Block N. (2005). Two neural correlates of consciousness. *Trends in Cognitive Sciences*, *9*(2), 46–52. https://doi.org/10.1016/j.tics.2004.12.006

Block, N. (1995). On a confusion about a function of consciousness. *Behavioral and Brain Sciences*, *18*(2), 227–287. https://doi.org/10.1017/S0140525X00038188

Bonnel, A. M., & Miller, J. (1994). Attentional effects on concurrent psychophysical discriminations: Investigations of a sample-size model. *Perception & Psychophysics*, *55*(2), 162–179. https://doi.org/10.3758/BF03211664

Bourassa, M. È., Vachon, F., & Brisson, B. (2015). Failure of temporal selectivity: Electrophysiological evidence for (mis)selection of distractors during the attentional blink. *Psychophysiology*, 52(7), 933–941. https://doi.org/10.1111/psyp.12426

Bowman, H., & Wyble, B. (2007). The simultaneous type, serial token model of temporal attention and working memory. *Psychological review*, *114*(1), 38. https://doi.org/10.1037/0033-295X.114.1.38

Bowman, H., Filetti, M., Alsufyani, A., Janssen, D., & Su, L. (2014). Countering countermeasures: Detecting identity lies by detecting conscious breakthrough. *PLoS One*, *9*(3), e90595. https://doi.org/10.1371/journal.pone.0090595

Bowman, H., Filetti, M., Janssen, D., Su, L., Alsufyani, A., & Wyble, B. (2013). Subliminal salience search illustrated: EEG identity and deception detection on the fringe of awareness. *PLoS One*, *8*(1), e54258. https://doi.org/10.1371/journal.pone.0054258

Bradley, M. T., & Janisse, M. P. (1981). Accuracy demonstrations, threat, and the detection of deception: Cardiovascular, electrodermal, and pupillary measures. *Psychophysiology*, *18*(3), 307–315. https://doi.org/10.1111/j.1469-8986.1981.tb03040.x

Brady, T. F., & Alvarez, G. A. (2011). Hierarchical encoding in visual working memory: Ensemble statistics bias memory for individual items. *Psychological Science*, *22*(3), 384–392. https://doi.org/10.1177/0956797610397956

Broadbent, D. E., & Broadbent, M. H. (1987). From detection to identification: Response to multiple targets in rapid serial visual presentation. *Perception & Psychophysics, 42*(2), 105–113. https://doi.org/10.3758/BF03210498

Brooks, J. L., Zoumpoulaki, A., & Bowman, H. (2016). Data-driven region-of-interest selection without inflating Type I error rate. *Psychophysiology*, *54*(1), 100-113. https://doi.org/10.1111/psyp.12682

Burnett, K. E., d'Avossa, G., & Sapir, A. (2013). Matching cue size and task properties in exogenous attention. *The Quarterly Journal of Experimental Psychology,* *66*(12), 2363–2375. https://doi.org/10.1080/17470218.2013.780086

Cabestrero, R., Crespo, A., & Quirós, P. (2009). Pupillary dilation as an index of task demands. *Perceptual and Motor Skills*, *109*(3), 664–678. https://doi.org/10.2466/pms.109.3.664-678

Carrasco M. (2011). Visual attention: the past 25 years. *Vision Research*, *51*(13), 1484–1525. https://doi.org/10.1016/j.visres.2011.04.012

Castiello, U., & Umiltà, C. (1990). Size of the attentional focus and efficiency of processing. *Acta Psychologica, 73*(3), 195–209. https://doi.org/10.1016/0001-6918(90)90022-8

Cavanagh, J. F., & Frank, M. J. (2014). Frontal theta as a mechanism for cognitive control. *Trends in Cognitive Sciences*, *18*(8), 414–421. https://doi.org/10.1016/j.tics.2014.04.012

Cavanagh, J.F., Frank, M.J., Klein, T.J., & Allen, J.J.B. (2010). Frontal theta links prediction errors to behavioral adaptation in reinforcement learning. *Neuroimage*, *49*(4), 3198–3209. https://doi.org/10.1016/j.neuroimage.2009.11.080

Che, X., Lian, H., Zhang, F., Li, S., & Zheng, Y. (2024). The Reactivation of working memory representations affects attentional guidance. *Psychophysiology*, *61*(3), e14514. https://doi.org/10.1111/psyp.14514

Chen, I. Y., Karabay, A., Mathôt, S., Bowman, H., & Akyürek, E. G. (2023). Concealed identity information detection with pupillometry in rapid serial visual presentation. *Psychophysiology, 60*(1), e14155. https://doi.org/10.1111/psyp.14155

Chen, I. Y., Mathot, S., van der Mijn, R., Karabay, A., Bowman, H., & Akyurek, E. G. (2025). Concealed personally familiar face detection with EEG in rapid serial visual presentation. *PsyArXiv*. https://doi.org/10.31234/osf.io/axp4w_v1

Chennu, S., Craston, P., Wyble, B., & Bowman, H. (2009). Attention increases the temporal precision of conscious perception: Verifying the Neural-ST Model. *PLoS Computational Biology*, *5*(11), e1000576. https://doi.org/10.1371/journal.pcbi.1000576

Chun, M. M., & Jiang, Y. (1998). Contextual cueing: Implicit learning and memory of visual context guides spatial attention. *Cognitive Psychology, 36*(1), 28–71. https://doi.org/10.1006/cogp.1998.0681

Chun, M. M., & Jiang, Y. (1999). Top-down attentional guidance based on implicit learning of visual covariation. *Psychological Science, 10*(4), 360–365. https://doi.org/10.1111/1467-9280.00168

Chun, M. M., & Potter, M. C. (1995). A two-stage model for multiple target detection in rapid serial visual presentation. *Journal of Experimental Psychology: Human Perception and Performance*, *21*(1), 109–127. https://doi.org/10.1037/0096-1523.21.1.109

Chunharas, C., Rademaker, R. L., Brady, T. F., & Serences, J. T. (2022). An adaptive perspective on visual working memory distortions. *Journal of Experimental Psychology: General*, *151*(10), 2300–2323. https://doi.org/10.1037/xge0001191

Cohen, M. A., Keefe, J., & Brady, T. F. (2023). Perceptual awareness occurs along a graded continuum: No evidence of all-or-none failures in continuous reproduction tasks. *Psychological Science, 34(9), 1033–1047. https://doi.org/10.1177/09567976231186798*

Cohen, M. X., & Donner, T. H. (2013). Midfrontal conflict-related theta-band power reflects neural oscillations that predict behavior. *Journal of Neurophysiology*, *110*(12), 2752–2763. https://doi.org/10.1152/jn.00479.2013

Cohen, N., Moyal, N., & Henik, A. (2015). Executive control suppresses pupillary responses to aversive stimuli. *Biological Psychology, 112*, 1–11. https://doi.org/10.1016/j.biopsycho.2015.09.006

Cowan, N. (2001). The magical number 4 in short-term memory: A reconsideration of mental storage capacity. *Behavioral and Brain Sciences*, *24*(1), 87–114. https://doi.org/10.1017/S0140525X01003922

Craston, P., Wyble, B., Chennu, S., & Bowman, H. (2009). The attentional blink reveals serial working memory encoding: Evidence from virtual & human event-related potentials. *Journal of Cognitive Neuroscience*, *21*(3), 550–566. https://doi.org/10.1162/jocn.2009.21036

Dalski, A., Kovács, G., & Ambrus, G. G. (2022). Evidence for a general neural signature of face familiarity. *Cerebral Cortex*, *32*(12), 2590–2601. https://doi.org/10.1093/cercor/bhab366

Dehaene, S., Changeux, J. P., Naccache, L., Sackur, J., & Sergent, C. (2006). Conscious, preconscious, and subliminal processing: A testable taxonomy. *Trends in Cognitive Sciences*, *10*, 204–211. https://doi.org/10.1016/j.tics.2006.03.007

Dehaene, S., Kerszberg, M., & Changeux, J. P. (1998). A neuronal model of a global workspace in effortful cognitive tasks. *Proceedings of the National Academy of Sciences of the United States of America*, *95*(24), 14529–14534. https://doi.org/10.1073/pnas.95.24.14529

Dehaene, S., Sergent, C., & Changeux, J. P. (2003). A neuronal network model linking subjective reports and objective physiological data during conscious perception. *Proceedings of the National Academy of Sciences of the United States of America*, *100*(14), 8520–8525. https://doi.org/10.1073/pnas.1332574100

Dell'Acqua, R., Dux, P. E., Wyble, B., Doro, M., Sessa, P., Meconi, F., & Jolicoeur, P. (2015). The attentional blink impairs detection and delays encoding of visual information: Evidence from human electrophysiology. *Journal of*

Cognitive Neuroscience, *27*(4), 720–735. https://doi.org/10.1162/jocn_a_00752

Dell'Acqua, R., Jolicoeur, P., Pesciarelli, F., Job, R., & Palomba, D. (2003). Electrophysiological evidence of visual encoding deficits in a cross-modal attentional blink paradigm. *Psychophysiology*, *40*(4), 629–639. https://doi.org/10.1111/1469-8986.00064

Desimone, R., & Duncan, J. (1995). Neural mechanisms of selective visual attention. *Annual Review of Neuroscience*, *18*, 193–222. https://doi.org/10.1146/annurev.ne.18.030195.001205

Di Lollo, V., Kawahara, J. I., Shahab Ghorashi, S. M., & Enns, J. T. (2005). The attentional blink: Resource depletion or temporary loss of control? *Psychological Research*, 69, 191-200. https://doi.org/10.1007/s00426-004-0173-x

Dionisio, D. P., Granholm, E., Hillix, W. A., & Perrine, W. F. (2001). Differentiation of deception using pupillary responses as an index of cognitive processing. *Psychophysiology*, *38*(2), 205–211. https://doi-org /10.1111/1469-8986.3820205

Donkin, C., Nosofsky, R. M., Gold, J. M., & Shiffrin, R. M. (2013). Discrete-slots models of visual working-memory response times. *Psychological Review*, *120*(4), 873–902. https://doi.org/10.1037/a0034247

Duncan, J., Martens, S., & Ward, R. (1997). Restricted attentional capacity within but not between sensory modalities. *Nature*, *387*(6635), 808–810. https://doi.org/10.1038/42947

Duncan, J., Ward, R. & Shapiro, K. (1994) Direct measurement of attentional dwell time in human vision. *Nature, 369*(6478), 313–315. https://doi.org/10.1038/369313a0

Dux, P. E., & Harris, I. M. (2007). Viewpoint costs occur during consolidation: Evidence from the attentional blink. *Cognition, 104*(1), 47–58. https://doi.org/10.1016/j.cognition.2006.05.004

Dux, P. E., & Marois, R. (2009). The attentional blink: A review of data and theory. *Attention, Perception & Psychophysics*, *71*(8), 1683–1700. https://doi.org/10.3758/APP.71.8.1683

Egeth, H. (2018). Comment on Theeuwes's characterization of visual selection. *Journal of Cognition, 1*(1). https://doi.org/10.5334/joc.29

Eriksen, C. W., & St. James, J. D. (1986). Visual attention within and around the field of focal attention: A zoom lens model. *Perception & Psychophysics, 40*(4), 225–240. https://doi.org/10.3758/BF03211502

Eriksen, C. W., & Yeh, Y. Y. (1985). Allocation of attention in the visual field. *Journal of Experimental Psychology: Human Perception and Performance, 11*(5), 583. https://doi.org/10.1037/0096-1523.11.5.583

Failing, M., & Theeuwes, J. (2018). Selection history: How reward modulates selectivity of visual attention. *Psychonomic Bulletin & Review, 25*(2), 514–538. https://doi.org/10.3758/s13423-017-1380-y

Farwell, L. A., & Donchin, E. (1991). The truth will out: Interrogative polygraphy ("lie detection") with event-related potentials. *Psychophysiology*, *28*, 531–547. https://doi.org/10.1111/ j.1469-8986.1991.tb01990.x

Faul, F., Erdfelder, E., Lang, A. G., & Buchner, A. (2007). G* Power 3: A flexible statistical power analysis program for the social, behavioral, and biomedical sciences. *Behavior Research Methods*, *39*(2), 175-191. https://doi.org/10.3758/BF03193146

Fougnie, D., & Alvarez, G. A. (2011). Object features fail independently in visual working memory: Evidence for a probabilistic feature-store model. *Journal of Vision*, *11*(12), 1–12. https://doi.org/10.1167/11.12.1

Fougnie, D., Suchow, J. W., & Alvarez, G. A. (2012). Variability in the quality of visual working memory. *Nature Communications*, *3*(1), 1–8. https://doi.org/10.1038/ncomms2237

Fuggetta, G., Lanfranchi, S., & Campana, G. (2009). Attention has memory: Priming for the size of the attentional focus. *Spatial Vision, 22*(2), 147-159. https://doi.org/10.1163/156856809787465618

Gamer, M. (2011). Detecting concealed information using autonomic measures. In B. Verschuere, G. Ben-Shakhar, & E. Meijer (Eds.), *Memory detection: Theory and application of the concealed information test* (pp. 12–23). Cambridge University Press. https://doi.org/10.1017/cbo9780511975196.003

Gamer, M., & Berti, S. (2010). Task relevance and recognition of concealed information have different influences on electrodermal activity and event-related brain potentials. *Psychophysiology*, *47*(2), 355–364. https://doi.org/10.1111/j.1469-8986.2009.00933.x

Gamer, M., Verschuere, B., Crombez, G., & Vossel, G. (2008). Combining physiological measures in the detection of concealed information. *Physiology & Behavior*, *95*(3), 333–340. https://doi.org/10.1016/j.physbeh.2008.06.011

Ganis, G., Kosslyn, S. M., Stose, S., Thompson, W. L., and Yurgelun-Todd, D. A. (2003). Neural correlates of different types of deception: an fMRI investigation. *Cerebral Cortex*, *13*(8), 830–836. https://doi.org/10.1093/cercor/13.8.830

Gati, I., & Ben-Shakhar, G. (1990). Novelty and significance in orientation and habituation: A feature-matching approach. *Journal of Experimental Psychology: General*, *119*(3), 251–263. https://doi.org/10.1037/0096-3445.119.3.251

Geng, J. J., & Behrmann, M. (2002). Probability cuing of target location facilitates visual search implicitly in normal participants and patients with hemispatial neglect. *Psychological Science, 13*(6), 520–525. https://doi.org/10.1111/1467-9280.00491

Geng, J. J., & Behrmann, M. (2005). Spatial probability as an attentional cue in visual search. *Perception & Psychophysics, 67*(7), 1252–1268. https://doi.org/10.3758/BF03193557

Gilzenrat, M. S., Nieuwenhuis, S., Jepma, M., & Cohen, J. D. (2010). Pupil diameter tracks changes in control state predicted by the adaptive gain theory of locus coeruleus function. *Cognitive, Affective, & Behavioral Neuroscience*, *10*(2), 252–269. https://doi.org/10.3758/CABN.10.2.252

Goodhew, S. C., Shen, E., & Edwards, M. (2016). Selective spatial enhancement: Attentional spotlight size impacts spatial but not temporal perception. *Psychonomic Bulletin & Review, 23*(4), 1144–1149. https://doi.org/10.3758/s13423-015-0904-6

Greenwood, P. M., & Parasuraman, R. (1999). Scale of attentional focus in visual search. *Perception & Psychophysics, 61*(5), 837–859. https://doi.org/10.3758/BF03206901

Greenwood, P. M., & Parasuraman, R. (2004). The scaling of spatial attention in visual search and its modification in healthy aging. *Perception & Psychophysics, 66*, 3–22. https://doi.org/10.3758/BF03194857

Gresch, D., Boettcher, S. E. P., Gohil, C., van Ede, F., & Nobre, A. C. (2024). Neural dynamics of shifting attention between perception and working-memory contents. *Proceedings of the National Academy of Sciences of the United States of America*, *121*(47), e2406061121. https://doi.org/10.1073/pnas.2406061121

Gronau, Q. F., Van Erp, S., Heck, D. W., Cesario, J., Jonas, K. J., & Wagenmakers, E. J. (2017). A Bayesian model-averaged meta-analysis of the power pose effect with informed and default priors: the case of felt power. *Comprehensive Results in Social Psychology, 2*(1), 123–138. https://doi.org/10.1080/23743603.2017.1326760

Hajcak, G., MacNamara, A., & Olvet, D. M. (2010). Event-related potentials, emotion, and emotion regulation: an integrative review. *Developmental Neuropsychology*, *35*(2), 129–155. https://doi.org/10.1080/87565640903526504

Hajilou, O. (2020). *Face Perception and Recognition, on the Fringe of Human Awareness*. University of Kent (United Kingdom).

Hardman, K. O. (2016). CatContModel: Categorical and continuous working memory models for delayed estimation tasks (version 0.8.0) [Computer software]. https://github.com/hardmanko/CatContModel

Hardman, K. O., Vergauwe, E., & Ricker, T. J. (2017). Categorical working memory representations are used in delayed estimation of continuous colors. *Journal of Experimental Psychology: Human Perception and Performance, 43*(1), 30–54. https://doi.org/10.1037/xhp0000290

Hayden, B. Y., & Gallant, J. L. (2005). Time course of attention reveals different mechanisms for spatial and feature-based attention in area V4. *Neuron*, *47*(5), 637-643. https://doi.org/10.1016/j.neuron.2005.07.020

Hommel, B., & Akyürek, E. G. (2005). Lag-1 sparing in the attentional blink: Benefits and costs of integrating two events into a single episode. *The Quarterly Journal of Experimental Psychology Section A*, *58*(8), 1415-1433. https://doi.org/10.1080/02724980443000647

Honts, C. R., Devitt, M. K., Winbush, M., & Kircher, J. C. (1996). Mental and physical countermeasures reduce the accuracy of the concealed knowledge test. *Psychophysiology*, *33*(1), 84–92. https://doi.org/10.1111/j.1469-8986.1996.tb02111.x

Hubner, R. (2000). Attention shifting between global and local target levels: The persistence of level-repetition effects. *Visual Cognition, 7*(4), 465–484. https://doi.org/10.1080/135062800394612

JASP Team (2022). JASP (Version 0.16.4.0) [Computer software]. https://jasp - stats.org

Jiang, Y. V., Swallow, K. M., Rosenbaum, G. M., & Herzig, C. (2013). Rapid acquisition but slow extinction of an attentional bias in space. *Journal of Experimental Psychology: Human Perception and Performance, 39*(1), 87–99. https://doi.org/10.1037/a0027611

Jolicœur, P. (1998). Modulation of the attentional blink by on-line response selection: Evidence from speeded and unspeeded Task1 decisions. *Memory & Cognition*, *26*(5), 1014-1032.https://doi.org/10.3758/BF03201180

Jolicœur, P. (1999). Concurrent response-selection demands modulate the attentional blink. *Journal of Experimental Psychology: Human Perception and Performance*, *25*(4), 1097. https://doi.org/10.1037/0096-1523.25.4.1097

Jolicœur, P., & Dell'Acqua, R. (1998). The demonstration of short-term consolidation. *Cognitive psychology*, *36*(2), 138–202. https://doi.org/10.1006/cogp.1998.0684

Jolicœur, P., & Dell'Acqua, R. (1999). Attentional and structural constraints on visual encoding. *Psychological Research, 62*, 154–164. https://doi.org/10.1007/s004260050048

Kahana, M. J., Seelig, D., & Madsen, J. R. (2001). Theta returns. *Current Opinion in Neurobiology*, *11*(6), 739–744. https://doi.org/10.1016/S0959-4388(01)00278-1

Kahneman, D., & Beatty, J. (1966). Pupil diameter and load on memory. *Science*, *154*(3756), 1583–1585. https://doi.org/10.1126/science.154.3756.1583

Karabay, A., & Akyürek, E. G. (2019). Temporal integration and attentional selection of color and contrast target pairs in rapid serial visual presentation. *Acta Psychologica, 196*, 56–69. https://doi.org/10.1016/j.actpsy.2019.04.002

Karabay, A., Wilhelm, S. A., de Jong, J., Wang, J., Martens, S., & Akyürek, E. G. (2022). Two faces of perceptual awareness during the attentional blink: Gradual and discrete. *Journal of Experimental Psychology: General*, *151*(7), 1520–1541. https://doi.org/10.1037/xge0001156

Klein, R. M., & Dick, B. (2002). Temporal dynamics of reflexive attention shifts: A dual-stream rapid serial visual presentation exploration. *Psychological Science*, *13*(2), 176-179. https://doi.org/10.1111/1467-9280.00432

Klimesch, W., Doppelmayr, M., Schimke, H., & Ripper, B. (1997). Theta synchronization and alpha desynchronization in a memory task. *Psychophysiology*, *34*(2), 169–176. https://doi.org/10.1111/j.1469-8986.1997.tb02128.x

Kool, W., Conway, A. R. A., & Turk-Browne, N. B. (2014). Sequential dynamics in visual short-term memory. *Attention, Perception, & Psychophysics*, *76*(7), 1885–1901. https://doi.org/10.3758/s13414-014-0755-7

Kranczioch, C., Debener, S., & Engel, A. K. (2003). Event-related potential correlates of the attentional blink phenomenon. *Cognitive Brain Research*, *17*(1), 177–187. https://doi.org/10.1016/S0926-6410(03)00092-2

Laeng, B., Ørbo, M., Holmlund, T., & Miozzo, M. (2011). Pupillary Stroop effects. *Cognitive Processing*, *12*(1), 13–21. https://doi.org/10.1007/s10339-010-0370-z

Lamme V. A. (2004). Separate neural definitions of visual consciousness and visual attention; a case for phenomenal awareness. *Neural Networks*, *17*(5-6), 861–872. https://doi.org/10.1016/j.neunet.2004.02.005

Lawrence, D. H. (1971). Two studies of visual search for word targets with controlled rates of presentation. *Perception & Psychophysics*, *10*(2), 85–89. https://doi.org/10.3758/BF03214320

Lawrence, R. K., Edwards, M., & Goodhew, S. C. (2020a). The impact of scaling rather than shaping attention: Changes in the scale of attention using global motion inducers influence both spatial and temporal acuity. *Journal of Experimental Psychology: Human Perception and Performance, 46*(3), 313–323. https://doi.org/10.1037/xhp0000708

Lawrence, R. K., Edwards, M., Talipski, L. A., & Goodhew, S. C. (2020b). A critical review of the cognitive and perceptual factors influencing attentional scaling and visual processing. *Psychonomic Bulletin & Review, 27*, 405–422. https://doi.org/10.3758/s13423-019-01692-9

Lefebvre, C. D., Marchand, Y., Smith, S. M., & Connolly, J. F. (2007). Determining eyewitness identification accuracy using event-related brain potentials (ERPs). *Psychophysiology*, *44*(6), 894–904. https://doi.org/10.1111/j.1469-8986.2007.00566.x

Lubow, R. E., & Fein, O. (1996). Pupillary size in response to a visual guilty knowledge test: New technique for the detection of deception. *Journal of Experimental Psychology: Applied*, *2*(2), 164–177. https://doi.org/10.1037/1076-898X.2.2.164

Luck, S. J., & Vogel, E. K. (1997). The capacity of visual working memory for features and conjunctions. *Nature*, *390*(6657), 279–284. https://doi.org/10.1038/36846

Luck, S. J., Hillyard, S. A., Mouloua, M., & Hawkins, H. L. (1996). Mechanisms of visual-spatial attention: Resource allocation or uncertainty reduction? *Journal of Experimental Psychology: Human Perception and Performance*, *22*(3), 725–737. https://doi.org/10.1037//0096-1523.22.3.725

Lykken, D. T. (1959). The GSR in the detection of guilt. *Journal of Applied Psychology*, *43*(6), 385–388. https://doi.org/10.1037/h0046060

Lykken, D. T. (1960). The validity of the guilty knowledge technique: The effects of faking. *Journal of Applied Psychology*, *44*(4), 258–262. https://doi.org/10.1037/h0044413

Lykken, D. T. (1974). Psychology and the lie detector industry. *American Psychologist*, *29*(10), 725–739. https://doi.org/10.1037/h0037441

Martens, S., & Wyble, B. (2010). The attentional blink: Past, present, and future of a blind spot in perceptual awareness. *Neuroscience & Biobehavioral Reviews*, *34*(6), 947–957. https://doi.org/10.1016/j.neubiorev.2009.12.005

Martens, S., Munneke, J., Smid, H., & Johnson, A. (2006). Quick minds don't blink: Electrophysiological correlates of individual differences in attentional selection. *Journal of Cognitive Neuroscience, 18*(9), 1423–1438. https://doi.org/10.1162/jocn.2006.18.9.1423

Mathôt, S., & Vilotijević, A. (2023). Methods in cognitive pupillometry: Design, preprocessing, and statistical analysis. *Behavior research methods, 55*(6), 3055–3077. https://doi.org/10.3758/s13428-022-01957-7

Mathôt, S., Berberyan, H., Büchel, P., Ruuskanen, V., Vilotijević, A., & Kruijne, W. (2023). Effects of pupil size as manipulated through ipRGC activation on visual processing. *NeuroImage*, *283*, 120420. https://doi.org/10.1016/j.neuroimage.2023.120420

Mathôt, S., Schreij, D. & Theeuwes, J. (2012). OpenSesame: An open-source, graphical experiment builder for the social sciences. *Behavior Research Methods, 44*, 314–324. https://doi.org/10.3758/s13428-011-0168-7

Matsuda, I., Nittono, H., Hirota, A., Ogawa, T., & Takasawa, N. (2009). Event-related brain potentials during the standard autonomic-based concealed information test. *International Journal of Psychophysiology*, *74*(1), 58–68. https://doi.org/10.1016/j.ijpsycho.2009.07.004

Meijer, E. H., Selle, N. K., Elber, L., & Ben-Shakhar, G. (2014). Memory detection with the Concealed Information Test: A meta analysis of skin conductance, respiration, heart rate, and P300 data. *Psychophysiology*, *51*(9), 879-904. https://doi.org/10.1111/psyp.12239

Meng, J., Meriño, L. M., Bigdely Shamlo, N., Makeig, S., Robbins, K., & Huang, Y. (2012). Characterization and robust classification of EEG signal from image RSVP events with independent time-frequency features. *PloS One*, *7*(9), e44464. https://doi.org/10.1371/journal.pone.0044464

Mertens, R., & Allen, J. J. B. (2008). The role of psychophysiology in forensic assessments: Deception detection, ERPs, and virtual reality mock crime scenarios. *Psychophysiology*, *45*(2), 286–298. https://doi.org/10.1111/j.1469-8986.2007.00615.x

Miller, G. A. (1956). The magical number seven, plus or minus two: Some limits on our capacity for processing information. *Psychological Review*, *63*(2), 81–97. https://doi.org/10.1037/h0043158

Müller, N. G., Bartelt, O. A., Donner, T. H., Villringer, A., & Brandt, S. A. (2003). A physiological correlate of the "zoom lens" of visual attention. *Journal of Neuroscience,* *23*(9), 3561–3565. https://doi.org/10.1523/JNEUROSCI.23-09-03561.2003

Navon, D. (2003). What does a compound letter tell the psychologist's mind? *Acta Psychologica*, *114*(3), 273-309. https://doi.org/10.1016/j.actpsy.2003.06.002

Nieuwenhuis, S., & de Kleijn, R. (2011). Consciousness of targets during the attentional blink: a gradual or all-or-none dimension? *Attention, Perception, and Psychophysics,* *73*, 364–373. https://doi.org/10.3758/s13414-010-0026-1

Nieuwenhuis, S., De Geus, E. J., & Aston-Jones, G. (2011). The anatomical and functional relationship between the P3 and autonomic components of the orienting response: P3 and orienting response. *Psychophysiology*, *48*(2), 162–175. https://doi.org/10.1111/j.1469-8986.2010.01057.x

Nieuwenstein, M. R., & Potter, M. C. (2006). Temporal limits of selection and memory encoding: A comparison of whole versus partial report in rapid serial visual presentation. *Psychological Science*, *17*(6), 471–475. https://doi.org/10.1111/j.1467-9280.2006.01730.x

Nieuwenstein, M. R., Chun, M. M., van der Lubbe, R. H., & Hooge, I. T. (2005). Delayed attentional engagement in the attentional blink. *Journal of*

Experimental Psychology: Human Perception and Performance, *31*(6), 1463. https://doi.org/10.1037/0096-1523.31.6.1463

Nigbur, R., Ivanova, G., & Stürmer, B. (2011). Theta power as a marker for cognitive interference. *Clinical Neurophysiology*, *122*(11), 2185–2194. https://doi.org/10.1016/j. clinph.2011.03.030

Nobre, A. C., & Gresch, D. (2025). How the brain shifts between external and internal attention. *Neuron*, *113*(15), 2382–2398. https://doi.org/10.1016/j.neuron.2025.06.013

Oberauer, K. (2021). Measurement models for visual working memory—A factorial model comparison. *Psychological Review*, *130*(3), 841-852. https://doi.org/10.1037/rev0000328

Oberauer, K., Lewandowsky, S., Farrell, S., Jarrold, C., & Greaves, M. (2012). Modeling working memory: An interference model of complex span. *Psychonomic Bulletin & Review*, *19*(5), 779–819. https://doi.org/10.3758/S13423-012-0272-4

Oberauer, K., Stoneking, C., Wabersich, D., & Lin, H. Y. (2017). Hierarchical Bayesian measurement models for continuous reproduction of visual features from working memory. *Journal of Vision*, *17*(5), 1–27. https://doi.org/10.1167/17.5.11

O'Craven, K. M., Downing, P. E., & Kanwisher, N. (1999). fMRI evidence for objects as the units of attentional selection. *Nature*, *401*(6753), 584–587. https://doi.org/10.1038/44134

Olivers, C. N., & Meeter, M. (2008). A boost and bounce theory of temporal attention. *Psychological Review*, *115*(4), 836. https://doi.org/10.1037/a0013395

Olivers, C. N., Van Der Stigchel, S., & Hulleman, J. (2007). Spreading the sparing: Against a limited-capacity account of the attentional blink. *Psychological Research*, *71*, 126-139. https://doi.org/10.1007/s00426-005-0029-z

Overgaard, M., Rote, J., Mouridsen, K., & Ramsøy, T. Z. (2006). Is conscious perception gradual or dichotomous? A comparison of report methodologies during a visual task. *Consciousness and Cognition, 15*(4), 700–708. https://doi.org/10.1016/j.concog.2006.04.002

Palmieri, H., Carrasco, M. (2024). Task demand mediates the interaction of spatial and temporal attention. *Scientific Reports*, *14*(1), 9228. https://doi.org/10.1038/s41598-024-58209-1

Pashler, H. (1988). Familiarity and visual change detection. *Perception & Psychophysics, 44*, 369–378. https://doi.org/10.3758/BF03210419

Pastukhov, A., Vonau, V., Stonkute, S., & Braun, J. (2013). Spatial and temporal attention revealed by microsaccades. *Vision Research*, *85*, 45–57. https://doi.org/10.1016/j.visres.2012.11.004

Peirce, J. W. (2007). PsychoPy-Psychophysics software in Python. *Journal of Neuroscience Methods*, *162*(1–2), 8–13. https://doi.org/10.1016/j.jneumeth.2006.11.017

Peirce, J. W. (2009). Generating stimuli for neuroscience using PsychoPy. *Frontiers in Neuroinformatics*, *2*(JAN), 10. https://doi.org/10.3389/neuro.11.010.2008

Peth, J., Suchotzki, K., & Gamer, M. (2016). Influence of countermeasures on the validity of the Concealed Information Test: Influence of countermeasures on CIT validity. *Psychophysiology*, *53*(9), 1429–1440. https://doi.org/10.1111/psyp.12690

Poggel, D. A., Treutwein, B., Calmanti, C., & Strasburger, H. (2006). Increasing the temporal g(r)ain: Double-pulse resolution is affected by the size of the attention focus. *Vision Research, 46*(18), 2998–3008. https://doi.org/10.1016/j.visres.2006.03.018

Poldrack R. A. (2007). Region of interest analysis for fMRI. *Social Cognitive and Affective Neuroscience*, *2*(1), 67–70. https://doi.org/10.1093/scan/nsm006

Polich, J. (2007). Updating P300: An integrative theory of P3a and P3b. *Clinical Neurophysiology*, *118*(10), 2128–2148. https://doi.org/10.1016/j.clinph.2007.04.019

Posner M. I. (1980). Orienting of attention. *The Quarterly Journal of Experimental Psychology*, *32*(1), 3–25. https://doi.org/10.1080/00335558008248231

Potter, M. C. (1976). Short-term conceptual memory for pictures. *Journal of Experimental Psychology: Human Learning and Memory*, *2*(5), 509–522. https://doi.org/10.1037/0278-7393.2.5.509

Potter, M. C., & Levy, E. I. (1969). Recognition memory for a rapid sequence of pictures. *Journal of Experimental Psychology*, *81*(1), 10–15. https://doi.org/10.1037/h0027470

Potter, M. C., Staub, A., & O'Connor, D. H. (2002). The time course of competition for attention: Attention is initially labile. *Journal of Experimental Psychology: Human Perception and Performance*, *28*(5), 1149. https://doi.org/10.1037/0096-1523.28.5.1149

Potter, M.C., Nieuwenstein, M., Strohminger, N. (2008). Whole report versus partial report in RSVP sentences. *Journal of Memory and Language, 58* (4), 907–915. https://doi.org/10.1016/j.jml.2007.12.002

Ptito, A., Arnell, K., Jolicoeur, P., & Macleod, J. (2008). Intramodal and crossmodal processing delays in the attentional blink paradigm revealed by event-related potentials. *Psychophysiology, 45*(5), 794–803. https://doi.org/10.1111/j.1469-8986.2008.00677.x

Querino, E., dos Santos, L., Ginani, G., Nicolau, E., Miranda, D., Romano-Silva, M., & Malloy-Diniz, L. (2015). Cognitive effort and pupil dilation in controlled and automatic processes. *Translational Neuroscience*, *6*(1), 168–173. https://doi.org/10.1515/tnsci-2015-0017

R Core Team (2022). R: A language and environment for statistical computing. R Foundation for Statistical Computing, Vienna, Austria. URL https://www.R-project.org/.

Raymond, J. E., Shapiro, K. L., & Arnell, K. M. (1992). Temporary suppression of visual processing in an RSVP task: An attentional blink? *Journal of Experimental Psychology: Human Perception and Performance*, *18*(3), 849–860. https://doi.org/10.1037/0096-1523.18.3.849

Renard, Y., Lotte, F., Gibert, G., Congedo, M., Maby, E., Delannoy, V., Bertrand, O. & Lécuyer, A. (2010). OpenViBE: An open-source software platform to design, test, and use brain–computer interfaces in real and virtual environments. *Presence*, *19*(1), 35-53. https://doi.org/10.1162/pres.19.1.35

Rensink, R. A. (2015). A function-centered taxonomy of visual attention. In: Coates, P., Coleman, S. (Eds.), *Phenomenal Qualities: Sense, Perception, and Consciousness*. Oxford University Press, Oxford, pp. 347-375.

Ricker, T. J., & Hardman, K. O. (2017). The nature of short-term consolidation in visual working memory. *Journal of Experimental Psychology: General, 146*(11), 1551–1573. https://doi.org/10.1037/xge0000346

Ricker, T. J., Spiegel, L. R., & Cowan, N. (2014). Time-based loss in visual short-term memory is from trace decay, not temporal distinctiveness. *Journal of Experimental Psychology: Learning, Memory, and Cognition*, *40*(6), 1510–1523. https://doi.org/10.1037/xlm0000018

Robitaille, N., Jolicoeur, P., Dell'Acqua, R., & Sessa, P. (2007). Short-term consolidation of visual patterns interferes with visuo-spatial attention: Converging evidence from human electrophysiology. *Brain Research*, *1185*, 158–169. https://doi.org/10.1016/j.brainres.2007.09.004

Rolke, B., Heil, M., Streb, J., & Hennighausen, E. (2001). Missed prime words within the attentional blink evoke an N400 semantic priming effect. *Psychophysiology*, *38*(2), 165–174. https://doi.org/10.1111/1469-8986.3820165

Rosenfeld J. P. (2020). P300 in detecting concealed information and deception: A review. *Psychophysiology*, *57*(7), e13362. https://doi.org/10.1111/psyp.13362

Rosenfeld, J. P., Biroschak, J. R., & Furedy, J. J. (2006). P300-based detection of concealed autobiographical versus incidentally acquired information in target and non-target paradigms. *International Journal of Psychophysiology*, *60*(3), 251–259. https://doi.org/10.1016/j.ijpsycho.2005.06.002

Rosenfeld, J. P., Soskins, M., Bosh, G., & Ryan, A. (2004). Simple, effective countermeasures to P300-based tests of detection of concealed information. *Psychophysiology*, *41*(2), 205–219. https://doi.org/10.1111/j.1469-8986.2004.00158.x

Schmidt, B. K., Vogel, E. K., Woodman, G. F., & Luck, S. J. (2002). Voluntary and automatic attentional control of visual working memory. *Perception & Psychophysics*, *64*(5), 754-763. https://doi.org/10.3758/BF03194742

Schupp, H. T., Cuthbert, B. N., Bradley, M. M., Cacioppo, J. T., Ito, T., & Lang, P. J. (2000). Affective picture processing: the late positive potential is modulated by motivational relevance. *Psychophysiology*, *37*(2), 257-261. https://doi-org/10.1111/1469-8986.3720257

Schurgin, M. W., Wixted, J. T., & Brady, T. F. (2020). Psychophysical scaling reveals a unified theory of visual memory strength. *Nature Human Behaviour*, *4*(11), 1156-1172. https://doi-org/10.1038/s41562-020-00938-0

Schwarz, G. (1978). Estimating the dimension of a model. *The Annals of Statistics*, *6*(2), 461–464. https://doi.org/10.2307/2958889

Sergent, C., & Dehaene, S. (2004). Is consciousness a gradual phenomenon? Evidence for an all-or-none bifurcation during the attentional blink. *Psychological Science, 15*(11), 720–728. https://doi.org/10.1111/j.0956-7976.2004.00748.x

Sergent, C., Baillet, S., & Dehaene, S. (2005). Timing of the brain events underlying access to consciousness during the attentional blink. *Nature Neuroscience*, *8*(10), 1391–1400. https://doi.org/10.1038/nn1549

Sessa, P., Luria, R., Verleger, R., & Dell'Acqua, R. (2007). P3 latency shifts in the attentional blink: Further evidence for second target processing postponement. *Brain Research*, *1137*, 131–139. https://doi.org/10.1016/j.brainres.2006.12.066

Seymour, T. L., Baker, C. A., & Gaunt, J. T. (2013). Combining blink, pupil, and response time measures in a concealed knowledge test. *Frontiers in Psychology*, *3*(614). https://doi.org/10.3389/fpsyg.2012.00614

Shapiro, K. L., Raymond, J. E., & Arnell, K. M. (1994). Attention to visual pattern information produces the attentional blink in rapid serial visual presentation. *Journal of Experimental Psychology: Human Perception and Performance, 20*(2), 357–371. https://doi.org/10.1037/0096-1523.20.2.357

Shen, D., and Alain, C. (2011). Temporal attention facilitates short-term consolidation during a rapid serial auditory presentation task. *Experimental Brain Research*, *215*, 285–292. https://doi.org/10.1007/s00221-011-2897-3

Simons, D. J., & Chabris, C. F. (1999). Gorillas in our midst: Sustained inattentional blindness for dynamic events. *Perception*, *28*(9), 1059-1074. https://doi.org/10.1068/p281059

Sokolov, E. N. (1963). *Perception and the Conditioned Reflex*. Pergamon Press.

Squires, N. K., Squires, K. C., & Hillyard, S. A. (1975). Two varieties of long-latency positive waves evoked by unpredictable auditory stimuli in man. *Electroencephalography and Clinical Neurophysiology*, *38*(4), 387–401. https://doi.org/10.1016/0013-4694(75)90263-1

Suchow, J. W., Brady, T. F., Fougnie, D., & Alvarez, G. A. (2013). Modeling visual working memory with the MemToolbox. *Journal of Vision*, *13*(10), 9–9. https://doi.org/10.1167/13.10.9

Sy, J. L., Miao, H.-Y., Marois, R., & Tong, F. (2021). Conscious perception can be both graded and discrete. *Journal of Experimental Psychology: General, 150*(8), 1461–1475. https://doi.org/10.1037/xge0001009

Tang, M. F., Ford, L., Arabzadeh, E., Enns, J. T., Visser, T. A. W., & Mattingley, J. B. (2020). Neural dynamics of the attentional blink revealed by encoding orientation selectivity during rapid visual presentation. *Nature Communications*, *11*(1), 1–14. https://doi.org/10.1038/s41467-019-14107-z

Tesche, C. D., & Karhu, J. (2000). Theta oscillations index human hippocampal activation during a working memory task. *Proceedings of the National Academy of Sciences of the United States of America*, *97*(2), 919-924. https://doi.org/10.1073/pnas.97.2.919

Theeuwes, J. (2018). Visual selection: Usually fast and automatic; seldom slow and volitional. *Journal of Cognition, 1*(1), Article 29. https://doi.org/10.5334/joc.13

Theeuwes, J., Belopolsky, A., & Olivers, C. N. (2009). Interactions between working memory, attention and eye movements. *Acta Psychologica*, *132*(2), 106–114. https://doi.org/10.1016/j.actpsy.2009.01.005

Theeuwes, J., Bogaerts, L., & van Moorselaar, D. (2022). What to expect where and when: How statistical learning drives visual selection. *Trends in Cognitive Sciences, 26*(10), 860–872. https://doi.org/10.1016/J.TICS.2022.06.001

Thiruvasagam, S., & Srinivasan, N. (2021). Gradedness of visual awareness depends on attentional scope: Global perception is more graded than local perception. *Consciousness and Cognition, 94*, 103174. https://doi.org/10.1016/J.CONCOG.2021.103174

Turatto, M., Benso, F., Facoetti, A., Galfano, G., Mascetti, G. G., & Umiltà, C. (2000). Automatic and voluntary focusing of attention. *Perception & Psychophysics, 62*, 935–952. https://doi.org/10.3758/BF03212079

van den Berg, R., & Ma, W. J. (2018). A resource-rational theory of set size effects in human visual working memory. *eLife*, *7*. https://doi.org/10.7554/ELIFE.34963

van den Berg, R., Awh, E., & Ma, W. J. (2014). Factorial comparison of working memory models. *Psychological Review*, *121*(1), 124–149. https://doi.org/10.1037/a0035234

van den Berg, R., Shin, H., Chou, W. C., George, R., & Ma, W. J. (2012). Variability in encoding precision accounts for visual short-term memory limitations. *Proceedings of the National Academy of Sciences of the United States of America*, *109*(22), 8780–8785. https://doi.org/10.1073/pnas.1117465109

van der Mijn, R. (2023). Opensesame-plugin-RSVP (Version 0.11) [Computer software]. https://github.com/robbertmijn/opensesame-plugin-RSVP

Verschuere, B., Ben-Shakhar, G., & Meijer, E. (Eds.). (2011). *Memory detection: Theory and application of the concealed information test*. Cambridge University Press. https://doi.org/10.1017/CBO9780511975196

Verschuere, B., Crombez, G., De Clercq, A., & Koster, E. H. (2004). Autonomic and behavioral responding to concealed information: differentiating orienting and defensive responses. *Psychophysiology*, *41*(3), 461-466. https://doi.org/10.1111/j.1469-8986.00167.x

Vogel, E. K., & Luck, S. J. (2002). Delayed working memory consolidation during the attentional blink. *Psychonomic Bulletin & Review*, *9*(4), 739–743.

Vogel, E. K., Luck, S. J., & Shapiro, K. L. (1998). Electrophysiological evidence for a postperceptual locus of suppression during the attentional blink. *Journal of Experimental Psychology: Human Perception and Performa*nce, *24*(6), 1656–1674. https://psycnet.apa.org/doi/10.1037/0096-1523.24.6.1656

Vul, E., Hanus, D., & Kanwisher, N. (2009). Attention as inference: Selection is probabilistic; responses are all-or-none samples. *Journal of Experimental Psychology: General, 138*(4), 546–560. https://doi.org/10.1037/a0017352

Wang, B., & Theeuwes, J. (2018). Statistical regularities modulate attentional capture. *Journal of Experimental Psychology: Human Perception and Performance, 44*(1), 13–17. https://doi.org/10.1037/xhp0000472

Wang, B., van Driel, J., Ort, E., & Theeuwes, J. (2019). Anticipatory distractor suppression elicited by statistical regularities in visual search. *Journal of Cognitive Neuroscience, 31*(10), 1535–1548. https://doi.org/10.1162/jocn_a_01433

Wetzels, R., Matzke, D., Lee, M. D., Rouder, J. N., Iverson, G. J., & Wagenmakers, E. J. (2011). Statistical evidence in experimental psychology: An empirical comparison using 855 t tests. *Perspectives on Psychological Science, 6*(3), 291-298. https://doi-org.proxy-ub.rug.nl/10.1177/1745691611406923

Wiese, H., Anderson, D., Beierholm, U., Tüttenberg, S. C., Young, A. W., & Burton, A. M. (2022). Detecting a viewer's familiarity with a face: Evidence from event-related brain potentials and classifier analyses. *Psychophysiology*, *59*(1), e13950. https://doi.org/10.1111/psyp.13950

Wiese, H., Ingram, B. T., Elley, M. L., Tüttenberg, S. C., Burton, A. M., & Young, A. W. (2019). Later but not early stages of familiar face recognition depend strongly on attentional resources: Evidence from event-related brain potentials. *Cortex*, *120*, 147–158. https://doi.org/10.1016/j.cortex.2019.06.004

Wilken, P., & Ma, W. J. (2004). A detection theory account of change detection. *Journal of Vision*, *4*(12), 11–11. https://doi.org/10.1167/4.12.11

Wolff, M. J., Jochim, J., Akyürek, E. G., & Stokes, M. G. (2017). Dynamic hidden states underlying working-memory-guided behaviour. *Nature Neuroscience, 20*, 864-871. https://doi.org/10.1038/nn.4546

Wyble, B., Bowman, H., & Nieuwenstein, M. (2009). The attentional blink provides episodic distinctiveness: Sparing at a cost. *Journal of Experimental Psychology: Human Perception and Performance, 35*(3), 787–807. https://doi.org/10.1037/a0013902

Wyble, B., Potter, M. C., Bowman, H., & Nieuwenstein, M. (2011). Attentional episodes in visual perception. *Journal of Experimental Psychology: General*, *140*(3), 488–505. https://doi.org/10.1037/a0023612

Young, A. W., & Burton, A. M. (2018). Are we face experts? *Trends in Cognitive Sciences*, *22*(2), 100–110. https://doi.org/10.1016/j.tics.2017.11.007

Zhang, W., & Luck, S. J. (2008). Discrete fixed-resolution representations in visual working memory. *Nature*, *453*(7192), 233–235. https://doi.org/10.1038/nature06860

Zhao, S., Xie, J., Zhai, M., Zhou, Y., Ma, F., Feng, C., & Feng, W. (2025). Early perceptual locus of suppression during the attentional blink. *Journal of Experimental Psychology: General*, *154*(2), 457–475. https://doi.org/10.1037/xge0001660

Ziegel, E. R. (2003). The Elements of Statistical Learning. *Technometrics*, *45*(3), 267–268. https://doi.org/10.1198/tech.2003.s770

Zivony, A., Lamy, D. (2022). What processes are disrupted during the attentional blink? An integrative review of event-related potential research. *Psychonomic Bulletin & Review*, *29*, 394–414. https://doi.org/10.3758/s13423-021-01973-2

English Summary

We investigated how visual cognitive processes unfold under temporal constraints using the rapid serial visual presentation (RSVP) paradigm. In a typical RSVP task, stimuli are presented sequentially at the same spatial location, usually at a rate of 10 items per second. This paradigm imposes high temporal pressure on the visual system while effectively controlling other variables, such as spatial confounds. Therefore, RSVP is a suitable tool to investigate how cognitive resources are allocated to process items in quick succession.

An interesting phenomenon that emerges in the dual-target RSVP paradigm is the attentional blink (AB). The AB refers to the impairment in reporting a second target (T2) when it appears shortly after the first target (T1), usually between 200 and 500 ms. The AB provides an ideal platform to examine processing limitations because it allow for a direct comparison between two time-interval conditions: 1) short intervals, during which the identification of T2 is significantly impaired; 2) longer intervals, during which no 'blink' occurs and T2 is reported normally.

This dissertation hence utilizes the RSVP and AB paradigms to examine the visual cognition under temporal constraints with regard to three specific aspects:

1. Whether working memory consolidation failure during the AB is a discrete, all-or-none process, or a gradual loss of representational quality (Chapter 2).

2. If spatial attention can be flexibly adjusted under time pressure and how this adjustment influences the discrete or graded nature of conscious awareness (Chapter 3).

3. How internal memory representations guide attention and whether this process can be captured by physiological signals for covert information detection (Chapter 4).

In Chapter 2, we analyzed data derived from continuous report tasks embedded in the AB paradigm to investigate the nature of working memory failures. The analysis included four distinct datasets: three obtained from different laboratories (Asplund et al., 2014; Karabay et al., 2022; Tang et al., 2020) and one from a new experiment conducted for this study. We conducted a systematic comparison of seven computations models, including "slot" models (standard mixture, slot, slots plus resource models) and variable precision models. Our results consistently showed that models incorporating a discrete guessing component ("slot" models) provided the best fit at both group and individual levels. Simulation analyses confirmed that these models accurately reproduce the "blink" pattern. In contrast, the standard VP model failed to capture impaired representations during the blink window, unless a guessing parameter was added. These findings support the view that working memory (WM) consolidation in the

tested tasks is a capacity-limited process where targets either enter memory successfully or fail entirely, with failures resulting in pure guessing.

In Chapter 3, we investigated whether participants can adaptively control their attentional scale under temporal constraints. In this study, we assumed that changes in the nature of T2 awareness, specifically indexed by its representational precision, would indicate whether attentional scaling had been successfully implemented. We manipulated the T1 location using session-wise, trial-wise, or statistical regularities. We then analyzed T2 performance using mixture modeling to dissociate the probability of conscious access from representational precision. Our results showed that precision decreased when session-wise cues and statistical regularities were implemented, indicating that a broad attentional scale was successfully induced in these contexts. In contrast, trial-wise cues failed to modulate precision, suggesting that immediate, trial-by-trial adaptation is not possible in this condition. These findings demonstrate that while spatial attention can be adjusted to influence the nature of conscious awareness, such spatial control depends on stable explicit cues or implicit learning of regularities rather than immediate adjustments.

In Chapter 4, we applied the RSVP paradigm to the practical domain of concealed information detection to investigate how internal memory representations influence temporal attention. Specifically, we embedded personally familiar faces as task-irrelevant probes within the RSVP streams within a gender-based target detection task. We then utilized four physiological measures: ERP (P3) amplitude, theta-band power, pupil size, and pupil size change to assess covert recognition. We found that all indicators successfully distinguished familiar probes from neutral control stimuli at the group level. However, at the individual level, although ERP and theta-band power signals provided reliable detection for most participants, pupillary responses were less effective. This is likely due to the difficulty of isolating relatively slow-developing pupillary signals in high-speed RSVP paradigms. Furthermore, by integrating neural and pupillary signals, we found that combined inference compensated to some extent for limitations of single measures.

In sum, these chapters explore how the human cognitive system processes information under temporal constraints using computational modeling, behavioral performance, and physiological measures. Across three empirical studies, we demonstrate that the cognitive system regulates information flow via reactive gating, proactive spatial scaling, and memory-driven priority signals. Specifically, our findings show that while working memory and conscious access in typical AB tasks are primarily governed by discrete, all-or-none capacity limits, the nature of awareness remains flexible and can be proactively configured by adjusting the attentional scale. Furthermore, internal memory representations can automatically capture processing resources even without overt report, a process that can be

reliably tracked through neural signals. Overall, this work suggests that temporal constraints provide a window into the dynamic nature of human cognition, illustrating how this system adaptively manages information processing under such pressure.

Nederlandse Samenvatting

We hebben onderzocht hoe visuele cognitieve processen zich ontvouwen onder tijdsdruk met behulp van het *Rapid Serial Visual Presentation* (RSVP) paradigma. In een typische RSVP-taak worden stimuli sequentieel op dezelfde ruimtelijke locatie gepresenteerd, meestal met een snelheid van 10 items per seconde. Dit paradigma legt een hoge tijdsdruk op het visuele systeem, terwijl andere variabelen, zoals ruimtelijke factoren, effectief onder controle worden gehouden. Daarom is RSVP een geschikt instrument om te onderzoeken hoe cognitieve middelen worden ingezet om stimuli in snelle opeenvolging te verwerken.

Een interessant fenomeen dat optreedt in het *dual-target* RSVP-paradigma is de *attentional blink* (AB). De AB verwijst naar de beperking in het rapporteren van een tweede doelstimulus (T2) wanneer deze kort na de eerste doelstimulus (T1) verschijnt, meestal tussen 200 en 500 ms. De AB biedt een ideaal platform om verwerkingsbeperkingen te onderzoeken, omdat het een directe vergelijking mogelijk maakt tussen twee tijdsinterval-condities: 1) korte intervallen, waarbij de identificatie van T2 sterk beperkt is; en 2) langere intervallen, waarbij geen 'blink' optreedt en T2 normaal wordt gerapporteerd.

Dit proefschrift maakt dan ook gebruik van de RSVP- en AB-paradigma's om visuele cognitie onder tijdsdruk te onderzoeken op drie specifieke aspecten:

1. Of het falen van de consolidatie in het werkgeheugen tijdens de AB een discreet "alles-of-niets"-proces is, of een geleidelijk verlies van representatieve kwaliteit (**Hoofdstuk 2**).

2. Of ruimtelijke aandacht flexibel kan worden aangepast onder tijdsdruk en hoe deze aanpassing de discrete of graduele aard van het bewuste bewustzijn beïnvloedt (**Hoofdstuk 3**).

3. Hoe interne geheugenrepresentaties de aandacht sturen en of dit proces kan worden vastgelegd door fysiologische signalen voor de detectie van verborgen informatie (**Hoofdstuk 4**).

In **Hoofdstuk 2** we hebben gegevens geanalyseerd van *continuous report tasks* die zijn ingebed in het AB-paradigma om de aard van werkgeheugen-fouten te onderzoeken. De analyse omvatte vier verschillende datasets: drie verkregen uit verschillende laboratoria en één uit een nieuw experiment dat voor deze studie is uitgevoerd. We hebben een systematische vergelijking uitgevoerd van zeven computationele modellen, waaronder "slot"-modellen (standaard mixture, slot, slots plus resource modellen) en *variable precision* modellen. Onze resultaten toonden consistent aan dat modellen met een discreet gokelement ("slot"-modellen) de beste fit boden op zowel groeps- als individueel niveau. Simulatie-analyses bevestigden dat deze modellen het "blink"-patroon nauwkeurig reproduceren. In tegenstelling hiermee slaagde het standaard VP-model er niet in om de verstoorde representaties tijdens het *blink*-venster vast te leggen, tenzij er een gokparameter

aan werd toegevoegd (waarmee wordt verondersteld dat de proefpersoon simpelweg raadt naar de identiteit van de doelstimulus). Deze bevindingen ondersteunen de opvatting dat consolidatie in het werkgeheugen (WM) in de geteste taken een capaciteitsbeperkt proces is waarbij targets ofwel succesvol in het geheugen worden opgenomen of volledig falen, waarbij falen resulteert in puur gokken.

In **Hoofdstuk 3** we hebben onderzocht of deelnemers hun aandachtsschaal (*attentional scale*, d.w.z. de grootte van het gebied waar ze aandacht aan besteden) adaptief kunnen aansturen onder temporele beperkingen. In deze studie gingen we ervan uit dat veranderingen in de aard van het T2-bewustzijn, specifiek geïndexeerd door de representatieve precisie, zouden aangeven of *attentional scaling* succesvol was geïmplementeerd. We manipuleerden de T1-locatie met behulp van sessie-gebonden cues, trial-gebonden cues of statistische regelmatigheden. Vervolgens analyseerden we de T2-prestaties met behulp van *mixture modeling* om de waarschijnlijkheid van bewuste toegang te scheiden van representatieve precisie. Onze resultaten toonden aan dat de precisie afnam wanneer sessie-gebonden cues en statistische regelmatigheden werden geïmplementeerd, wat aangeeft dat in deze contexten met succes een brede aandachtsschaal werd geïnduceerd. In tegenstelling hiermee slaagden trial-gebonden cues er niet in de precisie te moduleren, wat suggereert dat onmiddellijke, trial-voor-trial adaptatie in deze conditie niet mogelijk is. Deze bevindingen tonen aan dat hoewel ruimtelijke aandacht kan worden aangepast om de aard van het bewustzijn te beïnvloeden, een dergelijke ruimtelijke controle afhankelijk is van stabiele expliciete cues of van het impliciet leren van regelmatigheden, maar niet van directe, ad-hoc aanpassingen.

In **Hoofdstuk 4** we hebben het RSVP-paradigma toegepast op het praktische domein van de detectie van verborgen informatie om te onderzoeken hoe interne geheugenrepresentaties de temporele aandacht beïnvloeden. Specifiek hebben we persoonlijk bekende gezichten ingebed als taak-irrelevante *probes* in de snelle RSVP stimulusstromen in een op geslacht gebaseerde doeldetectietaak. Vervolgens gebruikten we vier fysiologische maten: ERP (P3) amplitude, theta-band vermogen, pupilgrootte en pupilgrootte-verandering om de mate van herkenning te meten. We vonden dat alle indicatoren bekende *probes* met succes onderscheidden van neutrale controlestimuli op groepsniveau. Op individueel niveau bleken pupillaire reacties echter minder effectief, hoewel ERP en theta-band vermogenssignalen voor de meeste deelnemers betrouwbare detectie boden. Dit is waarschijnlijk te wijten aan de moeilijkheid om de relatief traag verlopende pupillaire signalen te isoleren in snelle RSVP-paradigma's. Bovendien vonden we, door neurale en pupillaire signalen te integreren, dat gezamenlijke inferentie de beperkingen van individuele maten tot op bepaalde hoogte compenseerde.

Samenvattend onderzoeken deze hoofdstukken hoe het menselijke cognitieve systeem informatie verwerkt onder temporele beperkingen, gebruikmakend van computationeel modelleren, gedragsprestaties en fysiologische metingen. In drie empirische studies tonen we aan dat het cognitieve systeem de informatiestroom reguleert via reactieve gating, proactieve ruimtelijke schaling en geheugengestuurde prioriteitssignalen. Specifiek laten onze bevindingen zien dat terwijl het werkgeheugen en de bewuste toegang in doorsnee AB taken primair worden bepaald door discrete, "alles-of-niets" capaciteitslimieten, de aard van het bewustzijn flexibel blijft en proactief kan worden geconfigureerd door de aandachtsschaal aan te passen. Bovendien kunnen interne geheugenrepresentaties automatisch cognitieve middelen aanspreken, zelfs zonder expliciete rapportage, een proces dat betrouwbaar kan worden gevolgd via neurale signalen. Over het geheel genomen suggereert dit werk dat temporele beperkingen een venster bieden op de dynamische aard van de menselijke cognitie en illustreren ze hoe dit systeem de informatieverwerking adaptief beheert onder dergelijke druk.

Acknowledgements

If you had asked me on day one how I felt about starting a PhD, I would have told you how excited and curious I was. If you had asked me somewhere in the middle, you probably would have just heard a lot of complaining. I quickly learned that a PhD isn't just about doing research; it's a massive test of patience and mental stamina. Now, finally standing at the finish line, looking back at all the frustrating moments and exhausting days, my main feeling is simply gratitude. This journey took a lot out of me, and I am incredibly grateful for the people who walked alongside me and supported me through it all.

First and foremost, my deepest gratitude goes to my supervisors, **Elkan and Aytaç**.

Elkan, it is hard to believe how much time has passed since our very first phone interview. I can't remember exactly what I said about why I wanted to transition from biomedical engineering to cognitive psychology, but I still remember how excited and grateful I was when you welcomed me into your lab as a PhD student. It was your patience that allowed me to grow and find my footing in a completely different field. You always took my 'stupid' questions seriously, patiently explaining everything from basic terms to complicated neuroscience mechanisms. Your rigorous scientific attitude set a high standard for me. Thank you for your leadership and for guiding me through every major milestone – my first department talk, my first conference presentation, my first paper, and finally, the completion of this thesis.

Aytac, you are such a kind person and I am very glad to have you as my daily supervisor. During the first three years of my PhD, I can't count how many times I knocked on your office door to ask if you had a minute, and your answer was always yes. You guided me through every single detail of the research process. From designing experimental paradigms and running the experiments, to analyzing the data, and even handling the tedious paperwork, you always taught me with so much patience. I also want to thank you for all our small talks. You showed me how to navigate the inevitable ups and downs of a PhD, and how to approach difficult problems with a clear and calm mind. Thank you for everything.

To my dear paranymphs, **Sena and Zehan**, I am so lucky to have you two taking on this role. Thank you for being my 'boots on the ground' and taking care of all the complex graduation preparations while I was away from the Netherlands. You saved me from so much anxiety. I really couldn't have pulled this off without you, and I am so grateful to have you behind me. **Sena,** I am so glad to have met you and Sahcan—you two are such a lovely couple! You are such a sweet person, always smiling and incredibly genuine. **Zehan**, you always impressed me with your amazing outfits. In fact, your great sense of style actually inspired what we are going to wear for the defense!

To my friends from the **'百毒不侵' group**: our story started with that trip to Italy, which was my first real holiday after starting the PhD. Thank you for your continuous support. Thank you for being there for me when I was just settling down in the Netherlands, through the pandemic, during those times when we had nothing to do, and whenever I felt down. Thanks to our various sub-groups, my life in the Netherlands was full of joy.

To **Captain Wei,** strictly speaking, you are almost my matchmaker, haha! Thank you for your incredible leadership and organizational skills, which allowed us to just turn off our brains and enjoy our trips. Please keep it up and take me on more carefree adventures to enjoy life! **Nana and Xinya,** we came to Groningen together from the very first day. Having you by my side made my first time living abroad much less intimidating. I will always remember those early days when our apartments had barely any furniture, and we would sit on the floor to eat together and celebrate each other's birthdays. Thank you for your company and all those late-night chats. **Hao,** you are the best colleague ever! I loved our little weekday afternoon hangouts and gossiping with you in the office. You are always so kind. Thank you for your homemade Liangpi, your DIY bracelets, and for the warmth of always standing by my side no matter what.

I really appreciate the time I spent at the **E department.** Even though I wasn't physically sitting in the E office for the last two years of my PhD, I will always value the memories we made. To all my fellow PhDs who made this journey much more enjoyable—thank you for every shared lunch, every 'minnar', the E-outs, and our disco bowling nights. A special thanks to the people I spent the most time with: **Josh, Ivory, Yuanyuan, Sophia, Joost, Thomas, Tineke, Celina, Cherie, Veera, Ana, Mingming, Ahmet, Güven, Gülsen, and Maarten.** I also want to express my appreciation to **Mark N. and Wouter**; your helpful comments on my projects during our weekly lab meetings meant a lot to me. **Minou,** thank you for effortlessly sorting out all my administrative matters, and I will really miss our lovely little chats! Finally, a special thanks to **Monicque** for being my supervisor in the very beginning of my research path. I loved hearing your experiences in your research career, sharing our mutual appreciation for Chinese spices, and enjoying those wonderful summer barbecues at your place!

To my friends back in China, especially the ones who took up most of my WeChat storage: **Ping, Xiaoya, Xue, and Lele.** Thank you for listening to my endless complaints throughout this whole PhD journey. It would have been so much harder to get through without your (mostly online) company. You were always encouraging me, telling me that I could do this and handle whatever came my way. Sometimes, I think you believe in me more than I believe in myself.

Thank you to everyone in my **PhD support group.** Writing a thesis can be an incredibly isolating process, but sharing our struggles made it feel a little less lonely. It is a hard journey, but we all made it, or we will all make it in the end.

I also want to say a big thank you to my online friends from **暂停实验室.** It was all of you who taught me how to embrace my vulnerabilities and truly accept who I am.

接下来，我要把最深的感激留给我的家人。正是因为你们无底线的包容和支持，才有了今天的我。特别要感谢我的父母，**王建忠先生和李涛女士**。从小到大，无论我做出什么样的人生选择，你们总是无条件地支持我，并且永远坚定地相信我一定能做到。在这个离家万里、充满挑战的旅程中，你们始终是我最最坚强的后盾。爸爸妈妈，我爱你们！

And last but by no means least, **Carl.** This might actually be the hardest part to write in my acknowledgments. Thank you for your endless patience and understanding. Thank you for simply being there—through my anxiety, my boredom, my happiness, and my sadness. Through all the emotional rollercoasters of these past years, you were always right by my side. I am so incredibly happy to have spent the most colorful seven years of my life with you.Thank you for putting up with my endless nagging and all my weird quirks. Thank you for being the very first audience member whenever I prepared a conference presentation, and for always being the first (and most patient) participant for my tedious experiments. I feel like I can't possibly fit all my heartfelt words into this one page, so I will leave the rest for our wedding ceremony. I just hope you don't cry too much by then!